Ancillary Ligand Effects in Zirconium(IV) Aminoborollide and Nitrogen Chelated Pt(II) Complexes

Thesis by

Antek G. Wong-Foy

In Partial Fulfillment of the Requirements
for the Degree of
Doctor of Philosophy

California Institute of Technology
Pasadena, California

2002
(Defended October 1, 2001)

For My Family & Melanie

Acknowledgments

I have been extremely fortunate to have worked for and with Prof. John Bercaw. He is a brilliant scientist of the highest order, whose high work standards and ability to focus on the crux of important problems, think critically about them, then devise creative solutions are truly inspirational. He is an advisor *par excellence* and I am particularly grateful to John for his patience and support in allowing me incredible scientific freedom to work on challenging problems and to learn from my mistakes. The Bercaw group is an amazing environment to do science where you learn, perhaps, the most important and certainly most difficult lesson of all; you learn how to teach yourself. I am truly grateful to Prof. Gui Bazan, my undergraduate advisor, who first urged me to come to Caltech.

I would like to acknowledge the help of Jay Labinger, a collaborator on the Pt project from its inception, whose formidable intellect has been an inexhaustible source of insight, and for making it to my defense, especially since I had forgotten to tell him the date! I would like to acknowledge my committee members Profs. Bob Grubbs, Harry Gray, Doug Rees, and Sunney Chan for helpful suggestions. I would especially like to thank Prof. Doug Rees for rescuing my committee by sitting in for Sunney on such short notice. Harry, your lectures were a *tour de force* of science and your encouragement during the roughest thesis writing moments was the light at the end of the tunnel.

Throughout the changing face of the Bercaw Mafia there have consistently been incredibly talented grad students who have generously shared their time, advice, and friendship with me. Andy Kiely, as well as being a wealth of inorganic knowledge, first introduced Cory Nelson (my partner in crime on the borollide project, and a hella'va shortstop) and me to the Bercaw vacuum line, extremely dry martinis, and Raymond Chandler. Bob Blake was the first inhabitant of 201 and taught me the history, intricacies, and reasons behind every piece of glassware on the high vac line, and schooled me every time on the pool tables. Susan Brookhart helped me outfit the line, but more importantly showed me to the wonders of Peet's in the mornings. Both Sharad Hajela and Tim Herzog are incredibly creative scientists who were always there to offer invaluable chemical advice over the not too-frequent midnight beer, and introduced me to just about every fast-food (i.e. sleaze) joint in town. Mike Abrams, who made an epic batch of Da-Gin, taught me to bring chemicals into the box and not the antechamber pump, and found a fabulous apartment for Melanie and me. Shannon Stahl was the first grad student to work on the Pt project and his intensity for science was matched only his intensity for hopping into the Buick for sleaze.

Jeff Yoder is a sharp chemist who knew how to dominate the vac line (i.e. distilling doubly labeled propylene through four traps and three manifolds) and was someone to commiserate with about jobs. As well as leading the HOGS to their only C-league championship during my time here, he was always willing to consume any amount of awful vodka (Grey Goose) and chicken feet. Your and Shelly's friendship and generosity are much appreciated. Annita Zhong was a much welcomed addition to 201, and our "subtle discussions" about chemistry, though they may have cleared out the computer room or lab on more than one occasion, really helped me to think about problems indepthly. Seva (Shilov) Rostovsev has been a tremendous colleague on the Pt project as well as a fountain of knowledge with regards to the current literature. He also had a knack for naming most of the group computers, and a penchant for the phrase "monkey, heh?" Chris (Theory/JAG) Brandow was always willing to help out with any computational questions and demonstrated that roasted duck necks are digestible.

The Bercaw group has also had a number of amazing postdocs and visiting scientists who have had considerable influence on me. Shigenobu Miyake was a fine addition to 201 and showed me how to use a garden hose for a canula. I'm glad he returned to Japan with something useful too: the ability to swear in English. Jim Gilchrist, Alex Muci, and Joseph Sadighi are all walking organic encyclopedias and (at least the last two) are experts on South Park. I am grateful for all their help and advice on nearly everything from NMR spectroscopy and ligand synthesis, to getting married in Vegas and smoking stogies on the toilet seat sculpture. Dario Veghini, aside from being a suave ladies man, was always there to translate any article that was written in the following languages: german, italian, french, or russian. Matt Holtcamp is a tremendous chemist and really broke open the Pt project. He was instrumental in getting me started on the Pt chemistry and can make a mean deer-chili, even if it's from road kill. Ola Wendt was a kineticist extraordinaire and changed the way kinetics are practiced in the group for the better. He was also partial to VON'S brand liquor and introduced me to the not-so-finer pleasures of Swedish vermouth at a certain going-away party. Lars Johannson introduced to the Pt project the use of trifluoroethanol as a solvent and was a source for fruitful discussions. He supplied the Swedish vermouth at his going-away party. John Scollard always begrudgingly provided us with multi gram quantities of the Pt-dimer, while keeping the computers in tip-top shape. He couldn't win a game of guts to save his life but he did appreciate steak wrapped in bacon. Chris Levy passed on the secrets of the Pt-dimer synthesis, was a damned good cook, and pressed everyone's buttons. But I still appreciate his and Jennifer's friendship, if not only to be invited over for dinner.

I would like to acknowledge the current members of the Bercaw Mafia for all their help and support during the last grueling months of writing. As in the past, they are a talented group

of individuals. Lily Ackerman is a truly fine scientist who has also crossed the periodic table from the early to the late transition metals, where she is already dominating. Your friendship, support, the occasional Camel Light, and the 99 balloons has really meant a lot to me these past few months. Sara (Man's pants) Klamo has always held a great perspective on research, a crazy sense of humor, and a caffeine habit that I've always admired. Her attention to detail will surely make her an Ola'esque kinetics guru. Endy Min, who really knows how to swing, throws a hella'va going-away party. The stereo in 201 is now yours, —please play the music loud, polymerizations don't like NPR. The title of senior Bercaw Mafia now belongs to Susan (Aloha!) Schoefer who has an under appreciated rye sense of humor and who introduced me to dirty martinis at Monty's. Jonathan (Shannon Jr/Barney) Owen was poised to take over the Pt project the day he joined the group and has a very bright future ahead of him as the nicknames imply, though whether in chemistry or kids' television, we're not sure. Christoph Balzarak is one of the nicest Germans I know, taking over the thankless job of computer czar, as well as one of the bravest; he tried going toe-to-toe with Joseph on politics. Cliff Barr and Alan Heyduk are phenomenal scientists and I wish I could have interacted more with them. Best of luck to Theo Agapie and David Weinberg, the newest of the Bercaw Mafia.

Thanks go to Pat Anderson and Dian Buchness for all their personalized help and advice and the best hairdresser in town. This place would be in shambles without them. Thanks to Rick Gerhardt for the fabulous line in 201. Many thanks also to Larry Henling and Mike Day for solving all the x-ray structures in this thesis.

I have been extremely blessed to have the unwavering support, love, and continuing prayers of my parents. They have always been willing to sacrifice whatever was necessary to help me succeed and I am truly indebted to them. I would also like to thank my younger brother, whose advice helped immensely during the writing of the first drafts of this thesis. It's amazing that, though we think completely differently from one another, we still share the same views and opinions.

Last, but not least, I would like to thank Melanie Sanford. It is not possible to measure or even put into words how much your encouragement, friendship, and love have meant to me since we met nearly six years ago. You have been here for me always, and in every way. I know I would not have been able to complete this thesis without you, and would have ended up as a dice degenerate. I hope that I will always be there for you too, and give back even a fraction of what you have given of yourself to me.

Abstract

The preparation of new chloro derivatives of pentamethylcyclopentadienyl aminoborollide complexes of Zr are described. Treatment of the dianions **1.9–1.12** with Cp^*ZrCl_3 yields $Cp^*\{\eta^5\text{-}C_4H_4BN(Si(CH_3)_3)_2\}ZrCl\cdot LiCl$ (**1.13**), $Cp^*\{\eta^5\text{-}C_4H_4BNC(CH_3)_3Si(CH_3)_3\}ZrCl\cdot LiCl$ (**1.14**), $[Cp^*\{\eta^5\text{-}C_4H_4BN(Et)CH_2CH_2NEt_2\}ZrCl_2Li]_2$ (**1.15**), and $Cp^*\{\eta^5\text{-}2,5\text{-}Ph_2C_4H_2BNMe_2\}ZrCl\cdot LiCl$ (**1.16**). The electronic spectra of these complexes were measured and compared to the parent complex $Cp^*\{\eta^5\text{-}C_4H_4BN(CHMe_2)_2\}ZrCl\cdot LiCl$ (**1.17a**) in THF solvent. In general, as the substituents directly bonded to nitrogen increase in size, a blue shift of the low energy, aminoborollide to zirconium charge transfer band (LMCT), occurs. λ_{max} decreases in the order **1.16** > **1.17a** > **1.14** > **1.15** ~ **1.13**. The anionic portions of complexes **1.13–1.16** have also been structurally characterized by x-ray crystallography. Although the changes are very small, in general a lengthened B–N bond correlates linearly with the observed blue shift of the LMCT band.

Studies directed towards the development of a Pt(II)-catalyzed oxidation of ethylene to ethylene glycol based on the Shilov system for alkane functionalization is described. The first step is the activation of ethylene towards nucleophilic attack by water to generate a Pt(II) β-hydroxyalkyl intermediate that is oxidized in a second step to the Pt(IV) β-hydroxyalkyl. Reductive elimination via an S_N2-type mechanism at the α-C of the Pt(IV) β-hydroxyalkyl liberates the oxidized product leaving the reduced Pt(II) center to bind another equivalent of olefin. The first system examined was the methyl ethylene complex $[(tmeda)PtMe(\eta^2\text{-}C_2H_4)][SbF_6]$, **2.2**. Nucleophilic attack at the bound ethylene was not observed; instead displacement of ethylene occurred. The bound ethylene in the neutral complexes *cis*-$Cl_2PtL(\eta^2\text{-}C_2H_4)$, (L = PPh_3 (**2.23**), $AsPh_3$ (**2.24**), Me_2SO (**2.25**)) and *trans*-$Cl_2Pt(\eta^2\text{-}C_2H_4)(C_5H_5N)$, **2.26** are susceptible towards attack by OH^-. Under catalytic conditions (excess ethylene and H_2O_2) decomposition of **2.23**, **2.24**, and **2.25** was observed. In **2.26**, 1 turnover was observed before decomposition occurred. The bound ethylene in the complex $[(tmeda)PtCl(\eta^2\text{-}C_2H_4)][ClO_4]$ is activated towards nucleophilic attack by water and OH^-, allowing the isolation of the Pt(II) β-hydroxyalkyl. This is rapidly oxidized to the Pt(IV) β-hydroxyalkyl by hydrogen peroxide. In the presence of HCl, it undergoes reductive elimination to yield 2-chloroethanol and $(tmeda)PtCl_2$. Unfortunately, this system also showed no catalytic activity.

The dicationic complexes $[(ArN{=}C(Me){-}C(Me){=}NAr)Pt(solv)_2]X_2$, (Ar = 2,6-$(CH_3)_2C_6H_3$; **3.5a**: solv = CH_3CN, X = $CF_3SO_3^-$, BF_4^-, SbF_6^-; **3.5b**: solv = $(CH_3)_2CO$, X = BF_4^-, SbF_6^-) and **3.6** $[(CyN{=}C(H){-}C(H){=}NCy)Pt(CH_3CN)_2]X_2$, (Cy = C_6H_{11}, X = OTf^-, BF_4^-, PF_6^-, SbF_6^-) were synthesized from the corresponding Pt dichlorides with 2 equiv. of AgX. The reaction of **3.5a** with 1-phenylpyrazole, 2-phenylpyridine, 2-vinylpyridine, and 2-(2-thienyl)pyridine in acetone affords the cyclometalated products **3.11–3.14** via intramolecular C–H activation of an sp^2 C–H bond of the unsaturated sidegroup. Pyridines with saturated groups at the 2-position do not undergo a similar cyclometalation reaction. **3.6** undergoes cyclometalation of one of the cyclohexyl groups, an example of sp^3 C–H bond activation. The later reaction proceeds only partway to completion, implying that an equilibrium has been reached; in the case where X = OTf^-, the equilibrium favors the starting dication. Furthermore, the intramolecular C–H activation occurs in trifluoroethanol but not in acetone under comparable conditions in contrast to the reactions of **3.5a** with the substituted pyridines.

The diaqua complexe $[(ArN{=}C(Me){-}C(Me){=}NAr)Pt(H_2O)_2]X_2$, **4.3**, (Ar = 2,6-$(CH_3)_2C_6H_3$; X = OTf^-, BF_4^-) decompose in aqueous solution to yield a red-orange precipitate. Spectroscopic characterization of the precipitate by ^1H, IR, and conductivity measurements is consistent with C_{2v} symmetric structure containing hydroxo groups. Confirmation of the dicationic, dinuclear Pt(II) complex, **4.4**, where the two Pt centers are bridged by two OH groups was revealed by x-ray crystallography.

Table of Contents

Chapter 1: Ligand Induced Perturbations of the LMCT Bands in Pentamethylcyclopentadienyl Aminoborollide Complexes of Zr

Abstract..... 1
Introduction..... 2
Results and Discussion..... 17
Conclusions..... 32
Experimental..... 32
References and Notes..... 43

Chapter 2: Possible Intermediates in a Catalytic Cycle for the Oxidation of Ethylene to Ethylene Glycol Based on the Shilov System

Abstract..... 49
Introduction..... 50
Results..... 54
Discussion..... 68
Experimental..... 72
References and Notes..... 79

Chapter 3: Intramolecular C–H Activation by Dicationic α-Diimine Supported Pt(II) Complexes

Abstract..... 82
Introduction..... 83
Results and Discussion..... 86
Experimental..... 100
References and Notes..... 109

Chapter 4: Synthesis and Characterization of a Dinuclear μ-Hydroxo–Bridged α-Diimine Pt(II) Complex

Abstract..... 113
Introduction..... 114
Results and Discusion..... 115
Conclusions..... 133
Experimental 134
References and Notes..... 137

Appendix 1: X-ray Crystallographic Data for 1.13a..... 141
Appendix 2: X-ray Crystallographic Data for 1.14a..... 144
Appendix 3: X-ray Crystallographic Data for 1.15..... 148
Appendix 4: X-ray Crystallographic Data for 1.16a..... 152
Appendix 5: X-ray Crystallographic Data for 3.12..... 154
Appendix 6: X-ray Crystallographic Data for 3.14..... 158
Appendix 7: X-ray Crystallographic Data for 4.4..... 161

List of Figures

Chapter 1: **Figure 1.** Neutral Sc and Y single component α-olefin and stereospecific α-olefin polymerization catalysts. 3

Figure 2. Isoelectronic, dianionic ligands and their possible coordination modes as Cp^- analogues. 5

Figure 3. Possible resonance contributors describing the bonding picture in aminoborollide complexes with transition metals. 14

Figure 4. Synthesis of 2,5-dihydroborolenes **1.4–1.6** Conditions: a) hexanes, –78 °C to rt; b) Et_2O, –78 °C to rt. 17

Figure 5. Labeled Diamond view of the anionic portion of **1.13a**. The cation, $Li(tmeda)_2$, has been omitted for clarity. Thermal ellipsoids are shown at 50% probability. 21

Figure 6. Labeled Diamond view of the anionic portion of **1.14a**. The cation, $Li(tmeda)_2$, has been omitted for clarity. Thermal ellipsoids are shown at 50% probability. 21

Figure 7. Labeled Diamond view of **1.15**. Thermal ellipsoids are shown at 30% probability. 22

Figure 8. Labeled Diamond view of the anionic portion of **1.16a**. The cation, $Li(THF)_4$, has been omitted for clarity. Thermal ellipsoids are shown at 50% probability. 22

Figure 9. Plot of LMCT bands of complexes **1.13a–1.17a** in visible region. 28

Figure 10. Plot of λ_{max} versus B–N bond length. 29

Figure 11. Correlation of λ_{max} and increase in B–N bond length for complexes **1.13a**, **1.14a**, and **1.17a**. 29

Chapter 2: **Figure 1.** $K[Cl_3Pt(\eta^2\text{-}C_2H_4)]$ (8.22 mM) catalyzed oxidation of ethylene (~3.5 atm) by Na_2PtCl_6 (123 mM) to 2-chloroethanol (▫) and ethylene glycol (▪) as a function of time. Total number of turnovers (○). 62

Chapter 3: **Figure 1**. Representative aryl and alkyl α-diimine ligands. 84

Figure 2. Labeled Diamond drawing of the cationic portion of **3.12** ($X = BF_4^-$) with ellipsoids at 50% probability. 92

Figure 3. Labeled Diamond drawing of the cationic portion of **3.14** ($X = BF_4^-$) with ellipsoids at 50% probability. 94

Chapter 4: **Figure 1**. α-aryldiimine ligated μ-hydroxo-bridged dimers of Pt(II). 116

Figure 2. Labeled Diamond drawing of the cationic portion of **4.4** ($X = OTf^-$) with ellipsoids at 50% probability. The two OTf^- anions and a disordered acetone molecule have been omitted for clarity). 117

Figure 3. Bent and planar 1,10-phenanthroline based Pt(II) μ-OH bridged dimers. 119

Figure 4. ^1H NMR of (a) μ-OH dimer **4.4** ($X = OTf^-$) in neutral D_2O; (b) diaqua **4.3** in 0.05M DOTf solution; (c) dihydroxy **4.6** in 0.1 M KOH in D_2O solution. (Peak intensities in the aryl and methyl regions are scale differently). 121

Figure 5. Electronic spectra of **4.3** (——, 1.12×10^{-4} M), **4.4** (– – –, 9.27×10^{-5} M), and **4.6** (---, 1.52×10^{-4} M). 122

Figure 6. Titration of **4.4** (7.61×10^{-5} M) with 0.100M NaOH. Mole ratios of added OH^-:**4.4** are 0:1(trace 1) and 2.8:1(trace 13). Further addition of NaOH does not result in additional changes to trace 13. 125

Figure 7. Alkyl and aryl region of the ^1H NMR in TFE-d_3 for the protonolysis of **4.7**, with DOTf. 132

List of Tables

Chapter 1: **Table 1.** Selected Intraligand and Zr–Borollide Distances (Å) and selected Intraligand Bond Angles (°). 23

Chapter 3: **Table 1.** Selected bond lengths and bond angles for the cationic portion of **3.12** ($X = BF_4^-$). 92

Table 2. Selected bond lengths and bond angles for the cationic portion of **3.14** ($X = BF_4^-$). 94

Chapter 4: **Table 1.** Selected bond lengths and bond angles for the cationic portion of **4.4** ($X = OTf^-$). 117

Table 2. Tabulated absorption maxima λ_{max} and molar absorptivities for **4.3**, **4.4**, and **4.6** in aqueous solution. 122

Chapter 1

Ligand Induced Perturbations of the LMCT Bands in Zr Pentamethylcyclopentadienyl Aminoborollide Complexes

Abstract

The preparation of new chloro derivatives of pentamethylcyclopentadienyl aminoborollide complexes of Zr are described. Double deprotonation of the 2,5-dihydroborolenes **1.4–1.7** with 2 equivalents of a lithium base affords the corresponding dianions **1.9–1.12**. Treatment of **1.9–1.12** with Cp^*ZrCl_3 yields $Cp^*\{\eta^5\text{-}C_4H_4BN(Si(CH_3)_3)_2\}ZrCl\cdot LiCl$ (**1.13**), $Cp^*\{\eta^5\text{-}C_4H_4BNC(CH_3)_3Si(CH_3)_3\}ZrCl\cdot LiCl$ (**1.14**), $[Cp^*\{\eta^5\text{-}C_4H_4BN(Et)CH_2CH_2NEt_2\}ZrCl_2Li]_2$ (**1.15**), and $Cp^*\{\eta^5\text{-}2,5\text{-}Ph_2C_4H_2BNMe_2\}ZrCl\cdot LiCl$ (**1.16**). The electronic spectra of these complexes were measured and compared to the parent complex $Cp^*\{\eta^5\text{-}C_4H_4BN(CHMe_2)_2\}ZrCl\cdot LiCl$ (**1.17a**) in THF solvent. In general, as the substituents directly bonded to nitrogen increase in size, a blue shift of the low energy aminoborollide to zirconium charge transfer band (LMCT), occurs. λ_{max} decreases in the order **1.16** > **1.17a** > **1.14** > **1.15** ~ **1.13**. The anionic portions of complexes **1.13–1.16** have also been structurally characterized by x-ray crystallography. Although the changes are very small, in general a lengthened B–N bond correlates linearly with the observed blue shift.

Introduction

Since its commercialization over four decades ago, the Ziegler-Natta polymerization of ethylene and α-olefins has grown into a multibillion dollar a year industry worldwide.[1-4] Estimates of global production have been placed in excess of 1.9 billion pounds annually,[4] totaling over 160 billion pounds.[5] Until recently, the mainstays of the industry have been heterogeneous catalysts comprised of mixtures of group 4 halides and alkyl aluminums or the alternative chromium on silica.[6] The advent of metallocene based, single-site, homogeneous catalysts, however, is rapidly changing this, as evident by the first plant initiated by Exxon in 1991 using these catalysts.[7-9] This renewed interest in metallocenes emerged from the discovery in 1980 by Sinn and Kaminsky that homogeneous mixtures of methylaluminoxane, or MAO, (MAO—partially hydrolyzed $AlMe_3$) combined in large excesses with group 4 bent-metallocenes, such as Cp_2MCl_2 (M = Ti, Zr, Hf; Cp = C_5H_5), produced highly active catalysts for the polymerization of ethylene and α-olefins.[10,11] The past two decades since have seen enormous research efforts in both academic and industrial laboratories directed towards the understanding and development of these single-site, homogeneous polymerization systems. These developments have been reviewed in numerous books and review articles.[12-16]

These homogeneous metallocene catalysts offer unprecedented control of the resulting macroscopic properties of the polymer by controlling various aspects of monomer enchainment at a molecular level through manipulation of the ancillary ligands. Unlike their heterogeneous counterparts, where multiple active sites are polymerizing with different, independent rate constants for enchainment, co-monomer incorporation

and chain termination, the single-site nature of homogeneous catalysts lead to polymers of low polydispersities and uniformly incorporated co-monomers.[5-13] This translates into the ability to control macroscopic properties of a polymer such as molecular weight, molecular weight distribution, the incorporation of different monomers and the absolute and relative stereochemistry of the polymer.[9,12,13]

A substantial body of work has now accumulated in support of the notion that the catalytically active species in metallocene based homogeneous Ziegler-Natta systems are cationic, 14-electron, d^0 alkyls or hydrides of the general composition $[Cp_2MR][WCA]$ (M = Ti, Zr, and Hf; WCA = "weakly coordinating anion"), where the key role of MAO is to first alkylate the metal center then subsequently remove a ligand.[17-19] Careful mechanistic studies carried out by the groups of Watson and Bercaw have utilized isoelectronic, 14-electron d^0, lanthanide and group 3 metallocenes to describe the nature of the active species, establish the role of co-activators, delineate the fundamental details of olefin insertion, and outline the requirements for stereoselectivity.[20-26] The culmination of which has resulted in the synthesis of the first single component, α-olefin polymerization catalyst based on scandium,[27,28] as well as the first yttrium containing single component, stereospecific α-olefin polymerization catalyst (Figure 1).[29,30]

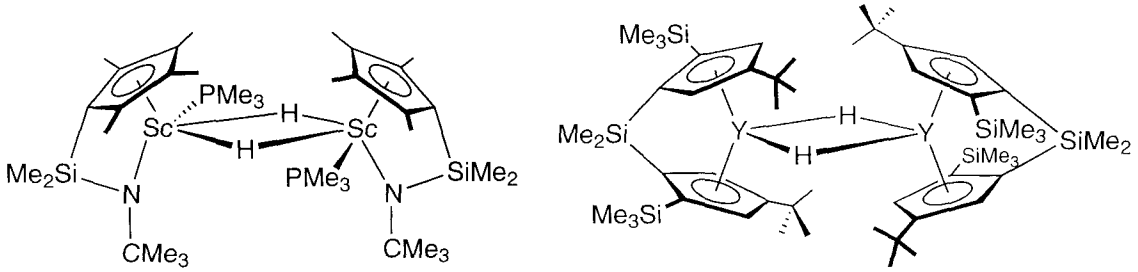

$[(Cp^*SiN^tBu)(PMe_3)Sc(H)]_2$ $[(S,S\text{-}Me_2Si(C_5H_2\text{-}2\text{-}SiMe_3\text{-}4\text{-}CMe_3)_2Y(H)]_2$

Figure 1. Neutral Sc and Y single component α-olefin and stereospecific α-olefin polymerization catalysts.

Encouraged by the successful preparation of these single component group 3 catalysts, efforts by various groups turned to developing neutral group 4 complexes for homogeneous olefin polymerizations. Complexes of this type were anticipated to combine the advantage of the single component nature of the neutral group three catalysts while retaining the high catalytic activity of the corresponding cations. One such strategy involves the replacement of one of the monoanionic Cp rings of a bent-metallocene with a dianionic 6π analogue. There are relatively few ligands of this general type, and those that have been employed in this context coordinate in either an η^5 or η^4 manner (Figure 2). Of these, the dicarbollide, the *nido*-carborane, and the aminoborollide dianions are both isoelectronic and isolobal to the Cp anion. This was first recognized by Hawthorne for the dicarbollide dianion, $[C_2B_9H_{11}]^{2-}$,[31,32] and since then a substantial number of metallacarboranes have been synthesized incorporating not only d and f-block metals[33-35] but also main group elements.[36]

η^5-dianionic ligands:

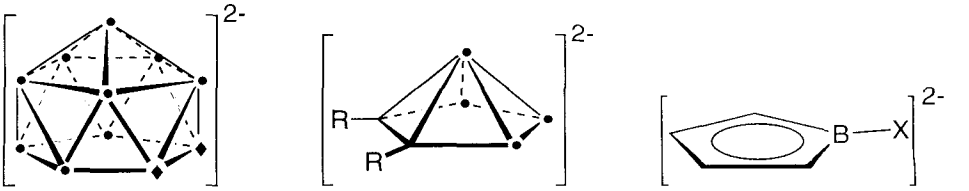

Dicarbollide
$[C_2B_9H_{11}]^{2-}$
(• = BH; ♦ = CH)

nido-Carborane
$[R_2C_2B_4H_4]^{2-}$
(• = BH; R = $SiMe_3$ or Et)

Borollide
$[C_5H_4BX]^{2-}$
(X = Ph, NMe_2, NEt_2, N^iPr_2)

η^4-dianionic ligands:

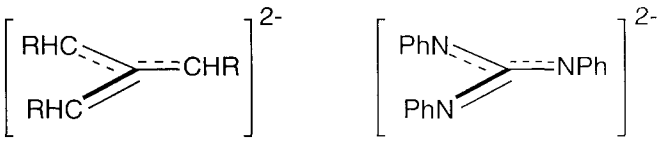

Trimethylenemethane
$[C(CHR)_3]^{2-}$
(R = H, Ph)

Triazamethylenemethane
$[C(CNPh)_3]^{2-}$

Figure 2. Isoelectronic, dianionic ligands and their possible coordination modes as Cp^- analogues.

Dicarbollide complexes of all the group 4 metals have been studied systematically by Jordan and coworkers. Both the Zr and Hf analogues show reactivity patterns quite characteristic of electrophilic d^0, 14–electron metallocenes. It came as a surprise then that the structure of what was presumed to be the mono-methyl Hf complex, [Cp*(η^5-$C_2B_9H_{11}$)HfMe] (Cp* = C_5Me_5), turned out to be an unsymmetrical dimer described as a Cp*(η^5-$C_2B_9H_{11}$)Hf^+ fragment bridged to a Cp*$HfMe_2^+$ fragment by the terminal B–H bonds of a dicarbollide dianion.[37] The Zr analogue was formulated as having the same dimeric structure owing to the fact that it displayed similar spectral and analytical characteristics. These methyl complexes polymerize ethylene, oligomerize propylene, form adducts with Lewis bases, insert internal alkynes forming β-agostic complexes,

decompose to μ-CH_2 dimers, and undergo σ-bond metathesis with dihydrogen and dicarbollide C–H bonds (Scheme 1).[38-40]

Scheme 1

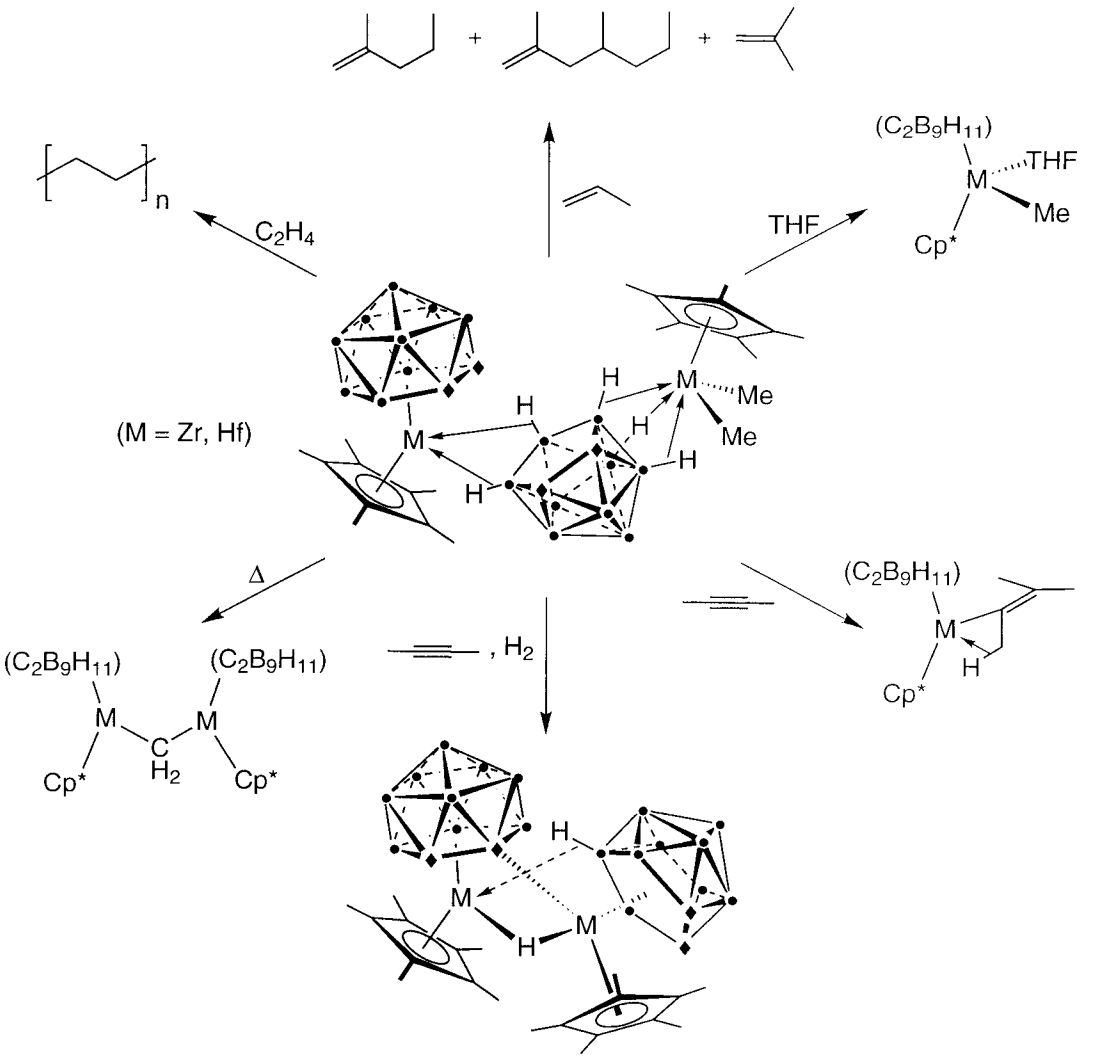

The corresponding Ti complex, Cp*($C_2B_9H_{11}$)TiMe, is monomeric due to the smaller radius of Ti versus Zr or Hf.[41] The electrophilic nature of the complex is demonstrated by its ability to dimerize ethylene, coordinate PMe_3, and insert internal alkynes and acetonitrile. Additionally, the methyl complex is unstable at rt and

undergoes irreversible σ-bond metathesis with one of the Cp* Me groups forming the fulvene derivative, $(\eta^6\text{-}C_5Me_4CH_2)(\eta^5\text{-}C_2B_9H_{11})Ti$ (Scheme 2).[42]

Scheme 2

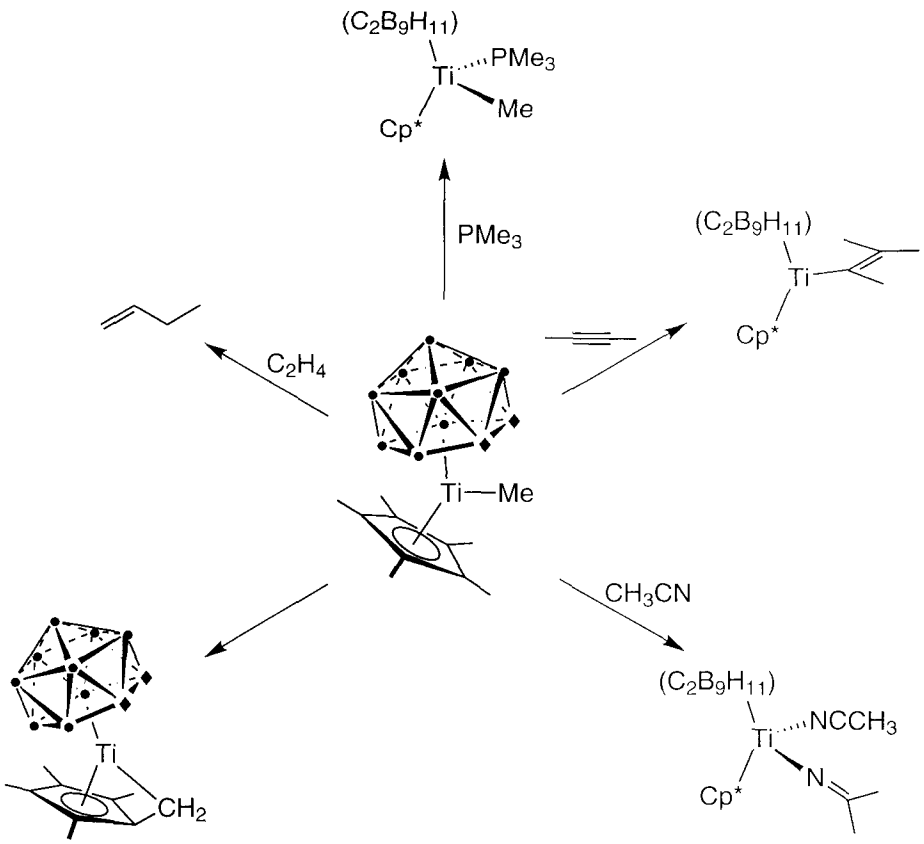

Finn, Grimes, and coworkers have extensively studied the smaller *nido*-carboranes, $[Et_2C_2B_4H_4]^{2-}$, on group V metals such as Nb and Ta, and recently on the group 4 metals, Ti and Zr.[43] These complexes show electrophilic behavior in their reactions with unsaturated substrates. The Ta(V) dimethyl complex, $Cp(\eta^5\text{-}Et_2C_2B_4H_4)TaMe_2$, inserts alkynes, nitriles, and isocyanides photochemically whereas the diphenyl complex reacts thermally with styrene and alkynes through an intermediate benzyne complex (Scheme 3).[44-46] In some of these reactions the carborane ligand is

rather non-innocent whereby the terminal B–H bonds participate in insertion chemistry with the unsaturated substrate.

Scheme 3

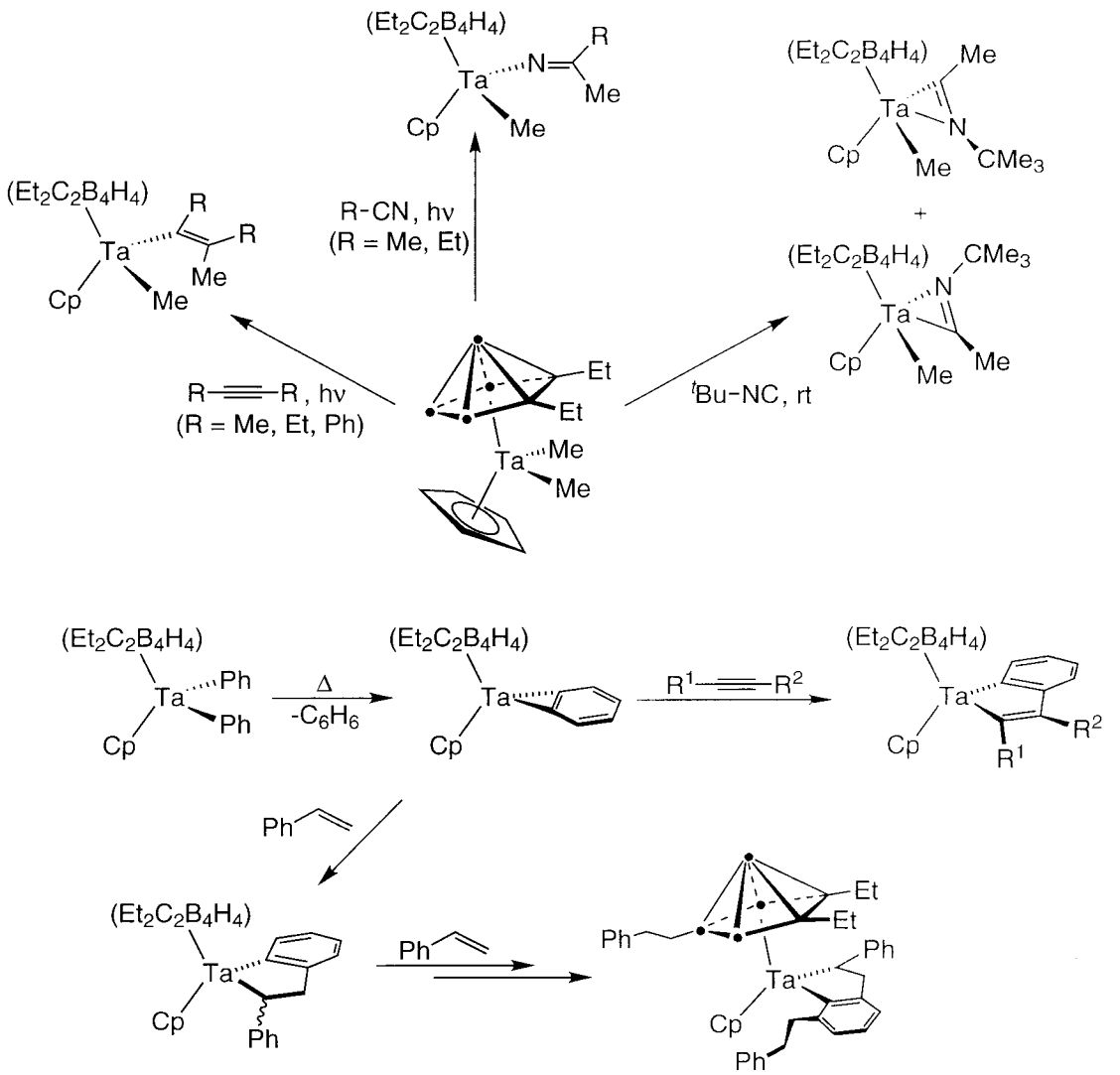

More recently, 14-electron, d^0, piano-stool type bis-phosphino complexes of Ti and Zr have been prepared. These were shown to be active ethylene polymerization catalysts in the presence of MAO (Scheme 4).[47]

Scheme 4

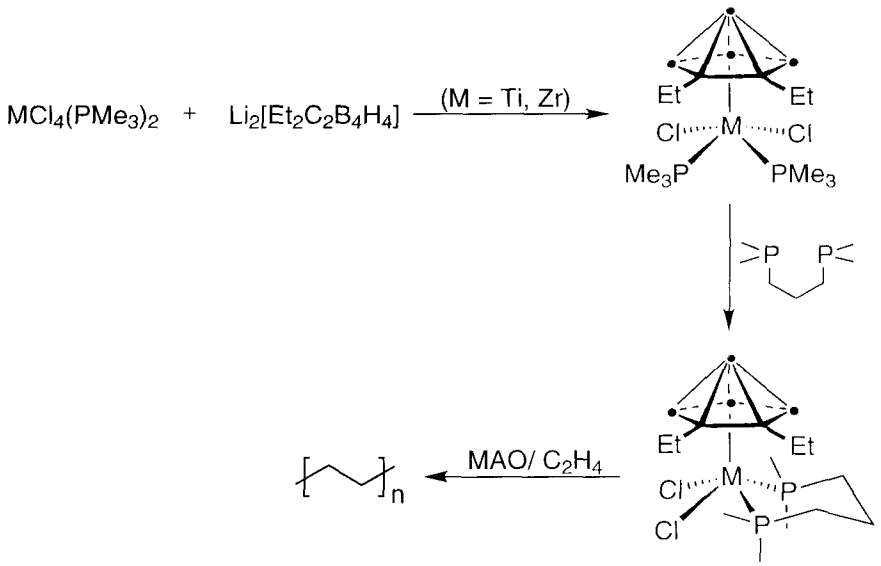

Hosmane and coworkers have similarly prepared a number of lanthanide and group 4 halide complexes with the *nido*-carborane, $[R_2C_2B_4H_4]^{2-}$ (R = $Si(CH_3)_3$).[35] Agostic B–H interactions are observed both with electropositive transition metals to give dimeric complexes and with lithium or magnesium counteranions to give "ate" complexes. In contrast to the Ta(V) complexes, the zirconate complex, $[Li(THF)_3][Cp^*(\eta^5\text{-}C_2B_4H_4(Si(CH_3)_3)_2ZrCl_2]$, does not undergo alkylation with lithium alkyls or Grignard reagents to any characterizable products (eq 1).[48]

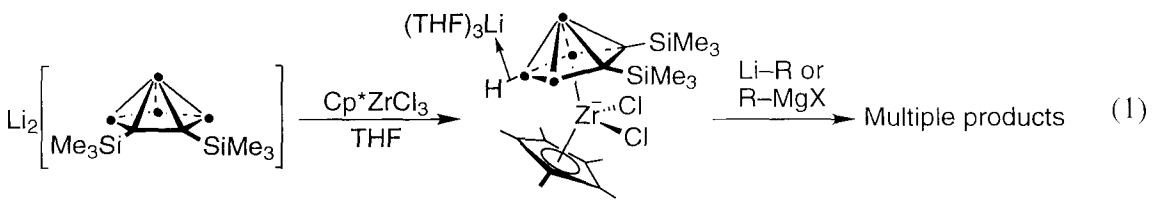

(1)

In the examples described above, the coordination chemistry at the metal center is significantly influenced by interactions with the electron rich B–H bonds of the ligands.

Efforts by the Bazan and Bercaw groups to design systems in which coordinating functionalities such as terminal B–H bonds are unavailable have led to studies of the trimethylenemethane ($[C(CH_2)_3]^{2-}$), the tribenzylidenemethane ($[C(CHPh)_3]^{2-}$), the triazabenzylidenemethane ($[C(NPh)_3]^{2-}$), and the diisopropylaminoborollide ($[C_4H_4BN^iPr_2]^{2-}$) dianions as ligands for group 4 metals. Bazan and coworkers have carried out extensive studies on Zr complexes containing the trimethylenemethane family of ligands.[49-51] The parent trimethylenemethane and tribenzylidenemethane ligands bind in an η^4 fashion and show characteristic electrophilic reactivity such as the coordination of LiCl to form either Zwitterions or discrete zirconate salts. Upon treatment with excess MAO, the LiCl adducts polymerize ethylene, 1,5-hexadiene, and co-polymerize ethylene with 1-hexene (Scheme 5).[50,51]

Scheme 5

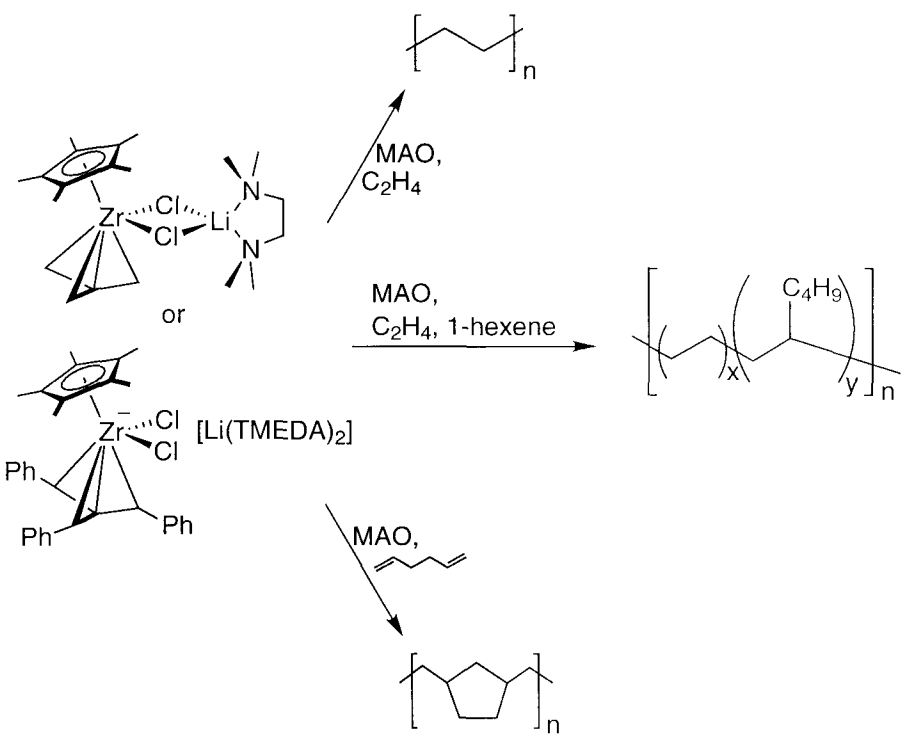

Alternatively the neutral d^0 complex, $Cp^*(\eta^4\text{-}C(CHPh)_3)ZrCH_3(THF)$,[50] can be accessed by treatment of Cp^*ZrMe_2Cl with $Li[PhCH_2C(CHPh)_2]$, (the mono-anion of the tribenzylidenemethane ligand). The resulting dimethyl complex undergoes intramolecular σ-bond metathesis liberating methane and generating the η^4- bound tribenzylidenemethane, similar to that reported by Bercaw and coworkers for a related Ta complex.[52] The electrophilic character of this complex is demonstrated by it coordination of THF, its tendency to undergo σ-bond metathesis with 2-butyne, and its ability to polymerize ethylene (Scheme 6). Replacement of the tribenzylidenemethane ligand with the trimethylenemethane ligand results in the methylene bridged dimer due to the reduced steric environment around the metal center.

Scheme 6

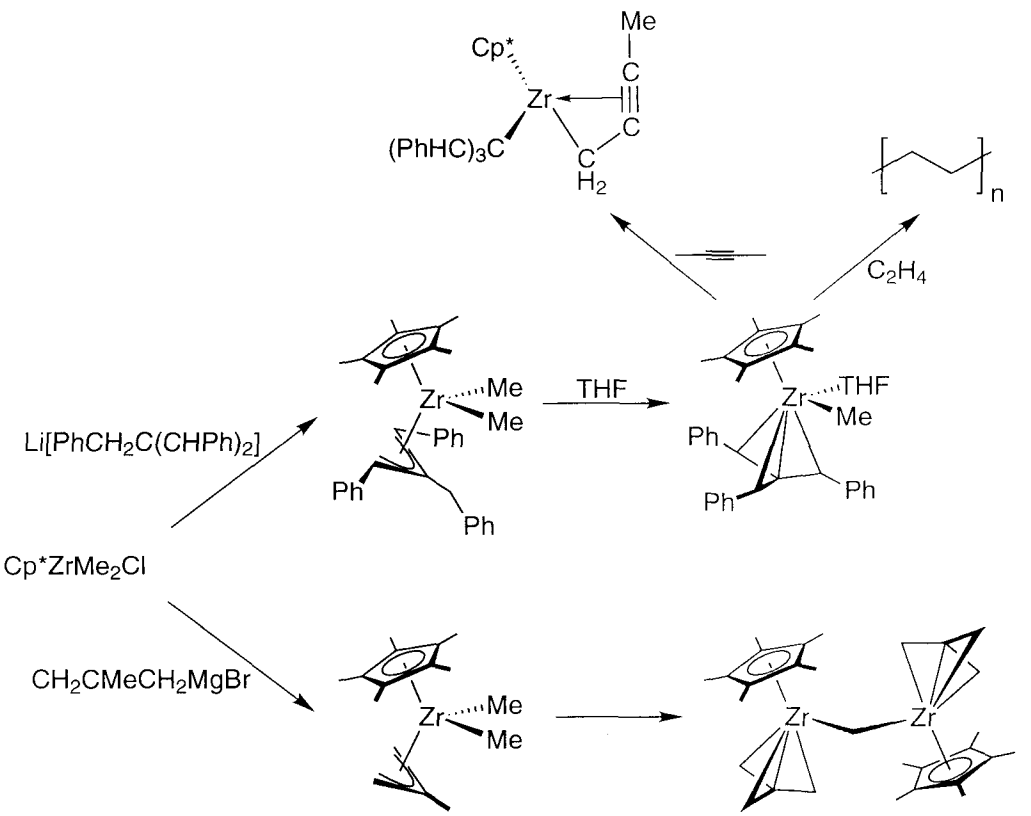

Finally unlike the parent ligand, the triazabenzylidenemethane ligand binds only in an η^2 fashion through two of the amide nitrogens to afford zwitterionic complexes of Zr (eq 2).[49]

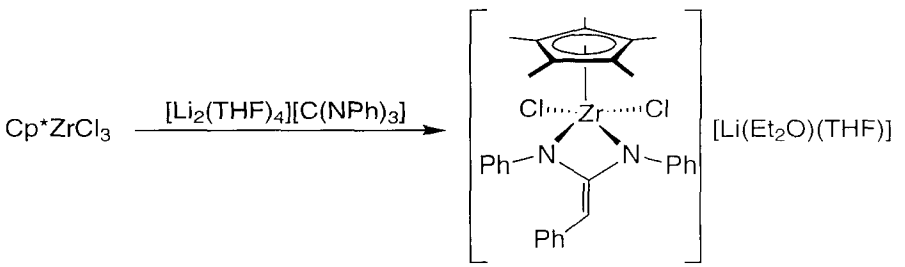

(2)

Bercaw and coworkers have focused on the use of the N,N-diisopropylaminoborollide ligand as a divalent Cp analogue for group 4 metals. The dianionic charge of this ligand can be understood in terms of replacing a neutral C–H vertex of the Cp anion with an anionic B–N fragment. Again, the electrophilic nature of Zr and Hf complexes containing this ligand is manifest in their tendency toward salt formation with halides and small alkyls.[53-55] Methide abstraction with $B(C_6F_5)_3$ generates the neutral mono-methyl Hf complex which is an active catalyst for ethylene polymerization (Scheme 7).[56]

Scheme 7

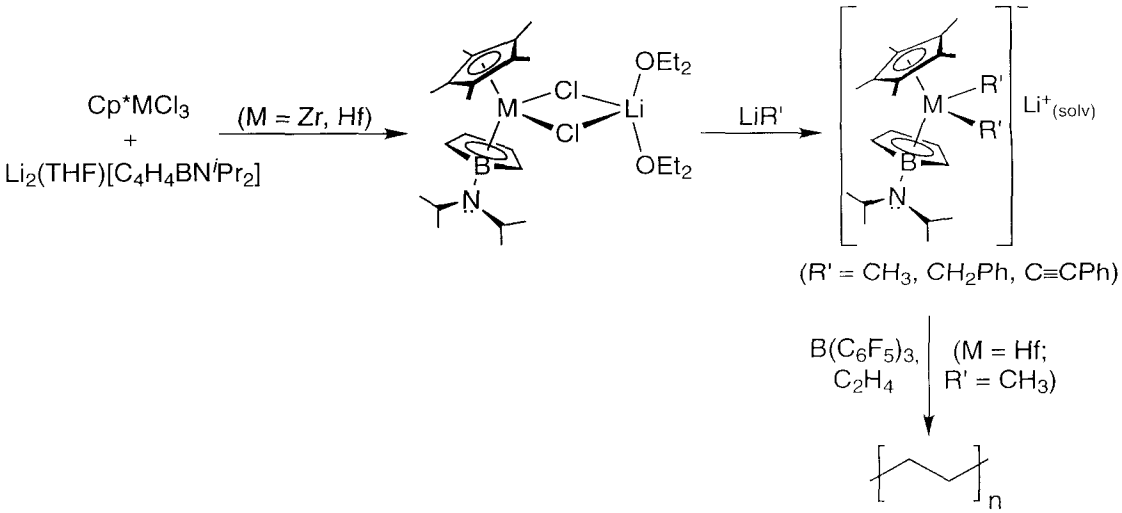

In contrast, treatment of the LiCl adducts with allylmagnesium bromide affords the neutral, d^0, η^3-allyl products, which are free of coordinated solvents or halides.[57] These η^3-allyl complexes polymerize ethylene, coordinate Lewis bases, and react via σ-bond metathesis with dihydrogen to hydrogenate the allyl ligand and produce the thermally unstable monomeric hydrides (Scheme 8).

Scheme 8

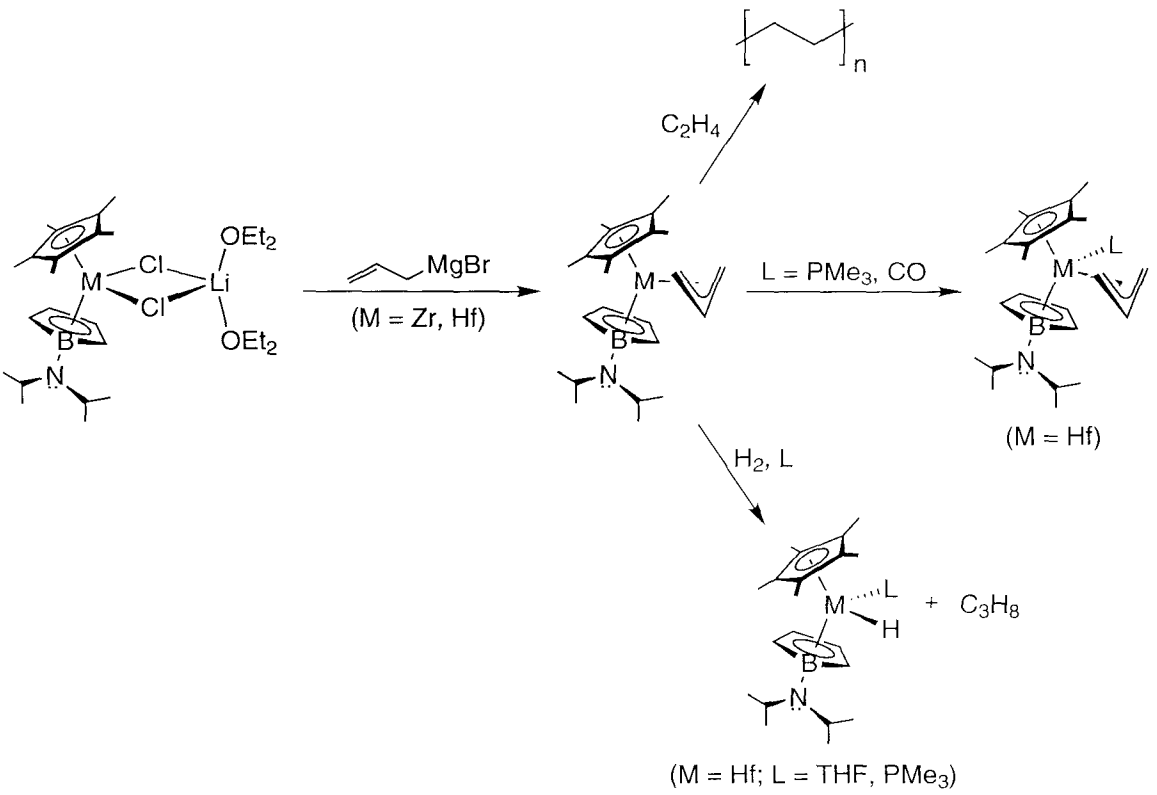

Unlike the previously described dianionic ligands, diisopropylaminoborollide contains a tunable B–N interaction, which has a profound effect on the structure and reactivity of its transition metal complexes. Three limiting resonance structures contributing to the overall bonding picture can be invoked and are illustrated in Figure 3.[53,57]

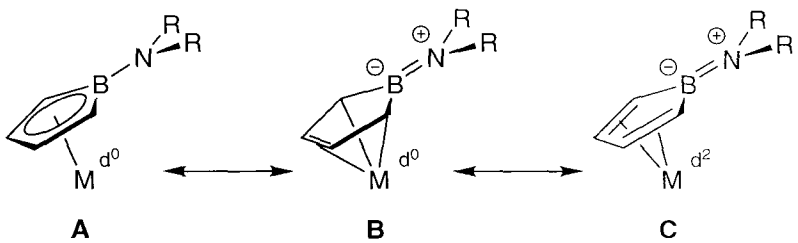

Figure 3. Possible resonance contributors describing the bonding picture in aminoborollide complexes with transition metals.

The first resonance structure is the dianionic aminoborollide adduct, **A** (η^5-L_2Z = η^5-LX_2), the second is the dianionic metallacyclopentene complex, **B** (η^4-LX_2), and the third is the neutral iminoborata-fulvene species, **C** (η^4-L_2). In resonance structures **A** and **B**, the transition metal is considered to be in its highest oxidation state, while in **C**, the metal can be viewed as being formally reduced by two electrons. Based on the available crystal structure data and on the electronic spectra of a series of related complexes, Bercaw and coworkers have suggested that the best description of the ground state for Zr and Hf metallocenes is a combination of the resonance structures **A** and **C**.[53,57] In contrast, due to the greater accessibility of the lower oxidation states of tantalum, Bazan and coworkers have suggested that resonance structures **B** and **C** best describe the bonding in Ta-borollide complexes.[58,59] Finally, Herberich has concluded that resonance structure **C** is the best valence bond description of the bonding in late transition metal complexes of this ligand.[60]

In addition to the bonding considerations described above, the presence of the Lewis basic amino group adjacent to the Lewis acidic metal center has been used in a cooperative fashion for the heterolytic cleavage of H–X bonds in acids, alcohols, thiols and terminal acetylenes (Scheme 9). However, to date these complexes have not demonstrated the ability to heterolytically cleave sp^2 and sp^3 C–H bonds.

Scheme 9

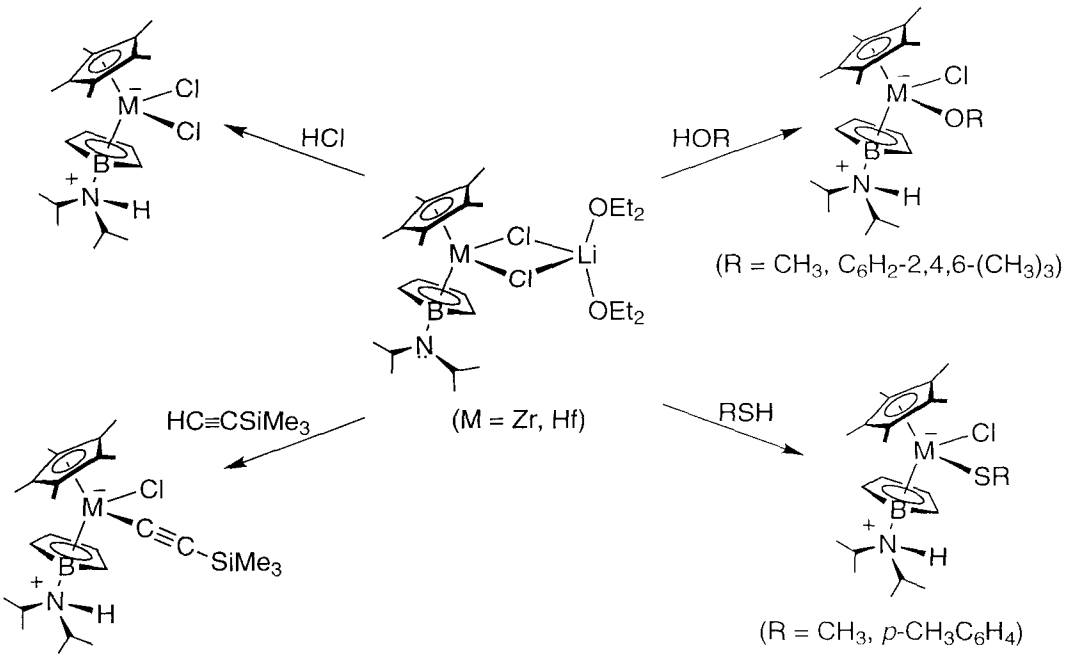

In contrast to most group(IV), d^0 bent metallocenes, the N,N-diisopropylaminoborollide complexes of Zr and Hf are deeply colored due to a weak aminoborollide to metal charge transfer transition (LMCT) in the visible region.[57] This transition is a direct consequence of π-donation from the lone pair on nitrogen to the empty p-orbital on boron. As a result, the energy of this LMCT transition should be a sensitive indicator of changes in electron density at the metal center. The goal of this project was to synthesize a series of sterically bulky aminoborollide complexes of Zr and Hf and to examine their LMCT transitions. Using the LMCT data in combination with solid state structural results, we hoped to directly probe the effects of ligand variation on the nature of the B–N bond and on the electronics at the metal center. Ultimately, these results could provide insights towards the design of superior group IV aminoborollide catalysts for H-X bond cleavage and olefin polymerization reactions.

Results and Discussion

Synthesis and Characterization of Cp*(Borollide)ZrCl·LiCl Complexes 1.13–1.16

A general synthetic route to the borollide ligands reported herein is outlined below. The ligand synthesis commences with the preparation of the 2,5-dihydroborolenes **1.4–1.6** (Figure 4), which is based on the methodology developed by Herberich for the parent, 1-(*N,N*-diisopropylamino)-2,5-dihydroborolene.[61]

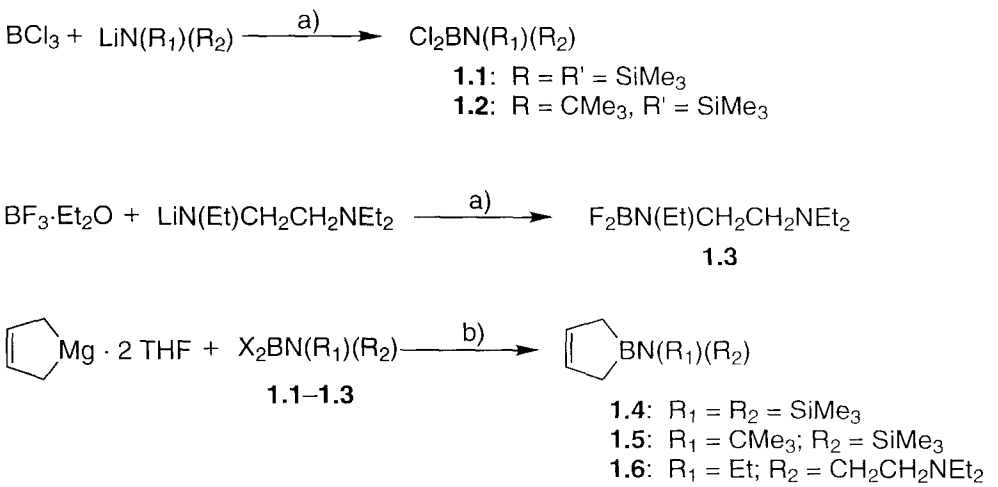

Figure 4. Synthesis of 2,5-dihydroborolenes **1.4–1.6** Conditions: a) hexanes, –78 °C to rt; b) Et_2O, –78 °C to rt.

Organoborondihalides **1.1** and **1.2** were prepared by treating a solution of BCl_3 in hexanes with the appropriate lithium amide at –78 °C. Alternatively, the boron was introduced as the difluoroboron reagent, **1.3**, derived from $BF_3{\cdot}OEt_2$. The use of **1.3** was necessary because the lithium amide, $LiN(Et)CH_2CH_2NEt_2$, contained Et_2O as a solvent of crystallization, and boron trihalides other than $BF_3{\cdot}OEt_2$ are known to cleave Et_2O.[62] Treatment of the appropriate organoborondihalides with magnesium-butadiene in Et_2O at low temperature afforded the *C*-unsubstituted 2,5-dihydroborolenes **1.4–1.6** in modest yield (41–43%).[63] Similarly, the *cis* and *trans* isomers of the *C*-substituted 2,5-diphenyl-

2,5-dihydroborolenes, **1.7** and **1.8**, were prepared by treatment of the magnesium reagent, $Mg(1,4\text{-}Ph_2C_4H_4)(THF)_3$, with Cl_2BNMe_2 and $Cl_2BN(i\text{-}Pr)_2$ respectively, according to a modification of Herberich's procedures (eq 3).[64]

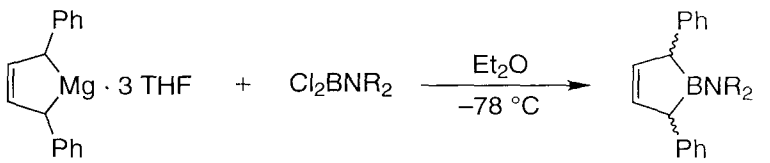

(3)

1.7: R = CH_3
1.8: R = $CH(CH_3)_2$

Double deprotonation of the 2,5-dihydroborolenes, **1.4–1.7**, with two equivalents of LDA or lithium tetramethylpiperidide (LiTMP) produced the corresponding dianions **1.9–1.12** in high yields, and treatment with one equivalent of Cp^*ZrCl_3 in toluene afforded the bent metallocene analogues **1.13–1.16** (Scheme 10).[65] In general, the di-lithio salts **1.9–1.12** could be generated in situ and used without isolation; however, in the case of the bent metallocene **1.13**, isolation of the THF adduct of **1.9**, $Li_2[C_4H_4BN(Si(CH_3)_3)_2](THF)$, yielded a cleaner product upon metallation with the zirconium precursor. Notably, all attempts to generate the dianion of **1.8** failed. Treatment of **1.8** with various lithium bases resulted in a color change to bright red, but ^1H NMR spectroscopy showed the formation of an intractable mixture of products. This was rather surprising, since LDA deprotonation of **1.7** to afford **1.12** proceeded cleanly at –78 °C to provide deep red solutions of this dianion.

Scheme 10

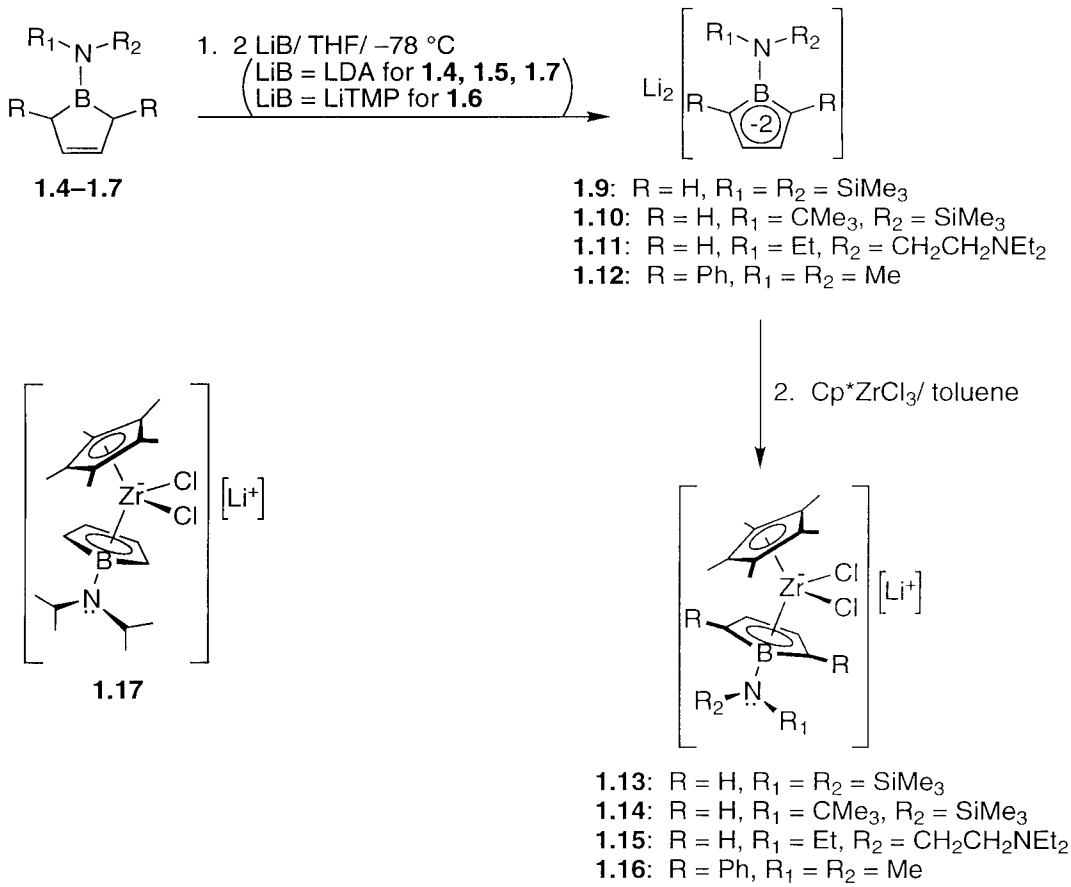

Like the parent zirconocene, Cp*{η^5-$C_4H_4BN(CHMe_2)_2$}ZrCl·LiCl (**1.17** in Scheme 10), the new metallocenes tenaciously hold on to LiCl and were often isolated as their LiCl adducts. THF and Et_2O readily coordinate to these materials, but can be removed by successive triturations with toluene and then washing with petroleum ether. In general, the LiCl adducts are sparingly soluble in hydrocarbon solvents. A notable exception is complex **1.13**, which is moderately soluble in petroleum ether, and, as a result, was isolated in low yield (12%).

X-ray Crystal Structure Determinations of Zirconates 1.13a–1.16a

In an effort to correlate the electronic spectroscopy of **1.13a–1.16a** with the ground state perturbation of B–N π-bonding, x-ray structure determinations of these complexes were undertaken. Diamond illustrations of the lithium solvated forms of **1.13–1.16** (designated as **1.13a–1.16a**) are shown in Figures 5–8, and selected bond lengths and bond angles are listed in Table 1.

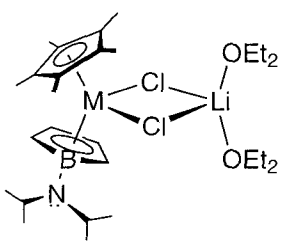

1.17a: (M = Zr)
1.18: (M = Hf)

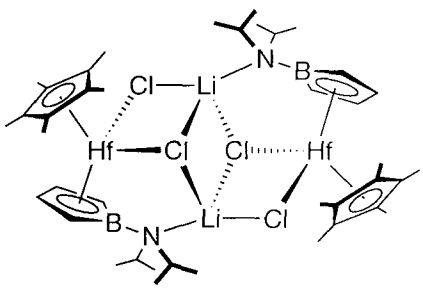

1.19

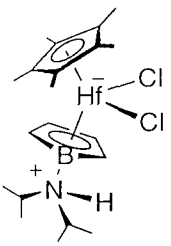

1.20

In general, x-ray quality crystals were grown from THF or from THF/tmeda solutions layered with petroleum ether. These coordinating solvent systems serve to bind the Li^+ ion and promote the formation of monomeric complexes such as **1.17a** and **1.18**. In the absence of a donor solvent, the lithium ions coordinate to the borollide nitrogen to form chloride bridged dimers (*e.g.*, complex **1.19**) and effectively eliminate π-donation from the nitrogen lone pair to boron. This is manifest in an increase of B–N bond length from 1.44 Å in **1.18** to 1.5 Å in **1.19**, as well as in a change of color from blue (in the former) to orange-red (in the latter).[53] Because this dimer does not reflect the true B–N bond order, we wanted to avoid its formation. Notably, previous studies have demonstrated that protonation at nitrogen (to afford the zwitterionic complex **1.20**) has a similar effect of "short circuiting" the π-interaction.[55]

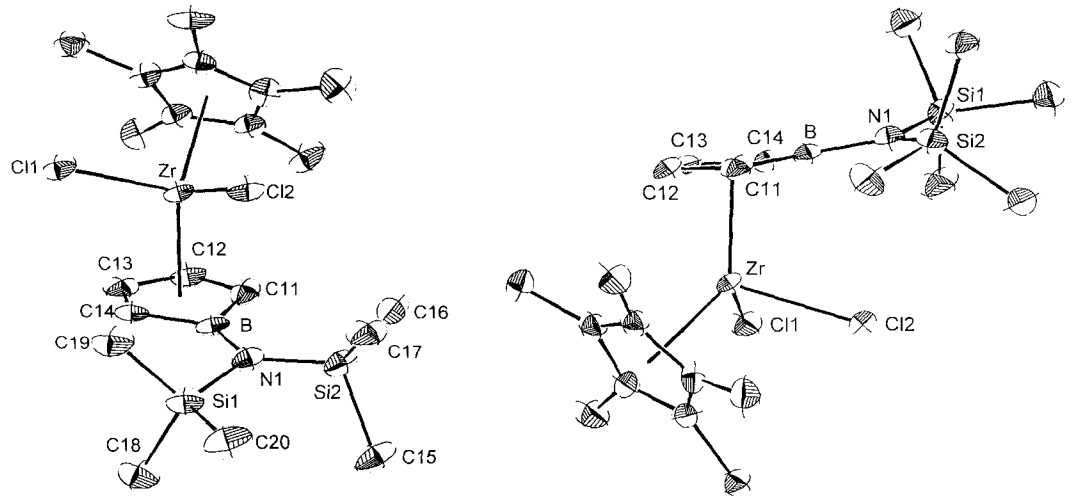

Figure 5. Labeled Diamond view of the anionic portion of **1.13a**. The cation, $Li(tmeda)_2$, has been omitted for clarity. Thermal ellipsoids are shown at 50% probability.

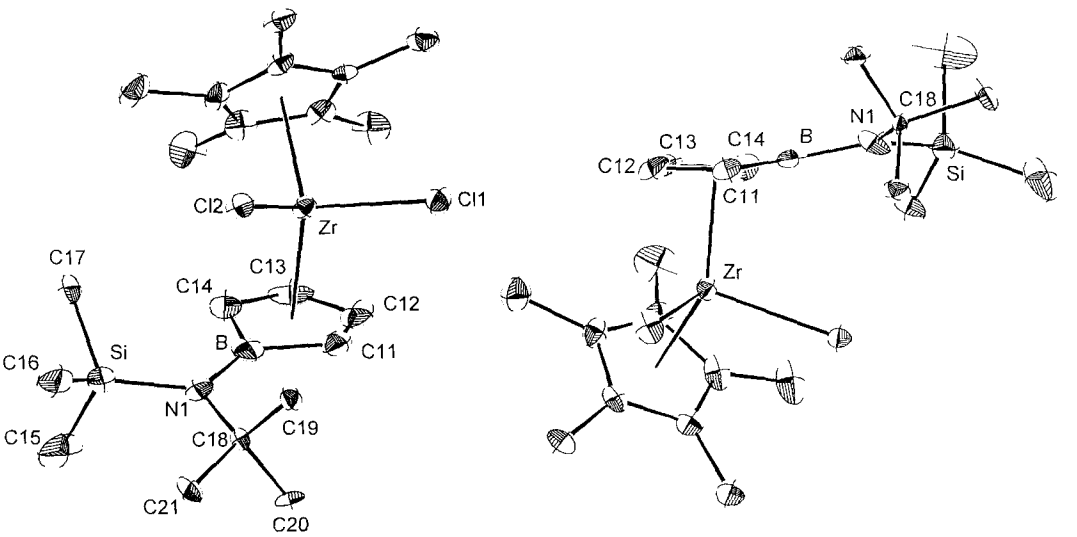

Figure 6. Labeled Diamond view of the anionic portion of **1.14a**. The cation, $Li(tmeda)_2$, has been omitted for clarity. Thermal ellipsoids are shown at 50% probability.

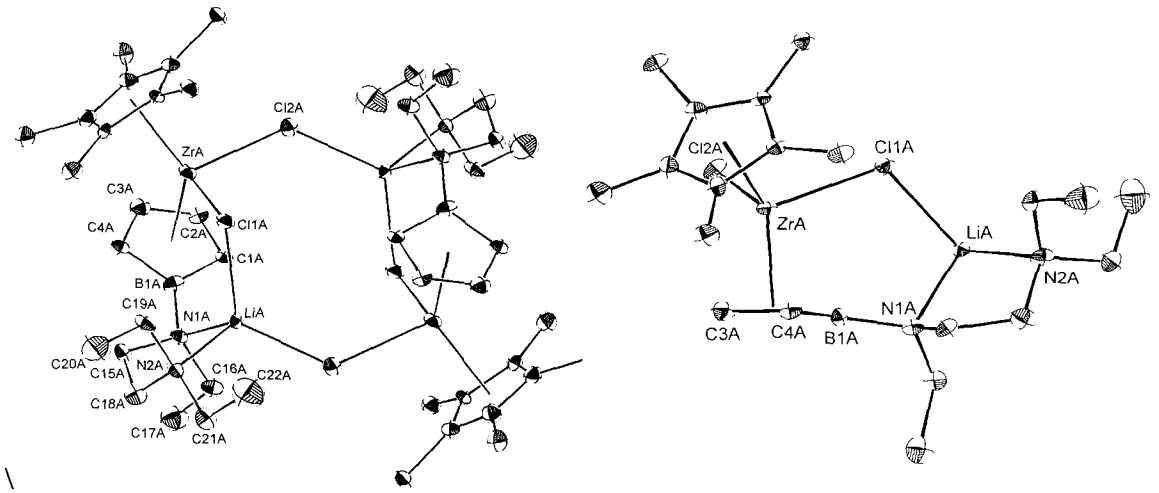

Figure 7. Labeled Diamond view of **1.15**. Thermal ellipsoids are shown at 30% probability.

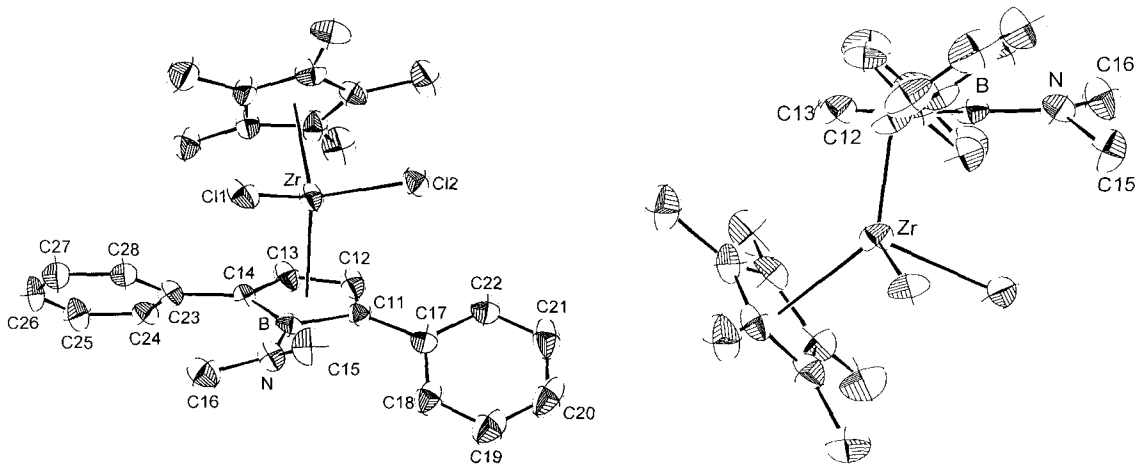

Figure 8. Labeled Diamond view of the anionic portion of **1.16a**. The cation, $Li(THF)_4$, has been omitted for clarity. Thermal ellipsoids are shown at 50% probability.

Table 1. Selected Intraligand and Zr–Borollide Distances (Å)[a]

	B–N	B–C_α	C_α–C_β	C_β–$C_{\beta'}$	$C_{\beta'}$–$C_{\alpha'}$	B–$C_{\alpha'}$	M–B	M–C_α	M–$C_{\alpha'}$	M–C_β	M–$C_{\beta'}$	M–Cent
1.13a	1.480(7)	1.561(7)	1.421(7)	1.402(8)	1.429(7)	1.524(8)	2.722(5)	2.469(4)	2.515(5)	2.383(4)	2.419(5)	2.172
1.14a[b]	1.457(8)	1.544(8)	1.419(8)	1.403(8)	1.413(8)	1.528(9)	2.747(6)	2.514(5)	2.484(6)	2.411(5)	2.416(5)	2.198
1.15	1.46(3)	1.50(3)	1.38(2)	1.31(3)	1.45(3)	1.49(3)	2.67(2)	2.515(19)	2.423(19)	2.400(18)	2.36(2)	2.158
1.16a	1.444(7)	1.539(7)	1.424(7)	1.384(7)	1.423(7)	1.555(8)	2.707(6)	2.580(5)	2.526(5)	2.413(5)	2.427(5)	2.206
1.17a[c]	1.433(11)	1.526(12)	1.404(12)	1.377(14)	1.423(12)	1.520(12)	2.714(9)	2.405(8)	2.518(8)	2.354(10)	2.439(10)	2.165
1.18[d]	1.435(9)	1.522(10)	1.390(11)	1.382(12)	1.442(11)	1.530(10)	2.693(8)	2.360(7)	2.498(7)	2.358(8)	2.418(8)	2.132
1.19[d]	1.509(6)	1.524(7)	1.434(7)	1.411(7)	1.437(7)	1.513(7)	2.654(5)	2.510(1)	2.501(5)	2.372(5)	2.417(5)	2.138
1.20[d]	1.580(8)	1.476(9)	1.418(9)	1.381(10)	1.424(9)	1.509(8)	2.624(6)	2.542	2.471	2.420	2.411	2.169

[a] Refers to atom designations below:
[b] See text regarding quality of structure analysis.
[c] Reference 55.
[d] Reference 53.

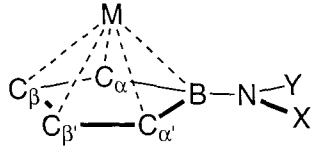

Table 1 (continued). Selected Intraligand Bond Angles and (°)[a]

	X, Y	B–N–X	B–N–Y	X–N–Y	Sum ∠ About N	Cp_{cent}–Zr–Bo_{cent}
1.13a	X = Y = Si	112.9(4)	124.9(4)	122.1(2)	359.9	131.6
1.14a[b]	X = Si, Y = C	124.7(3)	117.1(4)	118.2(3)	359.8	132.0
1.15	X = Y = C	114.3(17)	114.6(17)	115.2(16)	344.1	132.0
1.16a	X = Y = C	124.0(4)	121.3(4)	109.6(4)	354.9	132.7
1.17a[c]	X = Y = C	121.6(7)	123.5(7)	114.6(7)	359.7	132.7
1.18[d]	X = Y = C	120.7(6)	123.4(6)	115.6(6)	359.7	133.0
1.19[d]	X = Y = C	113.0(3)	114.2(3)	112.9(3)	340.1	132.0
1.20[d]	X = Y = C	116.5(7)	112.9(4)	114.3(3)	343.7	132.6

[a] Refer to atom designations below:

[b] See text regarding quality of structure analysis.

[c] Reference 55.

[d] Reference 53.

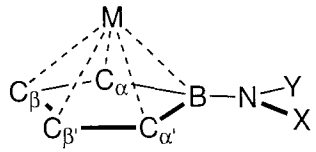

Complexes **1.13** and **1.14** were crystallized from petroleum ether layered solutions of THF and tmeda, and the Li^+ cations were coordinated by two equiv of tmeda to give **1.13a** and **1.14a**, respectively. For these complexes, the use of tmeda was necessary in order to obtain crystals suitable for diffraction. In contrast, x-ray quality crystals of complex **1.16** were obtained without the use of tmeda, and in this structure (**1.16a**) the Li^+ cation is fully solvated by four THF molecules. Complex **1.15** was crystallized as the neutral *dimer* from a 1 to 1 THF to tmeda solution layered with petroleum ether. This result indicates that the Li cation is tightly bound between the *N,N,N'*-triethylethylenediamine group on boron in **1.15**.

Comparison of the bond distances and bond angles to those of other aminoborollide complexes of Zr and Hf indicate that, in all cases, the borollide ligands are η^5-bound.[57,66] The B–N bond lengths in complexes **1.13a**, **1.14a**, and **1.16a** are slightly longer than those in the parent complex **1.17a** as well as those in the Hf analogue **1.18** (Table 1). The B–N bond distance in complex **1.13a** is particularly long (1.480(7) Å compared to 1.433(11) Å in **1.17a**), indicating that the boron-nitrogen interaction is significantly reduced. However, comparison to the B–N bond lengths of **1.19** (1.501(6) Å) and **1.20** (1.580(8) Å) reveals that there is still considerable double bond character in the B–N bond of **1.13a**. Additionally, the sum of the angles about nitrogen for **1.13a** and **1.14a** is effectively 360°, indicating that the nitrogen atom is sp^2 hybridized in both complexes. In contrast, complex **1.16a** shows only a slightly increased B–N bond distance relative to **1.17a**, but the sum of the angles around the nitrogen atom is only 355°, indicating slightly less sp^2 character than **1.13a**, **1.14a**, and **1.17a**.

The observed B–N bond distances and bond angles can be explained based on a combination of steric and electronic effects. In complexes **1.13a** and **1.14a**, the large TMS and ^{t}Bu substituents on nitrogen generate unfavorable steric interactions with the chlorides, resulting in a lengthening of the B–N bond relative to that of **1.17a**. In complex **1.16a**, the phenyl groups are canted at approximately 35° with respect to the borollide plane. This canting provides sufficient steric interaction to rotate the NMe_2 group slightly out of resonance, which is expected to lengthen the B–N bond. However, at the same time, the small size of the NMe_2 group results in increased σ-bonding to the electrophilic boron center, thus offsetting some of the increase in the B–N bond length resulting from steric interactions.

Finally, although the structure of **1.15** is given in Figure 7, discussion of its structural parameters remains tentative because crystals of this complex diffracted extremely poorly. However, despite this caveat, the observed structural parameters for **1.15** agree surprisingly well with those of the analogous Hf dimer **1.19**. For example, the B–N bond length in **1.15** (1.46(3) Å) is within error of that in **1.19** (1.509(6) Å). The metal–boron bond in **1.15** has shortened to 2.67(2) Å (as compared to 2.654(5) Å in **1.19**), indicating a stronger metal–boron interaction. Finally, the sum of the angles about the nitrogen in **1.15** is 344° compared to 340° for **1.19**.

Comparison of the LMCT Band in Complexes 1.13a–1.17a

Due to the instability of complexes **1.13a–1.17a** in most polar media, we initially used a toluene as a solvent for the investigation of their electronic spectroscopy. Importantly, however, comparing the electronic spectrum of these complexes in toluene

is problematic, because the extent to which the Li^+ cation is separated from the anionic Zr center can significantly affect the charge transfer transition.[67] In spite of this, only moderate solvatochromic shifts are observed on changing the solvent from toluene (dielectric constant = 2.38) to THF (dielectric constant = 7.4). For example, **1.17a** exhibits a LMCT band in the visible region at λ_{max} = 548 nm (ε = 681 M^{-1} cm^{-1}) in toluene, while in THF this band shifts to λ_{max} = 576 nm (ε = 873 M^{-1} cm^{-1}). The observed red shift is expected, since the more polar THF can better stabilize a build-up of charge in the excited state. The relatively small magnitude of the shift may indicate that only moderate dipole changes are associated with the excited state. A similar situation is well documented for titanocene complexes of the type Cp_2TiX_2, in which the solvatochromic shifts and the corresponding extinction coefficients are even smaller.[68-71]

We anticipated that changes to the sterics and electronics of the aminoborrolide ligands would be reflected in the electronic spectra of their Zr complexes. However, the tendency for the Li^+ cation to bind the aminoborollide nitrogen has complicated the analysis of these spectra. Association of the cation is expected to increase the energy of the LMCT transition relative to its baseline value. Cation binding is not expected to be a significant problem for complexes **1.13a** and **1.14a**, because their solid state structures indicate that the Li^+ is encapsulated by two tmeda molecules. In contrast, the x-ray structure of complex **1.15** shows that a Li^+ is clearly coordinated to the borollide nitrogen, and the cation will most likely remain in that position regardless of the solvent. However, in complexes **1.16a** and **1.17a** where the Li^+ is only coordinated by Et_2O or THF in the solid state, we cannot predict whether Li^+ will directly interact with the borollide nitrogen in solution.[72]

In order to minimize these complications and to obtain a true measure of the influence of sterics on the LMCT bands of **1.13a–1.17a**, absorption spectra were measured in THF where solvent-separated ion pairs are expected. This assumption is probably reasonable given that the structures of **1.13a**, **1.14a**, and **1.16a** (which were all crystallized from THF) showed the Li^+ to be well solvated. (The exception is of course complex **1.15**.) An overlay plot of the LMCT bands in the visible region is shown in Figure 9.

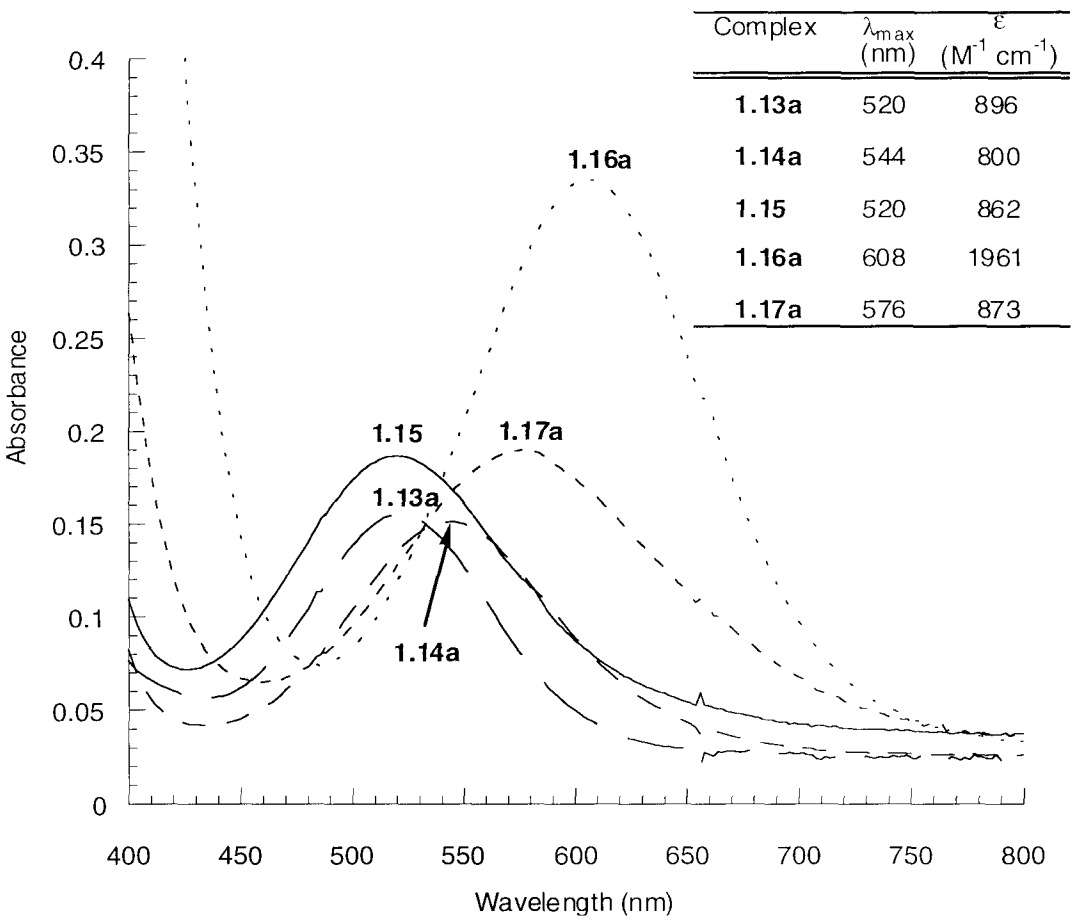

Figure 9. Plot of LMCT bands of complexes **1.13a–1.17a** in visible region.

Figure 9 shows that the range of wavelengths spanned is relatively small (approximately 90 nm), implying that there is a substantial amount of π-donation from nitrogen to boron in all the complexes under investigation. Within this range, however, complex **1.16a** exhibits the lowest energy LMCT band while compounds **1.13a** and **1.15** exhibit the highest. Figure 10 shows the absorption maxima plotted as a function of solid state B–N bond length.

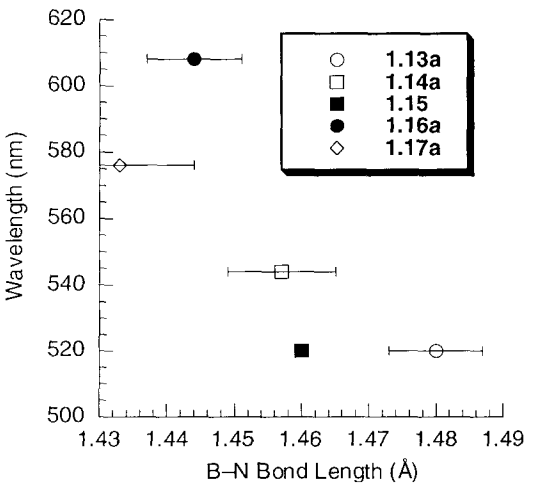

Figure 10. Plot of λ_{max} versus B–N bond length.

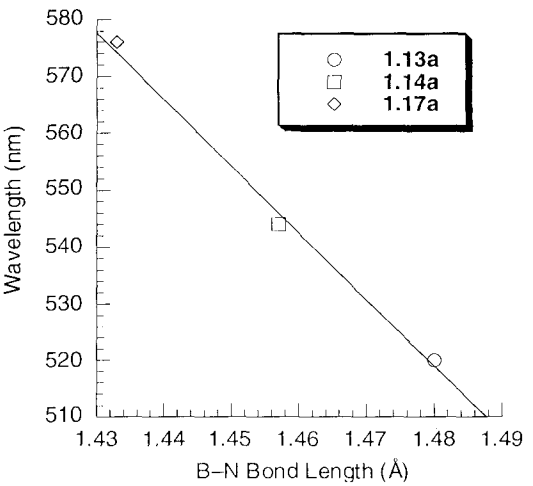

Figure 11. Correlation of λ_{max} and increase in B–N bond length for complexes **1.13a**, **1.14a**, and **1.17a**.

According to our original premise, as it becomes more difficult for the nitrogen to rotate into the geometry necessary for good π-overlap with boron (bonding is best described as being mainly from resonance structure **A** with very little contribution from **B** or **C** in Figure 3), the average B–N bond length will increase, and the LMCT band will blue shift to reflect this. Taken as a whole, there does not appear to be a correlation between B–N bond length and LMCT energy among the 5 complexes. However, if the points for **1.15** and **1.16a** are removed, then a linear relationship is obtained for the

remaining three complexes (Figure 11). As the substituents on nitrogen increase in size from two isopropyl groups (**1.17a**) to two trimethylsilyl groups (**1.13a**), a lengthening of the B–N bond length and a blue shift of the LMCT band is observed. These changes may be attributed to the increased steric interaction between the chlorides on Zr and the substituents on nitrogen. If rotation around the B–N bond requires the substituents to pass between the two chlorides (eq 4), then as the size of these substituents increase, the B–N bond length will naturally have to increase to allow this rotation to occur. Thus, the result of "stretching" the B–N bond is an increase in the rotational barrier.

(4)

This is indicated to some extent in the crystallographic results, and in all of the structures except for **1.15**, one of the substituents on nitrogen is positioned between the two chloride ligands. For example, Figure 5 shows that the trimethylsilyl group of **1.13a** resides between the two chlorides and has a distorted B–N–Si angle of 113° (this angle should be 120° for an sp^2 hybridized nitrogen). On the other hand, the Si–N–Si angle in this complex is 122°, reflecting the fact that the trimethylsilyl group prefers to sit between the chlorides in order to avoid unfavorable steric interactions with the other trimethylsilyl group. A similar distortion is observed for **1.14a** where now the smaller ^{t}Bu group resides between the chlorides.

Based on these considerations, the positions of **1.15** and **1.16a** in Figure 10 can be rationalized. As mentioned above, the structural parameters for **1.15** remain highly suspect, and the effect of the poor quality of this structure is reflected here. The error associated with the B–N bond length (1.46(3) Å) spans the entire axis in Figure 10. In all

likelihood the true B–N bond length is approximately 1.49 Å, which is more consistent with that of the Hf dimer **1.19** (1.509(6) Å). This places the position of **1.15** closer to **1.13a**, which is reasonable given that the chelated Li^+ should decrease the B–N interaction and lead to a blue shift of the LMCT band. For **1.16a**, the static structural parameters are not an accurate description of the dynamic situation in solution. As discussed above, the canted orientation of the phenyl groups on the borollide ring "gear" the NMe_2 group slightly out of resonance with the boron. However, in solution, the phenyl groups are rapidly rotating as shown by the equivalence of the ortho and meta protons in the ^1H NMR spectrum.[16] The rapid phenyl group rotation allows the NMe_2 group to rotate freely, as reflected by the low energy of the LMCT band. This result is also consistent with the suggestion that the relatively small methyl substituents do not have substantial steric interactions with the chlorides.

The electronic contributions to the LMCT band have thus far not been considered but are expected to play a role in stabilizing or destabilizing the ligand HOMO and/or metal LUMO. For example, the LMCT bands in decamethylcyclopentadienyl derivatives are red shifted in comparison to the unsubstituted derivatives due to destabilization of the HOMO by inductive effects of the methyl groups.[67] The electronic contribution to the LMCT band in the aminoborollide complexes examined herein should show a similar dependence on the various amino groups bonded to boron. For example, replacing the isopropyl groups of **1.17a** with two trimethylsilyl groups (**1.13a**) should result in a less donating amide, based on the σ^+ function for $CH(CH_3)_2$ ($\sigma^+ = -0.275$) versus $Si(CH_3)_3$ ($\sigma^+ = 0.093$).[73] Inductively, the trimethylsilyl is expected to stabilize the LUMO and lead to a blue shift of the LMCT. Thus, in this particular case, both steric and electronic factors lie

in the same direction. However, the subtle contributions of each effect remain unclear at this time, and it is not clear whether the other complexes show the same behavior.

Conclusions

Neutral aminoborollide zirconium complexes were synthesized containing different substitutents on the borollide nitrogen. The structures of the complexes **1.13a**, **1.14a**, **1.15**, and **1.16a** were determined by x-ray crystallography. The ligand-to-metal charge transfer bands were measured for these complexes. A modest blue shift was observed for λ_{max} as the substituents on nitrogen increase. A lengthening of the B–N bond was also observed and correlates with the shift to higher energy of the LMCT band. In general there is still considerable double bond character between the B and N atoms as determined by the crystallographic parameters.

Experimental

General Considerations: Standard high vacuum line, Schlenk, cannula, and inert atmosphere glove box techniques were employed to handle all air and/or moisture sensitive compounds as previously described.[74] Argon was purified by passage over MnO on vermiculite and activated 4Å sieves. Solvents were dried over Na/ benzophenone ketyl (THF, ether) or titanocene (toluene, pet ether).[75] NMR solvents: benzene-d_6 was dried over $LiAlH_4$ and then over Na metal; THF-d_8 was dried and stored over Na/ benzophenone ketyl. *n*-BuLi (1.6M in hexanes), $LiN[Si(CH_3)_3]_2$, $LiN(i\text{-}Pr)_2$, $(CH_3)_3SiNHC(CH_3)_3$, $(i\text{-}Pr)_2NH$, Et_3N, $Et_2NCH_2CH_2NHEt$, 2,2,6,6-tetramethylpiperidine, BCl_3 (1M in hexanes), $BF_3{\cdot}OEt_2$, $B(NMe_2)_3$, 1,3-butadiene, $ZrCl_4$, and Mg turnings were

all purchased from Aldrich. (*E,E*)-1,4-diphenyl-1,3-butadiene was purchased from Fluka. $Mg(C_2H_6)\cdot(THF)_2$,[76] $Cl_2BN(CH_3)_2$,[77] Cp^*ZrCl_3,[78] and $Cp^*\{\eta^5\text{-}C_4H_4BN(CHMe_2)_2\}ZrCl_2Li(Et_2O)_2$ (**1.17a**)[55] were prepared as previously reported.

^1H NMR and ^{13}C NMR spectra were taken on a General Electric QE300 (300.1 MHz for ^1H; 75.5 MHz for ^{13}C). Elemental analysis was carried out at the elemental analysis facility of the California Institute of Technology by Fenton Harvey on a Hewlett Packard 2400 analyzer. Infrared spectra were recorded on a Perkin–Elmer 1600 Series FTIR. UV-Vis spectra were recorded on a Hewlett-Packard 8452A and a Cary 14 spectrophotometer modified by OLIN using a 1.0 mm path length, air-free cell. X–ray crystallography was carried out on an Enraf-Nonius CAD-4 diffractometer under a cold stream of N_2 gas. Alternatively data was collected on a CCD area detector. Data reduction was done with Bruker SAINT v6.2. All structures were solved by direct methods using SHELXS-97 and refined with SHELXL-97.

$Cl_2BN(Si(CH_3)_3)_2$ (1.1). Under nitrogen in a 1 L 3-necked flask, 200 mL (0.200 mols) of BCl_3 in hexanes was added and cooled to –78 °C. To this was added a solution of 36.81 g (0.220 mol) $LiN[Si(CH_3)_3]_2$ in ~ 200 mL of petroleum ether. A white precipitate was formed immediately and stirring was continued for 15 minutes after addition at –78 °C. The bath was then removed and the reaction was allowed to warm to rt under stirring (8 h). Removal of solvent followed by a short-path vacuum distillation from 50–70 °C afforded 33.1 g (68.3%) of a clear liquid. ^1H NMR (C_6D_6): δ 0.27 (s, 18H, Si*Me*$_3$).

$Cl_2BNC(CH_3)_3Si(CH_3)_3$ (1.2). Under a flow of nitrogen a swivel frit apparatus was fitted with a 500 mL 3-necked flask (with two necks stoppered) on one end and a 250 mL round bottom flask on the other. 156 mL (0.102 mol) of a 0.655 M solution of $LiN(CH_3)_3Si(CH_3)_3$ in petroleum ether was added and cooled to –78 °C. The $LiN(CH_3)_3Si(CH_3)_3$ had been previously generated from 40 mL of $(CH_3)_3SiNHC(CH_3)_3$ in petroleum ether and 144 mL of *n*-BuLi (1.6 M in hexanes) at –20 °C. To this was added via cannula 100 mL (0.100 mol) of BCl_3 in hexanes. Immediately a white precipitate formed. After stirring for 15 min at –78 °C the reaction was allowed to warm to rt and stirred for another 2 h. This was then filtered and the solid on the frit was washed by recycling solvent. Removal of solvent in vacuo followed by a short-path vacuum distillation (60 °C fraction collected) afforded 9.00 g (39.8%) of a clear, colorless liquid. ^{1}H NMR (C_6D_6): δ 1.27 (s, 9H, $C(CH_3)_3$), 0.27 (s, 9H, $Si(CH_3)_3$).

$F_2BN(Et)CH_2CH_2NEt_2$ (1.3). A 500 mL 3-neck flask fitted with an N_2 inlet and two rubber stoppers was cooled to –55 °C and charged with $BF_3{\cdot}OEt_2$ (19.0 mL, 0.150 mol) and 200 mL Et_2O. To this was added via cannula $Li[N(Et)CH_2CH_2NEt_2]$ (22.5 g, 0.150 mol) in 200 mL Et_2O. (The $Li[N(Et)CH_2CH_2NEt_2]$ had been previously prepared from *n*-BuLi and $Et_2NCH_2CH_2NHEt$ in petroleum ether.) The reaction was stirred at –55 °C for 30 min after addition was complete. This was then allowed to warm to rt and stirred for 2 h. At this time a deep, red-brown viscous oil separated from the ethereal layer. Removal of solvent followed by two fractional distillations at 60 °C under full vacuum yielded 8.00 g (38.6%) of a clear colorless liquid. ^{1}H NMR (C_6D_6): δ 3.21 (q, 2H, ^3J = 6.9 Hz, $BNCH_2CH_3$), 2.59 (m, 2H, $BN(Et)CH_2CH_2$), 2.38 (m, 4H, $N(CH_2CH_3)_2$), 2.18 (t, 2H, ^3J =

6.3 Hz, BN(Et)CH_2CH_2), 1.21 (t, 3H, ^3J = 6.9 Hz, $BNCH_2CH_3$), 0.58 (t, 6H, ^3J = 6 Hz, $N(CH_2CH_3)_2$).

$C_4H_6BN(Si(CH_3)_3)_2$ (1.4). In a swivel frit apparatus fitted with a 2-necked flask, 1.66 g (7.46 mmol) of $Mg(C_2H_6)\cdot(THF)_2$ was suspended in 60 mL of Et_2O at –78 °C. To this was added 1.81g (7.46 mmol) of **1.1** via syringe. The reaction was allowed to warm to rt under stirring (2 h). This was filtered and solvent was removed under vacuum. Kugelröhr distillation at 55 °C under high vacuum yielded 0.700 g (41.7%) of a clear, colorless liquid. ^{1}H NMR (C_6D_6): δ 6.14 (s, 2H, $CHCH_2B$), 1.84 (s, 4H, $CHCH_2B$), 0.25 (s, 18H, $SiMe_3$).

$C_4H_6BNC(CH_3)_3Si(CH_3)_3$ (1.5). Synthesized as **1.4** above. In a swivel frit apparatus fitted with a 2-necked flask, 2.62 g (11.8 mmol) of $Mg(C_2H_6)\cdot(THF)_2$ was suspended in 90 mL of Et_2O at –78 °C. To this was added 2.67 g (11.8 mmol) of **1.2** via syringe. The reaction was stirred for 10 min then allowed to warm to rt under stirring (6 h). This was filtered and solvent was removed under vacuum. Kugelröhr distillation between 60–80 °C under high vacuum yielded 1.09 g (43.4%) of a clear, colorless liquid. ^{1}H NMR (C_6D_6): δ 6.10 (s, 2H, $CHCH_2B$), 1.93 (s, 4H, $CHCH_2B$), 1.23 (s, 9H, $C(CH_3)_3$), 0.2 (s, 9H, $Si(CH_3)_3$).

$C_4H_6BN(Et)CH_2CH_2NEt_2$ (1.6). Synthesized as **1.4** above. In a swivel frit apparatus fitted with a 2-necked flask, 2.00 g (8.98 mmol) of $Mg(C_2H_6)\cdot(THF)_2$ was suspended in 50 mL of Et_2O at –78 °C. To this was added 1.73 g (8.98 mmol) of **1.3** via syringe. The

reaction was stirred for 15 min then allowed to warm to rt under stirring overnight. This was filtered and solvent was removed under vacuum. Kugelröhr distillation between 60–80 °C under high vacuum yielded 1.09 g (43.4%) of a clear, colorless liquid. ^{1}H NMR (C_6D_6): δ 6.01 (s, 2H, C*H*CH_2B), 2.90 (t, 2H, ^3J = 6.3 Hz, BN(Et)C*H*$_2$$CH_3$), 2.82 (q, 2H, ^3J = 6.9 Hz, BNC*H*$_2$$CH_3$), 2.50 (m overlapping, 6H, BN(Et)CH_2C*H*$_2$, N(C*H*$_2$$CH_3$)$_2$), 1.62 (s, 4H, CHC*H*$_2$B), 0.83 (q, ^3J = 6.9 Hz, BNCH$_2$C*H*$_3$, N(CH$_2$C*H*$_3$)$_2$).

Mg(1,4-Ph$_2$C$_4$H$_4$)(THF)$_3$. This was prepared by a modification of the procedure by Nakamura and coworkers.[79] To a 500 mL 3-necked flask fitted with a condenser, an N_2 inlet adapter, and a septum, 12.0 g (494 mmol) Mg turnings were charged under an argon flush. THF (50 mL) was syringed in, followed by one crystal of I_2. 0.5 mL (5.08 mmol) 1,2-dibromoethane was then added via syringe and the red iodine color dissipated. The mixture was stirred till all the bubbling stopped. The clear THF solution was then cannula transfered away and fresh THF (100 mL) was added by syringe. This was followed by the addition of 11.0 g (53.3 mmol) (*E*, *E*)-1,4-diphenyl-1,3-butadiene dissolved in 50 mL of THF. Another 0.5 mL of 1,2-dibromoethane was added under vigorous stirring. After 30 minutes the color of the solution turned deep red. After stirring for 7 h at rt, an orange precipitate formed. The precipitate was cannula transferred away from the Mg onto a filter frit and washed once with THF (~ 10 mL). Drying under vacuum afforded 18.0 g (78.3%) of the tris THF adduct. This was used without further characterization.

2,5-$Ph_2C_4H_4BNMe_2$ (1.7). Prepared based on the method reported by Herberich.[64] 4.50 g (10.1 mmol) of $Mg(1,4\text{-}Ph_2C_4H_4)(THF)_3$ was suspended in 175 mL Et_2O at –78 °C. Next 1.27 g (10.1 mmol) Cl_2BNMe_2 was syringed onto the suspension. After addition the reaction was allowed to warm to rt and stirred for 24 h. At this point the solution was clear yellow with a precipitate that was slightly orange in color. The solution was filtered to yield a clear yellow solution. Removal of volatiles under vacuo afforded a yellow oil. This was Kugelröhr distilled at 180 °C under high vacuum (< 10^{-3} torr) to yield 1.00 g (38%) of a clear oil from which a white solid precipitated out upon standing suspended in a clear liquid. *cis: trans* = 2:1. ^{1}H NMR data is as reported.

$Li_2[C_4H_4BN(Si(CH_3)_3)_2](THF)$ (1.9). In a 50 mL Schlenk tube, a pre-cooled (–78 °C) solution of LDA (0.330 g, 3.1 mmol) dissolved in THF (40 mL) was cannula transferred to a –50 °C solution of **1.4** (0.349 g, 1.55 mmol) in petroleum ether (10 mL) in another 50 mL Schlenk tube. This was stirred for 3 h at –50 °C. The reaction was allowed to warm to rt and stirred for 30 min. The initially clear solution turned darker yellow as the solution warmed to rt. Additionally the Teflon coated stir bar was completely blackened. Solvent was quickly removed under vacuum and petroleum ether was added where an off white precipitate formed. This was cooled to –78 °C and the white flocculent precipitate was allowed to settle before the solvent was decanted via cannula. The solid was dried under vacuum to yield 223 mg (46.6%) of a sticky off white solid. ^{1}H NMR in C_6D_6 is consistent with 1 equivalent of THF coordinated. ^{1}H NMR (C_6D_6): δ 6.04 (br m, 2H, C*H*CHB), 4.83 (br m, 2H, CHC*H*B), 3.16 (br m, 4H, CH_2CH_2O), 1.08 (br m, 4H, CH_2CH_2O), 0.606 (s, 18H, $SiMe_3$).

Cp*{η^5-C$_4$H$_4$BN(Si(CH$_3$)$_3$)$_2$}ZrCl·LiCl (1.13). 223 mg (0.721 mmol) of **1.9** and 235 mg (0.707 mmol) of Cp*ZrCl$_3$ were charged into a swivel frit apparatus. Toluene (~ 25 mL) was then condensed in at –78 °C and stirred overnight as it warmed to rt. At this point the color of the solution had turned dark green. Removal of all volatiles afforded a maroon solid. Next Et$_2$O (~ 30mL) was condensed in at –78 °C, then stirred as the reaction warmed to rt. A deep blue solution formed as LiCl precipitated from solution. This was filtered and all volatiles were removed under vacuum to yield a yellow foam. Petroleum ether was then condensed in to give a clear reddish solution and a red-pink solid. Filtration of the red-pink solid and drying under vacuum afforded the solvent free complex (determined by ^{1}H NMR). This was then dissolved in THF to give a red/purple solution. Removal of THF under vacuum yielded a red-purple oil. Benzene (~ 30 mL) was condensed in and the resulting blue solution was carefully frozen. Lyophilization at rt overnight under dynamic vacuum afforded a rust-colored solid of which 56.2 mg (12.6%) was isolated. One equivalent of coordinated THF was determined from ^{1}H NMR in THF-d_8. ^{1}H NMR (THF-d_8): δ 5.13 (br m, 2H, C*H*CHB), 3.79 (br m, 2H, CHC*H*B), 3.62 (br m, 4H, CH$_2$C*H*$_2$O), 1.89 (s, 15H, Cp*Me*$_5$), 1.78 (m, 4H, C*H*$_2$CH$_2$O), 0.161 (s, 18H, Si*Me*$_3$). ^{13}C{^{1}H} NMR (THF-d_8): δ 118.03 (*C*HCHB), 116.77 (*C*$_5$Me$_5$), 99.34 (br, CH*C*HB), 68.23 (CH$_2$*C*H$_2$O), 26.44 (*C*H$_2$CH$_2$O), 12.62 (C$_5$*Me*$_5$), 6.07 (SiC(*C*H$_3$)$_3$). UV–vis (toluene) λ_{max}, nm (ε, M^{-1} cm^{-1}): 326 (2614), 398 (sh, 1197), 510 (398); (THF) λ_{max}, (ε, M^{-1} cm^{-1}): 320 (3176), 522 (628)

[Cp*{η^5-$C_4H_4BN(Si(CH_3)_3)_2$}$ZrCl_2$][$Li(TMEDA)_2$] (1.13a). A swivel frit apparatus was charged with 56.2 mg (0.273 mmol) of **1.13**. X-ray quality crystals were grown by adding excess TMEDA to a concentrated THF solution layered with petroleum ether at –35 °C. ^{1}H NMR (THF-d_8): δ 5.13 (br m, 2H, C*H*CHB), 3.79 (br m, 2H, CHC*H*B), 3.62 (br m, 4H, CH_2CH_2O), 1.89 (s, 15H, CpMe_5), 1.78 (m, 4H, CH_2CH_2O), 0.161 (s, 18H, SiMe_3). ^{13}C{^{1}H} NMR (THF-d_8): δ 118.03 (*C*HCHB), 116.77 (C_5Me_5), 99.34 (br, CH*C*HB), 68.23 (CH_2CH_2O), 26.44 (CH_2CH_2O), 12.62 (C_5Me_5), 6.07 ($SiC(CH_3)_3$) UV–vis (THF) λ_{max}, nm (ε, M^{-1} cm^{-1}): 324 (3521), 520 (896).

Cp*{η^5-$C_4H_4BNC(CH_3)_3Si(CH_3)_3$}$ZrCl$·$LiCl$ (1.14). Synthesized as **1.13** above. A solution of **1.5** (0.627 g, 3.00 mmol) in petroleum ether (20 mL) was added dropwise with stirring to a –78 °C solution of LDA (0.644 g, 6.01 mmol) in THF (30 mL) in a 50 mL Schlenk tube. The color of the solution was clear yellow at this point. After 15 min the –78 °C bath was removed and the mixture was allowed to warm to rt. This was stirred for 3 h after which all volatiles were removed under vacuum. To this residue was added 0.983 g (2.95 mmol) Cp*$ZrCl_3$, and the Schlenk tube was fitted to a swivel frit assembly. Toluene (~ 30 mL) was condensed onto the mixture at –78 °C and was stirred for 15 min. At this point the color of the reaction was dark green. A small amount of THF (~ 1 mL) was vac transferred onto this to yield a clear blue solution. This was stirred overnight at rt. This was filtered and all volatiles were removed under vacuum. Petroleum ether was condensed onto the mixture producing a purple solid that was filtered and washed by solvent recycle in the frit. In a new swivel frit assembly the purple solid was extracted with Et_2O. All volatiles were removed to yield a purple foam.

This foam was washed with petroleum ether (2 x 50 mL) and dried under vacuum to yield 0.545 g (35.3%) of a purple solid. ^{1}H NMR in THF-d_8 is consistent with no THF solvent molecules coordinated. ^{1}H NMR (THF-d_8): δ 5.21 (m, 2H, C*H*CHB), 3.80 (s, 2H, CHC*H*B), 1.93 (s, 15H, Cp*Me*$_5$), 1.39 (s, 9H, C(CH$_3$)$_3$), 0.292 (s, 9H, Si(CH$_3$)$_3$).

[Cp*{η^5-C$_4$H$_4$BNC(CH$_3$)$_3$Si(CH$_3$)$_3$}ZrCl$_2$][Li(TMEDA)$_2$] (1.14a). A swivel frit apparatus was charged with 140 mg (0.273 mmol) of **1.14**. 1 mL of TMEDA was condensed onto the solid, which did not dissolve. Next, just enough THF was condensed in to dissolve everything. Petroleum ether was then added and filtered to yield 62.1 mg (30%) of a light purple solid. X-ray quality crystals were grown from a concentrated THF solution layered with petroleum ether at –35 °C. ^{1}H NMR (THF-d_8): δ 5.21 (m, 2H, C*H*CHB), 3.80 (s, 2H, CHC*H*B), 2.30 (s, 8H, Me$_2$NC*H*$_2$), 2.15 (s, 12H, *Me*$_2$NCH$_2$), 1.93 (s, 15H, Cp*Me*$_5$), 1.39 (s, 9H, C(CH$_3$)$_3$), 0.292 (s, 9H, Si(CH$_3$)$_3$). ^{13}C{^{1}H} NMR (THF-d_8): 116.16 (*C*HCHB), 115.90 (*C*$_5$Me$_5$), 99.65 (br, CHCHB), 57.08 (Me$_2$NCH$_2$) 52.80 (*C*(CH$_3$)$_3$), 44.39 (*Me*$_2$NCH$_2$), 32.92 ((C(*C*H$_3$)$_3$), 10.75 (C$_5$*Me*$_5$), 6.72 (Si(*C*H$_3$)$_3$). UV–vis (toluene) λ_{max}, nm (ε, M^{-1} cm^{-1}): 294 (sh, 4647), 366 (2736), 608 (984); (THF) λ_{max}, nm (ε, M^{-1} cm^{-1}): 282 (7016.8), 342 (3470), 544 (800).

[Cp*{η^5-C$_4$H$_4$BN(Et)CH$_2$CH$_2$NEt$_2$}ZrCl$_2$Li]$_2$ (1.15) Synthesized as **1.13** above. A solution of **1.6** (0.300 g, 1.44 mmol) in petroleum ether (20 mL) was added dropwise with stirring to a –78 °C solution of LiTMP (0.423 g, 2.88 mmol) in THF (20 mL) in a 50 mL Schlenk tube. The color of the solution was clear yellow at this point. After 15 minutes the –78 °C bath was removed and the mixture was allowed to warm to rt. This

was stirred for 4 h after which all volatiles were removed under vacuum. To this residue was added 0.479 g (1.44 mmol) Cp*$ZrCl_3$, and the Schlenk tube was fitted to a swivel frit assembly. Toluene (~ 30 mL) was condensed onto the mixture at –78 °C and was stirred for 15 min, then stirred overnight at rt. At this point the color of the reaction was dark red-purple. This was then filtered and all volatiles were removed under vacuum. Petroleum ether was condensed onto the mixture producing a red-violet solid that was filtered and washed by solvent recycle in the frit. Drying under vacuum afforded 248 mg (33.7%) of a red-violet solid. X-ray quality crystals were grown from a concentrated THF solution layered with petroleum ether at –35 °C. ^{1}H NMR (THF-d_8): δ 5.34 (m, 2H, C*H*CHB), 4.05 (br, 2H, CHC*H*B), 3.08 (br, 2H, BNCH_2CH$_3$), 2.93 (t, 2H, ^3J = 6.3 Hz, BN(Et)CH_2CH$_2$), 2.67 (q, 4H, ^3J = 6.9 N(CH_2CH$_3$)$_2$), 2.60 (t, ^3J = 6.3 Hz, BN(Et)CH$_2$CH_2), 1.89 (s, 15H, C$_5$*Me*$_5$), 1.02 (t, 6H, ^3J = 6.9, N(CH$_2$CH_3)$_2$), 0.93 (t, 3H, ^3J = 6.9 Hz, BNCH$_2$CH_3). ^{13}C{^{1}H} NMR (THF-d_8): δ 119.61 (*C*HCHB), 118.93 (*C*$_5$Me$_5$), 97.37 (br, CH*C*HB), 53.40 (BN*C*H$_2$CH$_3$), 48.03 (BN(Et)*C*H$_2$CH$_2$), 46.50 (BN(Et)CH$_2$*C*H$_2$), 46.11 (N(*C*H$_2$CH$_3$)$_2$), 12.90 (BNCH$_2$*C*H$_3$), 12.49 (N(CH$_2$*C*H$_3$)$_2$), 10.38 (C$_5$*Me*$_5$). UV–vis (toluene) λ_{max}, nm (ε, M^{-1} cm^{-1}): 336 (2539), 582 (696); (THF) λ_{max}, nm (ε, M^{-1} cm^{-1}): 278 (7282), 324 (3856), 520 (862).

Cp*{η^5-2,5-Ph$_2$C$_4$H$_2$BNMe$_2$}ZrCl·LiCl (1.16). A solution of **1.7** (0.710 g, 2.72 mmol) in petroleum ether (20 mL) was added dropwise with stirring to a –78 °C solution of LDA (0.582 g, 5.43 mmol) in THF (20 mL) in a 50 mL Schlenk tube. The color of the solution was clear yellow at this point. After 15 minutes the –78 °C bath was removed and the mixture was allowed to warm to rt. The color of the solution slowly turned deep

red. This was stirred for overnight, after which all volatiles were removed under vacuum. To this residue was added 0.905 g (2.72 mmol) Cp*$ZrCl_3$, and the Schlenk tube was fitted to a swivel frit assembly. Toluene (~ 30 mL) was condensed onto the mixture at –78 °C and was stirred for 15 min. The reaction was then allowed to warm to rt and stirred for an additional 4 h. A fine white precipitate formed which could not be filtered away. All volatiles were removed under vacuum and fresh THF (~ 10 mL) was condensed in and stirred until a clear deep purple solution formed. THF was then removed under vacuum to yield a blue oil. Toluene (~ 30 mL) was transferred in and stirred at rt to yield a purple solution and a white precipitate. This was filtered followed by removal of all volatiles yielding a blue-purple foam. This foam was washed with petroleum ether (2x 50 mL) and dried under vacuum to yield 0.821 g (43%) of a green solid. ^{1}H NMR in THF-d_8 is consistent with no THF solvent molecules coordinated. ^{1}H NMR (THF-d_8): δ 7.39 (d, 4H, J = 8.4 Hz, *o*-H), 7.02 (t, J = 7.5 Hz, *m*-H), 6.78 (t, 2H, J = 7.5, *p*-H), 5.35 (s, 2H, C*H*CPhB), 2.73 (s, 6H, NMe_2), 1.76 (s, 15H, CpMe_5).

Cp*{η^5-2,5-$Ph_2C_4H_2$BNMe_2}ZrCl·LiCl(THF)$_4$ (1.16a). A swivel frit apparatus charged with 100 mg of **1.16** was dissolved in the minimum amount of THF possible. Petroleum ether was then added to precipitate a dark green-blue solid. ^{1}H NMR in THF-d_8 is consistent with 1.5 equivalents of THF coordinated. Dark green, x-ray quality crystals were obtained from layering a concentrated THF solution with petroleum ether and cooling to –35 °C for a week. Crystals obtained in this manner were of the *tetrakis*-THF solvate. ^{1}H NMR (THF-d_8): δ 7.39 (d, 4H, ^3J = 8.4 Hz, *o*-H), 7.02 (t, ^3J = 7.5 Hz, *m*-H), 6.78 (t, 2H, ^3J = 7.5, *p*-H), 5.35 (s, 2H, C*H*CPhB), 3.67 (m, 6H, CH_2CH_2O), 2.73 (s, 6H,

N*Me*$_2$), 1.83 (m, 6H, C*H*$_2$CH$_2$O), 1.76 (s, 15H, Cp*Me*$_5$). ^{13}C{^{1}H} NMR (C_6D_6): δ 146.49 (*C*HCPhB), 130.79 (*o-C*), 127.60 (*m-C*), 123.54 (*p-C*), 121.48 (*ipso-C*), 116.59 (*C*$_5$Me$_5$), 68.07 (*C*H$_2$*C*H$_2$O), 25.16 (*C*H$_2$CH$_2$O), 44.64 (N*Me*$_2$), 12.09 (C$_5$*Me*$_5$). UV–vis (toluene) λ_{max}, nm (ε, M^{-1} cm^{-1}): 374 (sh, 3904), 450 (sh, 1262), 556 (627); (THF) λ_{max}, nm (ε, M^{-1} cm^{-1}): 340 (11,789), 608 (1961).

References and Notes

1. Morse, P. M. *Chem. Eng. News* **1998**, 76 (Dec 11), 25.
2. Schut, J. H. *Plastics World* **1997**, (April), 27.
3. Rotman, D. *Chem. Week* **1996**, 158 (36), 37.
4. Thayer, A. N. *Chem. Eng. News* **1995**, 73 (Sept 11), 15.
5. Ittel, S. D.; Johnson, L. K.; Brookhart, M. *Chem. Rev.* **2000**, *100*, 1169.
6. Fink, G.; Steinmetz, B.; Joachim, Z.; Przybyla, C.; Tesche, B. *Chem. Rev.* **2000**, *100*, 1377.
7. Horton, A. D. *Trends Polym. Sci.* **1994**, *2*, 158.
8. Baker, J. *Europ. Chem. News* **1993**, (Oct 18), 22.
9. Chowdhury, J.; Moore, S. *Chem. Eng. News* **1993**, 71 (April), 34.
10. Sinn, H.; Kaminsky, W. *Adv. Organomet. Chem.* **1980**, *18*, 99.
11. Sinn, H.; Kaminsky, W.; Vollmer, H. J.; Woldt, R. *Angew. Chem.* **1980**, *92*, 396.
12. Alt, H. G.; Koeppl, A. *Chem. Rev.* **2000**, *100*, 1205.
13. Coates, G. W. *Chem. Rev.* **2000**, *1000*, 1223.
14. Angermund, K.; Fink, G.; Jensen, V. R.; Kleinschmidt, R. *Chem. Rev.* **2000**, *100*, 1457.

15. Kaminsky, W.; Scholz, V.; Werner, R. *Macromol. Symp.* **2000**, *159*, 9.

16. For some older reviews see: (a) Alt, H. G.; Samuel, E. *Chem. Soc. Rev.* **1998**, *27*, 323. (b) Kaminsky, W.; Sinn, H., Eds. *Transition Metals and Organometallics as Catalysts for Olefin Polymerization*; Springer-Verlag: Berlin, 1988. (c) Moehring, P. C.; Coville, N. J. *J. Organomet. Chem.* **1994**, *479*, 1. (d) Brintzinger, H. H.; Fischer, D.; Muelhaupt, R.; Rieger, B.; Waymouth, R. M. *Angew. Chem., Int. Ed. Engl.* **1995**, *34*, 1143. (e) Bochmann, M. *J. Chem. Soc., Dalton Trans.* **1996**, 255. (f) Janiak, C. In *Metallocenes*; Togni, A., Halterman, R. L., Eds.; Wiley-VCH: New york, 1998; Vol. 2. (g) Fink, G.; Mülhaupt, R.; Brintzinger, H. H., Eds. *Ziegler Catalysts*; Springer-Verlag: Berlin, 1995.

17. Jordan, R. F. *Adv. Organomet. Chem.* **1991**, *32*, 325.

18. Yang, X.; Stern, C. L.; Marks, T. J. *J. Am. Chem. Soc.* **1991**, *113*, 3623.

19. Hlatky, G. G.; Turner, H. W.; Weckman, R. R. *J. Am. Chem. Soc.* **1989**, *111*, 2798.

20. Watson, P. L.; Parshall, G. W. *Acc. Chem. Res.* **1985**, *18*, 51.

21. Watson, P. L. *J. Am. Chem. Soc.* **1982**, *104*, 337.

22. Burger, B. J.; Bercaw, J. E. *Abstr. Pap. Am. Chem. Soc.* **1987**, *193*, 23.

23. Parkin, G.; Bunel, E.; Burger, B. J.; Trimmer, M. S.; Vanasselt, A.; Bercaw, J. E. *J. Mol. Catal.* **1987**, *41*, 21.

24. Thompson, M. E.; Baxter, S. M.; Bulls, A. R.; Burger, B. J.; Nolan, M. C.; Santarsiero, B. D.; Schaefer, W. P.; Bercaw, J. E. *J. Am. Chem. Soc.* **1987**, *109*, 203.

25. Gilchrist, J. H.; Bercaw, J. E. *J. Am. Chem. Soc.* **1996**, *118*, 12021.

26. Grubbs, R. H.; Coates, G. W. *Acc. Chem. Res.* **1996**, *29*, 85.

27. Shapiro, P. J.; Cotter, W. D.; Schaefer, W. P.; Labinger, J. A.; Bercaw, J. E. *J. Am. Chem. Soc.* **1994**, *116*, 4623.

28. Shapiro, P. J.; Bercaw, J. E. *Abstr. Pap. Am. Chem. Soc.* **1990**, *199*, 381.

29. Coughlin, E. B.; Bercaw, J. E. *J. Am. Chem. Soc.* **1992**, *114*, 7606.

30. Coughlin, E. B., Ph.D. Thesis, California Institute of Technology, **1994**.

31. Hawthorne, M. F. *Acc. Chem. Res.* **1968**, *1*, 281.

32. Hawthorne, M. F.; Young, D. C.; Wagner, P. A. *J. Am. Chem. Soc.* **1965**, 1818.

33. Strauss, S. H. *Chem. Rev.* **1993**, *93*, 927.

34. Grimes, R. N. In *Comprehensive Organometallic Chemsitry II*; Wilkinson, G., Stone, F. G. A., Abel, E. W., Eds.; Pergamon Press: Oxford, U.K., 1995; Vol. 1, Chapter 9.

35. Saxena, A. K.; Hosmane, N. S. *Chem. Rev.* **1993**, *93*, 1081.

36. Todd, L. J. In *Comprehensive Organometallic Chemsitry II*; Wilkinson, G., Stone, F. G. A., Abel, E. W., Eds.; Pergamon Press: Oxford, U.K., 1995; Vol. 1, Chapter 7.

37. Crowther, D. J.; Swenson, D. C.; Jordan, R. F. *J. Am. Chem. Soc.* **1995**, *117*, 10403.

38. Crowther, D. J.; Baenziger, N. C.; Jordan, R. F. *J. Am. Chem. Soc.* **1991**, *113*, 1455.

39. Yoshida, M.; Crowther, D. J.; Jordan, R. F. *Organometallics* **1997**, *16*, 1349.

40. Yoshida, M.; Jordan, R. F. *Organometallics* **1997**, *16*, 4508.

41. Bei, X. H.; Young, V. G.; Jordan, R. F. *Organometallics* **2001**, *20*, 355.

42. Kreuder, C.; Jordan, R. F.; Zhang, H. M. *Organometallics* **1995**, *14*, 2993.

43. Grimes, R. N. *Coord. Chem. Rev.* **2000**, *200*, 773.

44. Grimes, R. N. *J. Organomet. Chem.* **1999**, *581*, 1.

45. Boring, E.; Sabat, M.; Finn, M. G.; Grimes, R. N. *Organometallics* **1998**, *17*, 3865.

46. Boring, E.; Sabat, M.; Finn, M. G.; Grimes, R. N. *Organometallics* **1997**, *16*, 3993.

47. Dodge, T.; Curtis, M. A.; Russell, J. M.; Sabat, M.; Finn, M. G.; Grimes, R. N. *J. Am. Chem. Soc.* **2000**, *122*, 10573.

48. Mao, S. S. H.; Tilley, T. D.; Rheingold, A. L.; Hosmane, N. S. *J. Organomet. Chem.* **1997**, *533*, 257.

49. Rodriguez, G.; Sperry, C. K.; Bazan, G. C. *J. Mol. Catal. A-Chem.* **1998**, *128*, 5.

50. Rodriguez, G.; Bazan, G. C. *J. Am. Chem. Soc.* **1997**, *119*, 343.

51. Bazan, G. C.; Rodriguez, G.; Cleary, B. P. *J. Am. Chem. Soc.* **1994**, *116*, 2177.

52. Mayer, J. M.; Curtis, C. J.; Bercaw, J. E. *J. Am. Chem. Soc.* **1983**, *105*, 2651.

53. Kiely, A. F., Ph.D. Thesis, California Institute of Technology, **1997**.

54. Quan, R. W., Ph.D. Thesis, California Institute of Technology, **1994**.

55. Quan, R. W.; Bazan, G. C.; Kiely, A. F.; Schaefer, W. P.; Bercaw, J. E. *J. Am. Chem. Soc.* **1994**, *116*, 4489.

56. Nelson, C. M., M.S. Thesis, California Institute of Technology, **1996**.

57. Pastor, A.; Kiely, A. F.; Henling, L. M.; Day, M. W.; Bercaw, J. E. *J. Organomet. Chem.* **1997**, *528(1-2)*, 65.

58. Sperry, C. K.; Bazan, G. C.; Cotter, W. D. *J. Am. Chem. Soc.* **1999**, *121*, 1513.

59. Sperry, C. K.; Cotter, W. D.; Lee, R. A.; Lachicotte, R. J.; Bazan, G. C. *J. Am. Chem. Soc.* **1998**, *120*, 7791.

60. Herberich, G. E.; Hessner, B.; Ohst, H.; Raap, I. A. *J. Organomet. Chem.* **1988**, *348*, 305.

61. Herberich, G. E.; Boveleth, W.; Hessner, B.; Hostalek, M.; Koeffer, D. P. J.; Ohst, H.; Soehnen, D. *Chem. Ber.* **1986**, *119*, 420.

62. March, J. *Advanced Organic Chemistry: Reactions, Mechanisms, and Structure*; Fourth ed.; John Wiley & Sons: New York, 1992.

63. Alternatively, the corresponding amino boron dichlorides **1.1** and **1.2** can be treated with two equivalents of allyl Grignard and subsequently ring-closed by metathesis using Grubbs's Ru catalyst to yield **1.4** and **1.5** in high yield.

64. Herberich, G. E.; Wagner, T.; Marx, H.-W. *J. Organomet. Chem.* **1995**, *502*, 67.

65. Herberich has previously prepared and structurally characterized the di-lithio salt **1.7** as its bis-TMEDA adduct in ref . No mention was made of the corresponding dianion of **1.8** or attempts at its synthesis.

66. Kiely, A. F.; Nelson, C. M.; Pastor, A.; Henling, L. M.; Day, M. W.; Bercaw, J. E. *Organometallics* **1998**, *17*, 1324.

67. Lever, A. B. P. *Electronic Spectroscopy of Inorganic Compounds*; 2nd ed.; Elsevier Science: Amsterdam, 1984.

68. Harrigan, R. W.; Hammond, G. S.; Gray, H. B. *J. Organomet. Chem.* **1974**, *81*, 79.

69. Vitz, E.; Brubaker, C. H., Jr. *J. Organomet. Chem.* **1974**, *84*, C16.

70. Vitz, E.; Brubaker, C. H., Jr. *J. Organomet. Chem.* **1976**, *104*, C33.

71. Tsai, Z.; Brubaker, C. H., Jr. *J. Organomet. Chem.* **1979**, *166*, 199.

72. Heteronuclear NMR such as ^{15}N and ^{6}Li as well as conductivity experiments could potentially help to sort out these issues, but unfortunately have not been done at this point.

73. Gordon, A. J.; Ford, R. A. *The Chemist's Companion*; John Wiley & Sons: New York, 1972.

74. Burger, B. J.; Bercaw, J. E. In *Experimental Organometallic Chemistry*; ACS Symposium Series 357; Wayda, A. L., Darensbourg, M. Y., Eds.; American Chemical Society: Washington, DC, 1987; pp 79-99.

75. Marvich, R. H.; Brintzinger, H. H. *J. Am. Chem. Soc.* **1971**, *93*, 2046.

76. Fujita, K.; Ohnuma, Y.; Yasuda, H.; Tani, H. *J. Organomet. Chem.* **1976**, *113*, 201.

77. Banister, A. J.; Greenwood, N. N.; Straughan, B. P.; Walker, J. *J. Chem. Soc.* **1964**, 995.

78. Lund, E. C.; Livinghouse, T. *Organometallics* **1990**, *9*, 2426.

79. Yasuda, H.; Kajihara, Y.; Mashima, K.; Nagasuna, K.; Lee, K.; Nakamura, A. *Organometallics* **1982**, *1*, 388.

Chapter 2

Possible Intermediates in a Catalytic Cycle for the Oxidation of Ethylene to Ethylene Glycol Based on the Shilov System

Abstract

Studies directed towards the development of a Pt(II)-catalyzed oxidation of ethylene to ethylene glycol based on the Shilov system for alkane functionalization is described. The first step is the activation of ethylene towards nucleophilic attack by water to generate a Pt(II) β-hydroxyalkyl. Oxidation of this intermediate in a second step affords a Pt(IV) β-hydroxyalkyl. In a third step reductive elimination via an S_N2-type nuclephilic attack at the α-C of the Pt(IV) β-hydroxyalkyl by water liberates the oxidized product leaving the reduced Pt(II) center to bind another equivalent of olefin. The first system examined was the methyl ethylene complex [(tmeda)PtMe(η^2-C_2H_4)][SbF_6] **2.2**. Even though it is cationic in nature, nucleophilic attack at the bound ethylene was not observed. Instead attack at the metal followed by displacement of ethylene occurred. The bound ethylene in the neutral complexes *cis*-$Cl_2PtL(\eta^2$-$C_2H_4)$, (L = PPh_3 (**2.23**), $AsPh_3$ (**2.24**), Me_2SO (**2.25**)) and *trans*-$Cl_2Pt(\eta^2$-$C_2H_4)(C_5H_5N)$ (**2.26**) are susceptible towards attack by OH^-. Under catalytic conditions (excess ethylene and H_2O_2) decomposition of **2.23**, **2.24**, and **2.25** was observed. With **2.26**, one turnover was observed of oxidized product, before decomposition occurred. The bound ethylene in the complex [(tmeda)PtCl(η^2-C_2H_4)][ClO_4] (**2.32**) is activated towards nucleophilic attack by water and OH^-, allowing the isolation of the Pt(II) β-hydroxyalkyl. This is rapidly oxidized to the Pt(IV) β-hydroxyalkyl by hydrogen peroxide. In the presence of HCl, it undergoes reductive elimination to yield 2-chloroethanol and (tmeda)$PtCl_2$. Unfortunately, this system also showed no catalytic activity.

Introduction

The direct and selective oxidation of simple alkanes presents a formidable challenge for organic and organometallic chemists. Despite considerable current research effort in the area, a general solution to this problem remains elusive.[1-3] The main obstacle does not involve the oxidation itself (which is generally thermodynamically favorable), but rather the control of its regio- and chemoselectivity.[2] The classic organic approach to alkane oxidation involves hydrogen atom abstraction from C–H bonds by HO· or RO· radicals. The regioselectivity of these reactions is directly related to the strength of the C–H bond in the substrate. As the C–H bond strength increases in the order *tertiary* < *secondary* < *primary* C–H, the relative reactivity towards H–atom abstraction by HO· or RO· radicals will be *tertiary* > *secondary* > *primary* C–H > methane. Chemoselectivity in these systems results from the decreased strength of C–H bonds that are directly attached to or adjacent to a more electronegative element. Thus, C–H bonds on partially oxidized carbon centers undergo faster H–atom abstraction than those on non-oxidized centers, resulting in an erosion of chemoselectivity as the reaction progresses. Alkanes can also undergo oxidation via H–anion abstraction by superacid electrophiles. These reactions produce the corresponding carbocations, and their regioselectivity is controlled by carbocation stability. This results in similar selectivity to radical reactions, because the stability of carbocations follows the relative ordering *tertiary* carbocation > *secondary* carbocation > *primary* carbocation > CH_3^+.

Transition metal reagents that do not operate by H· or H^- abstraction mechanisms may offer a solution to the problems of selectivity. Numerous transition metal mediated C–H bond activation reactions exhibit the regioselectivity pattern of *primary* C–H bonds

> *secondary* C–H bonds > *tertiary* C–H bonds. However, to date, only a few of these systems have proven capable of further functionalizing the alkane in a catalytic fashion. The Shilov system is a rare example of a transition metal-based alkane oxidation catalyst.[1,4,5] The catalytically active species in the Shilov system is the Pt(II) *bis*-aqua adduct $(Cl)_2Pt(OH_2)_2$ (derived from hydrolysis of $[PtCl_4]^{2-}$), and this complex catalyzes the oxidation of simple alkanes (*e.g.*, CH_3CH_3) to alcohols (*e.g.*, $HOCH_2CH_2OH$). The Pt(II) catalyst shows a number of remarkable features, including complete stability towards air and moisture as well as a preference for C–H bonds in the order *primary* > *secondary* >> *tertiary*. The mechanism of the Shilov reaction has been studied extensively, and the overall catalytic cycle is summarized in Scheme 1.[6] The first step of the cycle (which determines both the rate and selectivity of the overall reaction) involves the reversible C–H activation of an alkane by $(Cl)_2Pt(OH_2)_2$ to generate an alkylplatinum(II) intermediate and H^+. In the second step, this highly reactive platinum(II) alkyl species is oxidized by $[PtCl_6]^{2-}$ to generate an alkylplatinum(IV) adduct. Importantly, labeling studies have shown that the oxidation proceeds by electron transfer rather than alkyl transfer, suggesting that a more practical oxidant could potentially be substituted for $[PtCl_6]^{2-}$ in this reaction. In the final, product releasing step of the catalytic cycle, the alkyl Pt(IV) species undergoes reductive elimination of the oxidized alkane product (ROH or RCl) via an S_N2-type mechanism.

Scheme 1

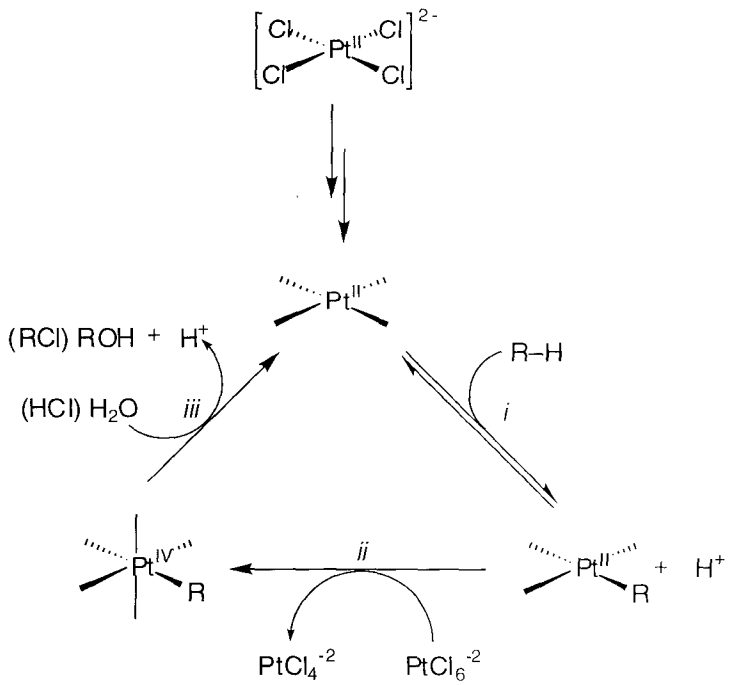

Net:

$$PtCl_6^{2-} + R\text{–}H + H_2O(Cl^-) \xrightarrow[120\ ^\circ C]{\text{cat. } PtCl_4^{2-}} R\text{–}OH(Cl) + PtCl_4^{2-} + 2\ HCl$$

The Shilov system exhibits excellent chemoselectivity because the initial oxidized products are generally stable towards further oxidation. For example, in a detailed study of ethane and ethanol oxidation, it was demonstrated that ethanol could be selectively oxidized to ethylene glycol and 2-chloroethanol in preference to acetaldehyde. Furthermore, the relative rates of C–H activation were H–CH_2CH_3 > H–CH_2CH_2OH > H–$CH(OH)CH_3$.[7-10] Importantly, appreciable amounts of a Pt(II) olefin complex, $[Cl_3Pt(\eta^2\text{-}C_2H_4)]^-$, were observed in solution during these studies, and it was later demonstrated that this complex was a kinetically viable intermediate in the oxidation of ethanol to ethylene glycol and 2-chloroethanol.[8,11,12]

Based on this precedent and on the propensity of Pt(II) to coordinate ethylene, we set out to demonstrate the catalytic oxidation of ethylene to ethylene glycol/2-

chloroethanol by Pt(II) complexes. A potential catalytic cycle for this reaction is outlined in Scheme 2. In a first step (i), the η^2-coordinated ethylene in complex **A** undergoes nucleophilic attack by water to generate a β-hydroxyalkyl Pt(II) complex (**B**) and H^+. Next, **B** is oxidized (in this case by hydrogen peroxide) to produce the corresponding Pt(IV) β-hydroxyalkyl adduct, **C** (step ii). Notably, a wide variety of oxidants including $PtCl_6^{2-}$, H_2O_2 and, ultimately, O_2 could potentially be used in this reaction. By analogy to the Shilov system, the α-carbon of **C** is expected to be susceptible to S_N2-type attack by water or chloride. In step iii, nucleophilic attack liberates ethylene glycol or 2-chloroethanol and the Pt(II) complex **D**. In a final step, an X-type ligand of **D** (in this case hydroxide) undergoes protonation followed by ligand substitution with ethylene to regenerate **A** and complete the catalytic cycle.

Scheme 2

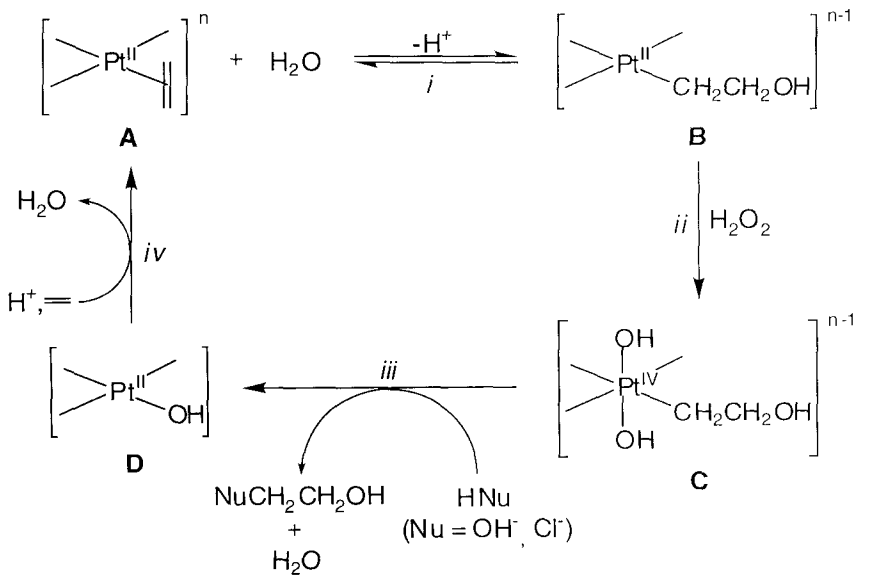

Results

Synthesis and Characterization of the Cationic Ethylene Complex [(tmeda)PtMe(η^2-C_2H_4)][SbF_6] (tmeda = N,N,N'N'-tetramethylethylenediamine) 2.2.

At the outset of this project, we set out to prepare the cationic ethylene complex [(tmeda)PtMe(η^2-C_2H_4)]$^+$, **2.2**. This complex was of particular interest because it might permit the use of dioxygen as the oxidant in the catalytic cycle shown in Scheme 2. This possibility was raised when our group reported that the neutral dimethyl complex (tmeda)$PtMe_2$ could be oxidized to the corresponding Pt(IV) hydroxo methoxy adduct with dioxygen in methanol (eq 1).[13]

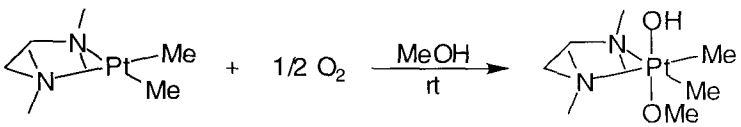

(1)

It was subsequently discovered that only dimethyl or diphenyl Pt(II) complexes were at high enough oxidation potentials to react with dioxygen in protic media.[14] Importantly, in our system, a dialkyl Pt(II) complex would be produced if a nucleophile such as water or hydroxide were to add to the bound olefin of **2.2** to yield the β-hydroxyethyl complex **2.3**. This might then be oxidized with dioxygen to afford the Pt(IV) methyl, β-hydroxyethyl species, **2.4** (eq 2).

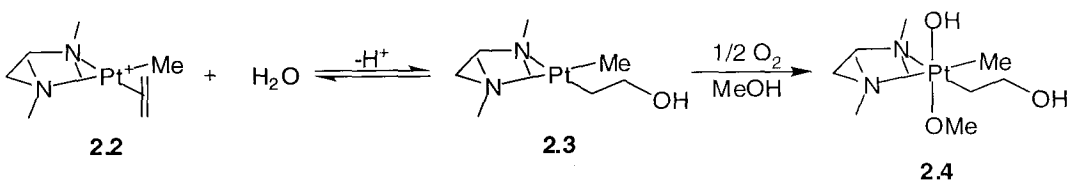

2.2 **2.3** **2.4**

(2)

Treatment of the neutral complex **2.1** with 1 equivalent of $AgSbF_6$ in CH_2Cl_2 under an atmosphere of ethylene afforded complex **2.2** in 88% isolated yield (eq 3).

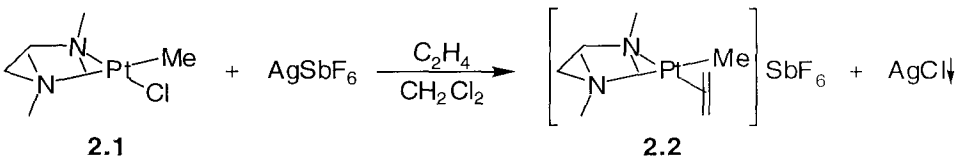

2.1 **2.2** (3)

The ^{1}H NMR spectrum of **2.2** shows a C_s symmetric complex in which the mirror plane lies in the square plane of the molecule. The resonances for the protons of the two NMe_2 groups appear as two singlets, while the diastereotopic methylene groups of the tmeda ligand appear as a pair of multiplets. The NMe_2 group *trans* to the ethylene moiety (δ 2.85 ppm) displays relatively strong coupling to ^{195}Pt ($^{3}J_{PtH}$ = 44.8 Hz), while that of the NMe_2 group *trans* to the Pt–Me group (δ 2.57 ppm) displays much weaker coupling to ^{195}Pt ($^{3}J_{PtH}$ = 14.8 Hz). The observed couplings are consistent with the greater trans influence of methyl compared to ethylene.[15] The methyl ligand of **2.2** appears at δ 0.36 ppm, and shows a $^{2}J_{PtH}$ coupling constant of 70.9 Hz. This value is somewhat low, particularly for a cationic complex, but is consistent with an observed decrease in $^{2}J_{PtH}$ coupling constant with decreasing electron density at platinum in the complexes (tmeda)PtMe(X). For example, the $^{2}J_{PtH}$ coupling constant for the methyl ligand of (tmeda)$PtMe_2$ is 85 Hz while that of (tmeda)PtMeCl is 79 Hz. At room temperature, the ethylene signal appears as a singlet [δ 3.87 ppm with ^{195}Pt satellites ($^{3}J_{PtH}$ = 67.5 Hz)] due to rapid rotation around the Pt–ethylene bond. Low temperature NMR studies to determine the barrier to ethylene rotation have not been carried out, but in related complexes this rotation could not be frozen out down to –80 °C.[16]

Notably, the choice of counteranion was critical to the successful isolation of the [(tmeda)Pt(Me)(η^2-C_2H_4)]$^+$ cation. For example, treating the dimethyl complex (tmeda)$PtMe_2$ with 1 equivalent of $H(Et_2O)_2BAr^F$ (BAr^F = B(3,5-$(CF_3)_2C_6H_3)_4$) at –20 °C

under an atmosphere of ethylene yielded the η^2-ethylene complex **2.5** along with traces of the Et_2O solvate **2.6** (eq 4). However, complex **2.5** was unstable is the absence of excess ethylene. When the atmosphere of ethylene was removed, the complex rapidly liberated the bound olefin and decomposed to a mixture of the chloride bridged platinum dimer, **2.7**, and other unidentified products (eq 5).

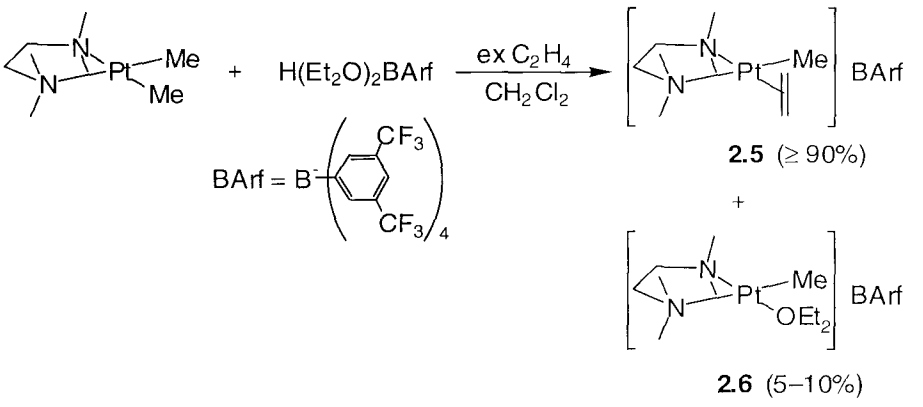

(4)

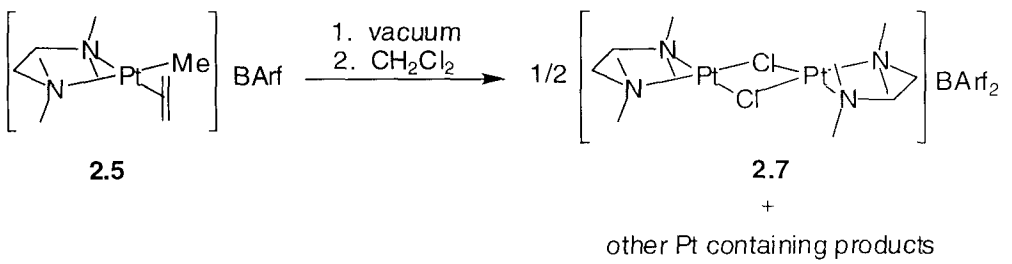

(5)

Treatment of a CH_2Cl_2 solution of **2.1** with $NaBAr^{f}$ under an atmosphere of ethylene for 24 hours at room temperature produced a complex mixture of starting material (**2.1**), η^2-ethylene complex **2.5** (~ 10%) and a methyl containing Pt species (δ 0.78 ppm, $^2J_{PtH}$ = 70 Hz). The latter was obtained in approximately 20% yield, and was tentatively assigned as either the CH_2Cl_2 solvated species **2.8**, or the bridging chloride complex **2.9** (eq 6). Eventually, this new product converted completely to the chloride-bridged dimer **2.7**. Attempts to cleave this dimer under an atmosphere of ethylene were

unsuccessful, even under high pressures of olefin (60 psig) and after long reaction times (>24 hr).

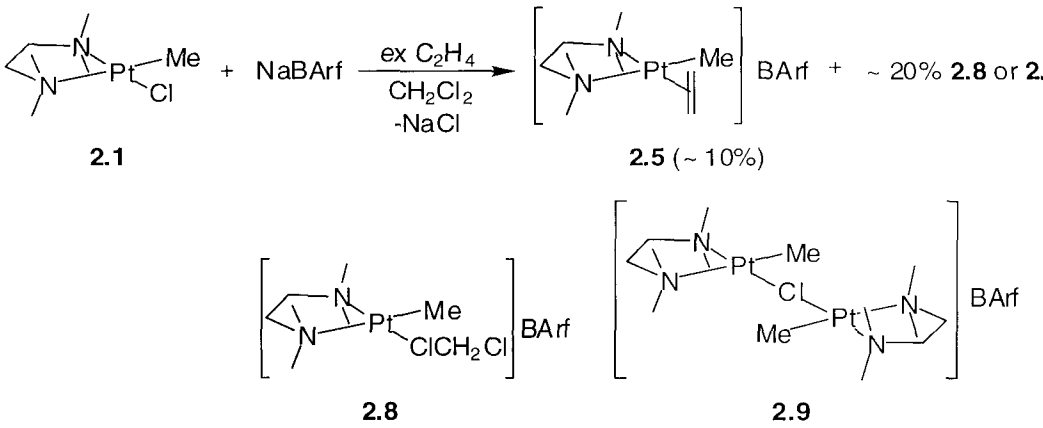

Finally, treatment of **2.1** with $AgBF_4$ in CH_2Cl_2 yielded a completely insoluble reaction mixture. When the reaction was carried out in methanol, **2.10** was observed in low yield (~ 5%), but the major product was the methanol solvated cation **2.11** (eq 7).

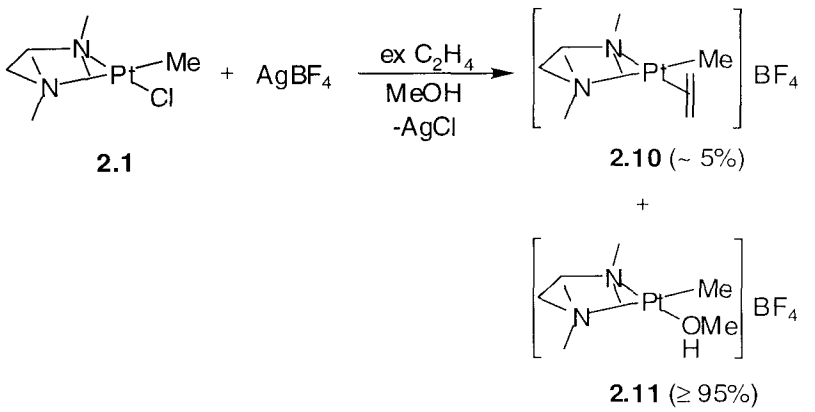

Attempted Oxidation of the Bound Ethylene in 2.2. With the ethylene complex **2.2** in hand, we examined the first step in the proposed catalytic cycle for olefin oxidation, namely, nucleophilic attack at the olefin to produce a σ-bound alkyl. Scheme 3

summarizes the reactivity of **2.2** towards nucleophiles in the presence and absence of oxidants.

Scheme 3

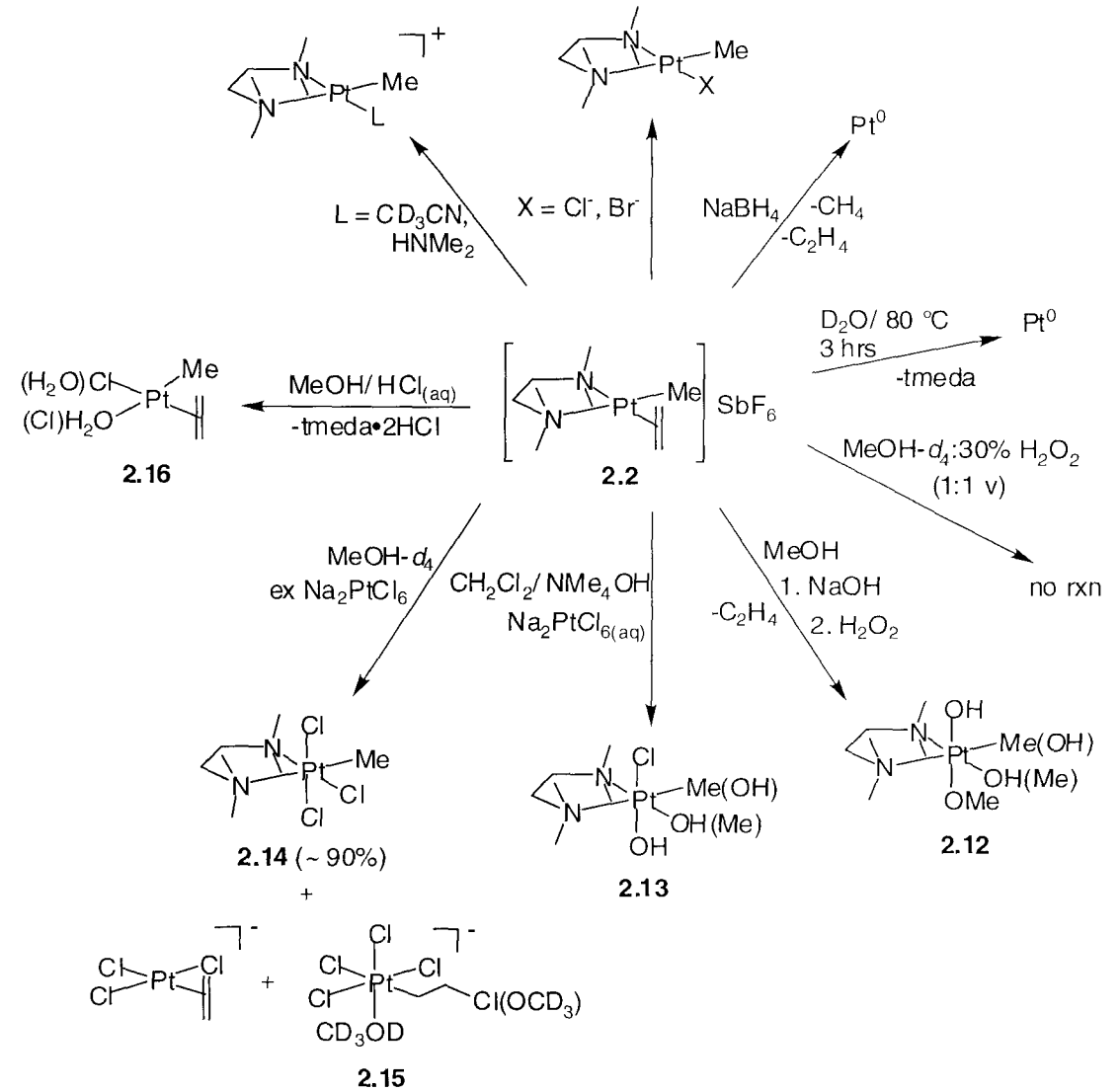

Unfortunately, none of the nucleophiles that were studied reacted with the coordinated ethylene of **2.2** to produce the desired σ-alkyl complex. Instead, the predominant reaction pathway involved nucleophilic attack at the metal center to displace the bound olefin and/or the tmeda ligand. Qualitatively, the rate of ligand substitution was very sensitive to the nature of the incoming nucleophile, suggesting that this reaction

proceeds by an associative mechanism. Ethylene was displaced instantaneously by bromide anion in CH_2Cl_2, while the reaction with chloride anion occurred over minutes under the same conditions. In CD_3CN, substitution of the bound ethylene proceeded cleanly over one week at room temperature. In contrast, dimethylamine reacted rapidly to liberate free ethylene, but this reaction produced a number of unidentified products in addition to the simple ligand substitution adduct. Bulkier amines such as N,N-diisopropylamine and N,N-dimethylaniline showed no reaction with complex **2.2**. Treatment of **2.2** with $NaBH_4$ in methanol at –78 °C resulted in the immediate liberation of gas (presumably ethylene and methane) accompanied by the precipitation of Pt^0. In general, complex **2.2** was not very thermally robust, and it decomposed rapidly at 80 °C in D_2O to form Pt^0. It is likely that the significant *trans* effect of both the methyl and ethylene ligands renders the tmeda ligand susceptible to ligand substitution with D_2O at elevated temperatures. In fact, doubly protonated tmeda was observed in this reaction mixture by ^1H NMR spectroscopy after 3 hours.

In a related system, the oxidation of the ethylene in $[Cl_3Pt(\eta^2\text{-}C_2H_4)]^-$ to 2-chloroethanol or ethylene glycol is believed to involve a (β-hydroxyethyl)Pt(II) intermediate (complex **B** in Scheme 2). This intermediate is only generated in steady state concentrations and has not been observed using common spectroscopic techniques. However, the addition of oxidants such as Cl_2 or $[PtCl_6]^{2-}$ has been shown to effectively trap the transient (β-hydroxyethyl)Pt(II) species by converting it to the more stable (β-hydroxyethyl)Pt(IV) adduct. Since a similar steady state situation may be operating in the present systems, an oxidant was added to the reactions of **2.2** with nucleophiles in order to trap any transiently generated (tmeda)Pt(II)(Me)(β-hydroxyethyl) products.

Treatment of methanol solutions of **2.2** with an excess of aqueous H_2O_2 resulted in no appreciable reaction. However, when the same reaction was carried out in the presence of excess hydroxide ion (in the form of a 0.1 N NaOH solution), the Pt(IV) adduct **2.12** was formed. Complex **2.12** was the major species observed by ^{1}H NMR spectroscopy and was tentatively assigned as the isomer in which the methyl group resides in the square plane of the octahedron, based on the known geometry of (tmeda)Pt(IV)(Me)(Cl)(OH)(OMe).[17] Addition of Na_2PtCl_6 to **2.2** in biphasic CH_2Cl_2/water mixtures containing NMe_4OH resulted in formation of the Pt(IV) complex **2.13**. Finally, treatment of **2.2** in methanol-d_4 with excess Na_2PtCl_6 produced **2.14**, presumably via oxidation of **2.1** (generated *in situ*) by an equivalent of $[PtCl_6]^{2-}$. Interestingly, free ethylene was not detected in the reaction mixture. Instead $Cl_3Pt(\eta^2$-$C_2H_4)$ was formed along with the β-chloroethyl Pt(IV) complex **2.15**. Additionally, another Pt–Me species was observed, but could not be identified. However, it does not appear to be the Pt(IV) methyl complex, $[Cl_5PtMe]^-$, which has been previously characterized.[11,18]

A final reactivity pattern was observed when methanol solutions of **2.2** were treated with an excess of concentrated HCl. In this reaction, the tmeda ligand was cleanly protonated off the metal center to yield a new Pt complex that is assigned as the chloroaqua adduct **2.16**. The ^{1}H NMR of this complex in CD_2Cl_2 is consistent with its formulation as **2.16**, and it contains a bound ethylene (δ 3.76 ppm, $^2J_{PtH}$ = 79.2 Hz), a bound water molecule (δ 1.58 ppm, $^2J_{PtH}$ = 96 Hz) and a methyl ligand (δ 0.56 ppm, $^2J_{PtH}$ = 81.0 Hz) in a 4:2:3 ratio.

Investigations of Pt(II) Ethylene Complexes Activated Towards Nucleophilic Attack. The reactivity of **2.2** indicated that catalytic turnover required a Pt(II) ethylene starting material in which the olefin is activated towards attack by H_2O.[19] There are still relatively few reports of well-defined, η^2-olefin complexes of platinum in which the bound olefin is susceptible towards nucleophilic attack. These include Zeise's anion ($[Cl_3Pt(\eta^2\text{-}C_2H_4)]^-$), the cationic complex $[(tmeda)PtCl(\eta^2\text{-}C_2H_4)][ClO_4]$ (**2.32**), and the neutral $Cl_2PtL(\eta^2\text{-}C_2H_4)$ complexes where L = PPh_3 (**2.23**), $ArPh_3$ (**2.24**), Me_2SO (**2.25**), or pyridine (**2.26**). Therefore, these different classes of olefin complexes were examined as potential catalysts.

Comparison of the Oxidation of Zeise's salt with Na_2PtCl_6 and H_2O_2.

First, the oxidation of Zeise's salt ($K[Cl_3Pt(\eta^2\text{-}C_2H_4)]$) in the presence of excess Na_2PtCl_6 and ethylene was examined. Treatment of $K[Cl_3Pt(\eta^2\text{-}C_2H_4)]$ with 15 equivalents of Na_2PtCl_6 under ~3.5 atm of ethylene at 45 °C yielded a 4.3:1 mixture of 2-chloroethanol to ethylene glycol. After 62 hrs a total of 5.5 turnovers were achieved with respect to the amount of $K[Cl_3Pt(\eta^2\text{-}C_2H_4)]$ added (Figure 1).

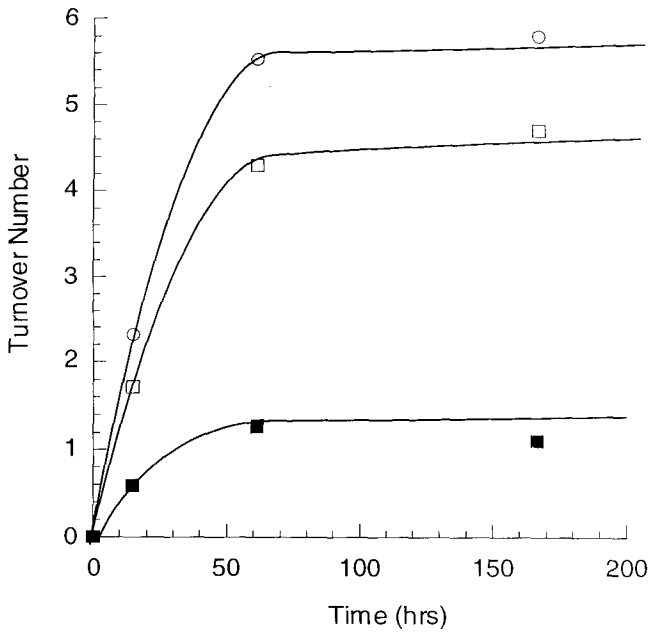

Figure 1. $K[Cl_3Pt(\eta^2\text{-}C_2H_4)]$ (8.22 mM) catalyzed oxidation of ethylene (~3.5 atm) by Na_2PtCl_6 (123 mM) to 2-chloroethanol (▫) and ethylene glycol (▪) as a function of time. Total number of turnovers (○).

After 166 hours, approximately 5.8 turnovers were observed, and traces of a gray solid began to precipitate from solution. At this point, the pH of the reaction mixture was between 0–1 as determined by pH paper. ^{1}H NMR analysis of the remaining solution showed the presence of significant quantities of the Pt ethylene complex. Additionally, ^{195}Pt NMR spectroscopy revealed that Pt(IV) complexes remained in solution. The gray precipitate was identified by ^{1}H NMR spectroscopy as the bridging chloride complex **2.17**, which had been reported previously by Sen and coworkers (eq 8).[20]

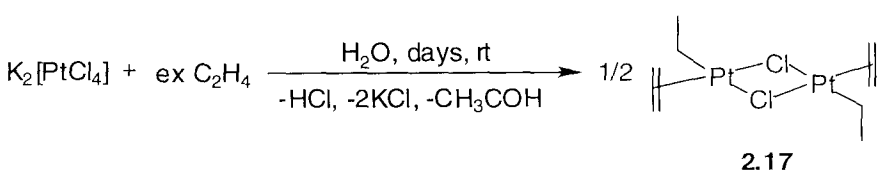

(8)

2.17

Next, oxidations of ethylene with $K[Cl_3Pt(\eta^2\text{-}C_2H_4)]$ using H_2O_2 as the oxidant were carried out. Addition of excess H_2O_2 to D_2O solutions of $K[Cl_3Pt(\eta^2\text{-}C_2H_4)]$ saturated with ethylene results in the formation of multiple Pt(IV) isomers, the structures of which are tentatively assigned as **2.18–2.20** (Scheme 4).

Scheme 4

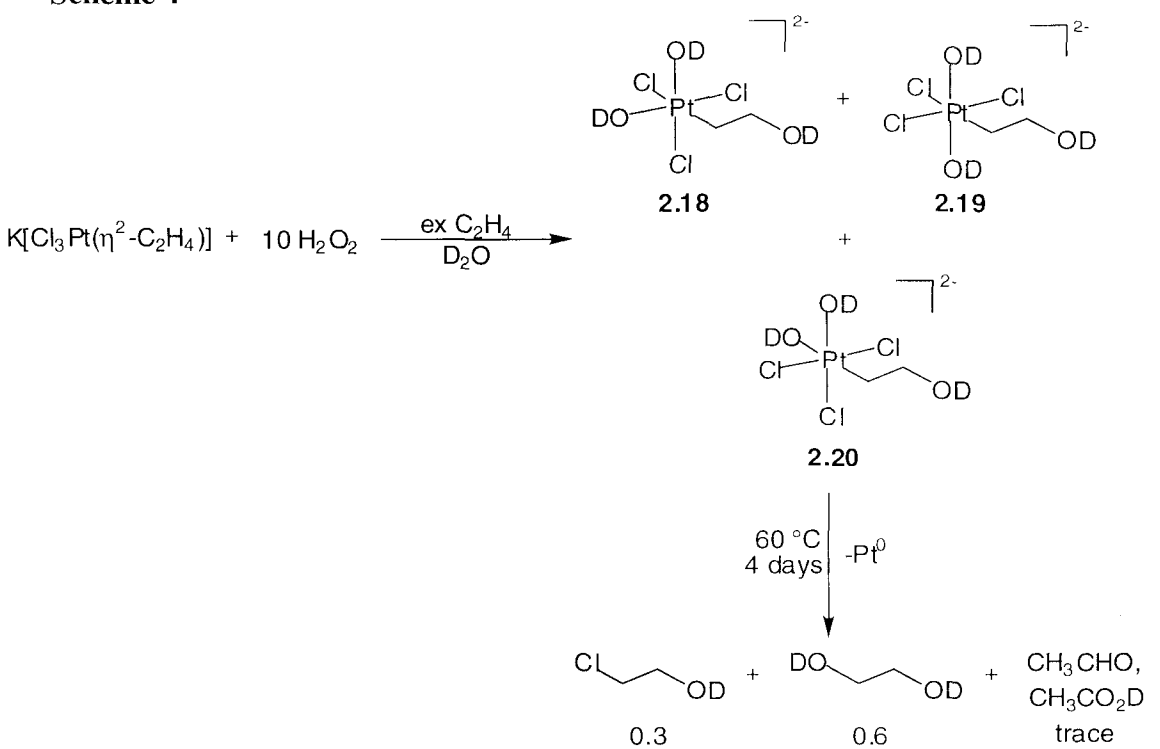

After heating for 4 days at 60 °C Pt^0 is formed in the NMR tube. Analysis of the products in solution gave ethylene glycol and 2-chloroethanol in a 2:1 ratio along with trace amounts of acetaldehyde and acetic acid. The ethylene glycol and the 2-chloroethanol account for approximately 90% of the ethylene from $[Cl_3Pt(\eta^2\text{-}C_2H_4)]^-$ that was added. Therefore, after 4 days less than 1 turnover was achieved. Heating these mixtures at 120 °C resulted in Pt^0 formation within 10 minutes. Carrying out the reaction in 1.0 M $HClO_4$

suppressed the formation of 2-chloroethanol entirely, but did not result in increased turnovers or in preventing Pt^0 deposition.

From the large amount of 2-chloroethanol produced, it was clear that part of the instability of the catalyst was because it was loosing Cl^- ligands in the product forming step. Therefore, reactions were carried out in NMR solvent mixtures consisting of DCl in D_2O. First, reactions were carried out without any added ethylene. Within minutes of addition of excess H_2O_2 to a solution of $K[Cl_3Pt(\eta^2\text{-}C_2H_4)]$ in 20% DCl/ D_2O at room temperature, conversion to a mixture of the β-chloroethyl (**2.21**) and β-hydroxyethyl species (**2.22**) was observed (Scheme 5). Heating this mixture at 45 °C for 12 hrs resulted in complete conversion to 2-chloroethanol. No other products were observed at this temperature; at 60 °C very small amounts of acetaldehyde, chloroacetaldehyde, acetic acid, and other unidentified products were observed. Reactions were then carried out with ethylene saturated DCl/D_2O solutions. Even after prolonged heating, there was no Pt^0 formation, but unfortuantely not more than 1 turnover was detected. Instead at significant concentrations of the starting ethylene complex, the orange Pt(IV) complex, $K_2PtCl_6 \cdot 6H_2O$, sometimes crystallized from solution (Scheme 5).

Scheme 5

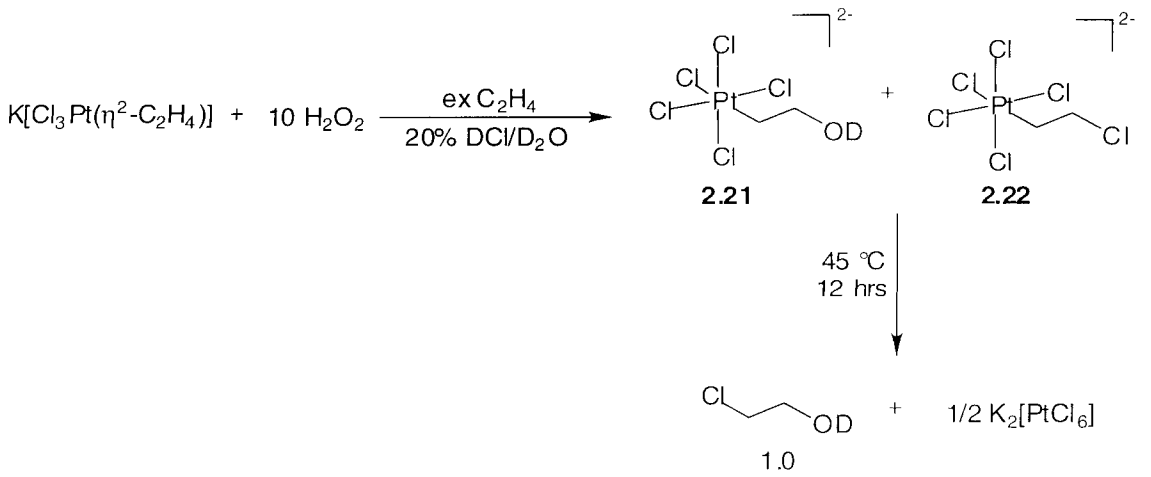

Thus the resulting product of reductive elimination, $[PtCl_4]^{2-}$, was being rapidly oxidized by excess H_2O_2 in solution before ethylene could substitute back into the coordination sphere of the platinum. Catalytic $SnCl_2$ is the additive of choice to increase the rate of olefin substitution into Pt(II) centers. Therefore, $SnCl_2$ was also tried in these reactions. However, in solution $SnCl_2$ will react with air to yield polymeric SnO_2. In the presence of H_2O_2, it was rapidly oxidized to SnO_2.

*Oxidation of the Bound Ethylene in Complexes of the Type (cis-$Cl_2PtL(\eta^2$-$C_2H_4)$ (L = PPh_3 (**2.23**), $AsPh_3$ (**2.24**), Me_2SO (**2.25**)) and trans-$Cl_2Pt(\eta^2$-$C_2H_4)(C_5H_5N)$, (**2.26**).*

Rapid addition of amines and pyridines to coordinated olefins in complexes **2.23–2.26** have been previously reported.[21] Therefore, these complexes were examined to see if the bound ethylene would be susceptible towards attack by OH^-. Treatment of a suspension of **2.23–2.25** in methanol with excess NaOH resulted in clear yellow solutions of the addition products **2.27–2.29** (eq 9).

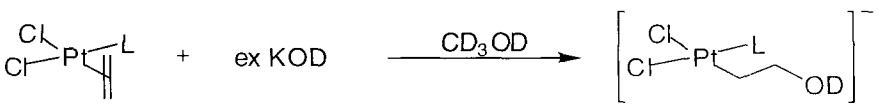

(9)

2.23: L = PPh_3
2.24: L = $AsPh_3$
2.25: L = Me_2SO

2.27: L = PPh_3
2.28: L = $AsPh_3$
2.29: L = Me_2SO

These complexes decompose over the course of 12 hours to black-brown solids. Oxidation reactions were next attempted. Excess H_2O_2 was added to suspensions of **2.23–2.25** in saturated ethylene solutions of methanol and heated to 60–80 °C. In all cases Pt^0 deposition occurred and only traces of acetaldehyde and acetic acid were observed in these reactions. By ^{31}P NMR all of the bound PPh_3 in **2.23** was oxidized to Ph_3PO. Based on this and the similarities in the aryl region in the ^1H NMR Ph_3AsO is expected as the major oxidized product in the reaction of **2.24** and H_2O_2. With **2.25** free Me_2SO was detected in solution by ^1H NMR.

The *trans* complex **2.26** also undoes nucleophilic attack at the bound ethylene to generate an approximate 5:1 mixture of the *trans* and *cis* σ-alkyl complexes **2.30** and **2.31** (eq 10). These complexes also decomposed slowly at room temperature.

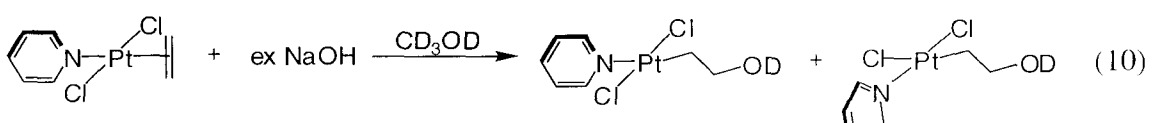

(10)

2.26 **2.30** **2.31**

However, in contrast to **2.23–2.25**, heating a CD_3OD/H_2O_2 solution of **2.26** at 60 °C in the absence of base produced a mixture of ethylene glycol and 2-chloroethanol. Interestingly, 2-methoxyethanol was not observed in any significant amount. Next, the reaction of **2.26** with H_2O_2 was carried out in the presence of excess ethylene in CD_3OD. After 4 days at 60 °C, Pt^0 deposition was observed. Analysis of the resulting solution showed the formation of approximately 1 equivalent total of ethylene glycol and 2-

chloroethanol per equivalent of $K[Cl_3Pt(\eta^2\text{-}C_2H_4)]$. In addition, significant quantities (~ 0.3 equivalents) of acetaldehyde and acetic acid were produced.

Oxidation of the Bound Ethylene in (tmeda)PtCl(η^2-C_2H_4)[ClO_4], 2.32.

In contrast to its methyl analog **2.2**, the chloride complex $[tmedaPtCl(C_2H_4)][ClO_4]$ **2.32** has been shown to be highly activated towards nucleophilic attack.[19] Protonolysis studies have revealed that the nucleophilic addition step is reversible, but in addition the Pt–C bond can also be cleaved.[22] However, the reaction of **2.32** with oxidants have not been reported to date.

Addition of solid **2.32** to an aqueous KOH solution affords the β-hydroxyalkyl species **2.33** in 80% isolated yield (eq 11).

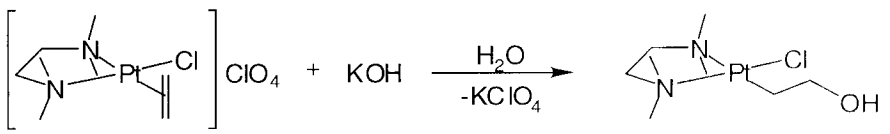

2.32 **2.33** (11)

Complex **2.33** was then cleanly oxidized to the corresponding β-hydroxyalkyl Pt(IV) species **2.34** upon treatment with H_2O_2 in methanol (eq 12). ^1H NMR spectroscopy in CD_3OD showed that the reaction afforded **2.34-*d*$_5$** in quantitative yield.

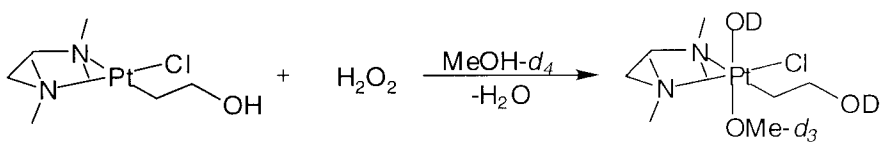

2.33 **2.34-*d*$_5$** (12)

Methanol-d_4 solutions of **2.34-*d*$_5$** were stable towards reductive elimination for days at 80 °C, even in the presence of excess OH^- (Scheme 6). However, the addition of an excess of HCl at 80 °C lead to reductive elimination to afford 2-chloroethanol and the

sparingly soluble complex (tmeda)$PtCl_2$. By ^1H NMR spectroscopy, the reaction of **2.34-d_5** with excess DCl in CD_3OD resulted in protonation of the Pt–OD group, as evidenced by a downfield shift of the peaks. However, the reductive elimination reaction was not completely clean and provided a variety of tmeda containing products. Furthermore, subjecting **2.32** to catalytic conditions (excess ethylene and H_2O_2) resulted in less than 1 turnover of ethylene glycol or 2-chloroethanol.

Scheme 6

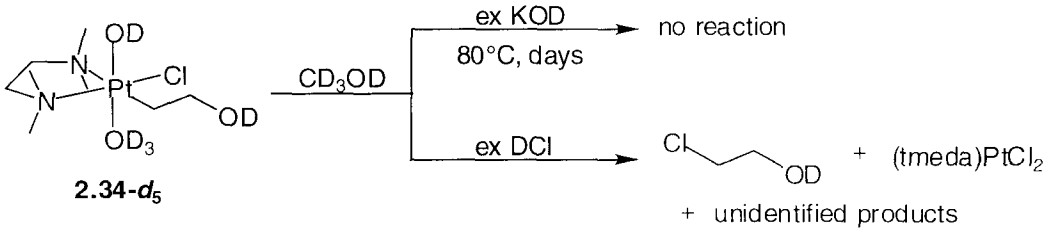

Discussion

In particular group 10 olefin complexes have been of interest since they are known to be key intermediates in important synthetic processes. One of the major processes is the Wacker oxidation, in which ethylene is oxidized to acetaldehyde in aqueous medium.[23] With Pt, this oxidation becomes one of ethylene to ethylene glycol. Recently there has been significant interest in using chelating nitrogen ligands in place of phosphine ligands with group 10 metals to generate highly active catalysts for a number of important transformations.[24] These nitrogen ligands are believed to be weaker donating ligands compared to the corresponding phosphine ligands and thus give rise to more electrophilic metal complexes. One example of this is the pentafluoropyridine complex [(tmeda)PtMe(NC_5F_5)][BArf], **2.35** (eq 13).[25] Pentafluoropyridine remains

unprotonated in 1N HNO_3 but is tightly bound by the 14 e⁻ fragment $[(tmeda)PtMe]^+$. **2.35** can activate hydrocarbons (benzene, cyclohexane, and methane) at 85 °C in pentafluoropyridine solvent (eq 13).[26]

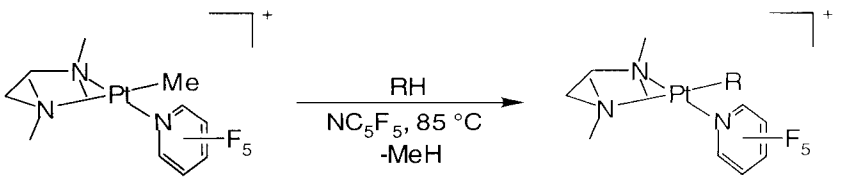

2.35 (13)

Coordination of an olefinic substrate to an electron deficient metal center serves to activate that substrate towards nucleophilic attack. Even traditionally unreactive alkenes such as ethylene, α-olefins, and internal olefins can become susceptible to attack upon coordination to a Lewis acidic metal. In general, the reactivity of the coordinated olefin increases as the metal center becomes more electron deficient.[27,28] Thus, cationic olefin complexes are typically more reactive than neutral olefin complexes, which in turn are more reactive than anionic species. Other factors, including coordinative saturation at the metal center and π-acidic ligands, can also facilitate attack at the olefin.

Based on these arguments, we anticipated that the Lewis acidic tmeda adduct **2.2** would be highly susceptible to nucleophilic attack at the olefin. However, as described above, this complex reacted exclusively *via* ligand substitution at the metal center. The nucleophilic addition product did not even appear to be generated in steady state concentrations, and could never be trapped by oxidation to the more stable Pt(IV) analog. The reactivity pattern of this cation stands in marked contrast to that of the *neutral* dichloro-olefin complexes ($cis\text{-}Cl_2PtL(\eta^2\text{-}C_2H_4)$) and to that of the *anionic* Zeise's salt. However, when the methyl ligand of **2.2** is substituted with a chloride (in **2.32**), the olefin

is once again activated towards nucleophilic attack. This observation suggests that the anomalous reactivity of **2.2** is a direct result of the CH_3 group. Methyl groups are well known to be excellent σ-donor ligands, and this feature appears to compensate for the electron deficiency at the cationic metal center of **2.2**. The increased electron density at Pt(II) results in increased back-bonding into the olefin π* orbital, thus disfavoring attack by an incoming nucleophile. Importantly, computational studies by Baird and coworkers appear to support this argument.[29]

Among the catalytic systems examined herein, the combination of Zeise's salt with $[PtCl_6]^{2-}$ or H_2O_2 afforded the most efficient and most selective formation of ethylene glycol/2-chloroethanol from ethylene. However, even in this case, a maximum of only 5.8 catalytic turnovers was achieved. With $[PtCl_6]^{2-}$ as the oxidant, the low turnover numbers (TON) can be understood in terms of the pH dependent equilibrium of the first step (nucleophilic attack on the coordinated olefin). This reaction has been studied in detail by Luinstra *et al.* by trapping the Pt(II) β-hydroxyethyl product *via* $[PtCl_6]^{2-}$ mediated oxidation.[11] In this system, the rate of Pt(IV) β-hydroxyethyl product formation showed an inverse 1st order dependence on H^+ concentration. In contrast, Halpern *et al.* showed that Zeise's salt can be rapidly oxidized to the Pt(IV) β-chloroethyl complex **2.22** with Cl_2 in 1 M HCl at room temperature.[30] Upon standing, this complex converted to the corresponding β-hydroxyethyl Pt(IV) species, which subsequently underwent reductive elimination to yield 2-chloroethanol. Halpern's result suggests that, even at high H^+ concentrations, the oxidation of a σ-alkyl Pt(II) adduct remains viable with the appropriate choice of oxidant. Alternatively, oxidation of $[Cl_3Pt(\eta^2\text{-}C_2H_4)]^-$ by

Cl_2 to yield the Pt(IV) ethylene complex $[Cl_5Pt(\eta^2\text{-}C_2H_4)]^-$ could occur prior to nucleophilic attack, but this has never been fully established.[10]

Hydrogen peroxide served as a good oxidant in reactions with Zeise's salt, and lead to clean conversion of coordinated ethylene to 2-chloroethanol in the presence of DCl. However, catalytic turnover with H_2O_2 could not be achieved, due to the slow kinetics of ethylene substitution relative to oxidation of $[PtCl_4]^{2-}$. In an effort to increase the rate of this ethylene substitution reaction, we turned to complexes containing stabilizing ligands. In systems containing soft, monodentate ligands (complexes **2.23–2.25**), ligand oxidation shut down the desired catalysis. In the pyridine ligated complex **2.26**, the chloride ligands were incorporated into the oxidized product during reductive elimination step. This resulted in a redistribution of ligands about platinum center following product formation, and ^1H NMR spectroscopy revealed a complex mixture of Pt(II) species. Finally, upon moving to the tmeda chelated complex **2.32** (the chloride analogue of **2.2**), the reductive elimination step became inefficient. Furthermore, the kinetics of olefin substitution at $(tmeda)Pt(Cl)_2$ remained slow compared to oxidation of this complex by H_2O_2.

Strukul has reported the catalytic oxidation of α-olefins to epoxides with H_2O_2 using bis-phosphine ligated Pt(II) complexes.[31] In these systems, the oxidation state of the Pt(II) center does not change throughout the course of the reaction, and, as a result, the peroxide can be used efficiently. If peroxide is to be used as the oxidant, similar strategies may be necessary in order to prevent deactivation of the catalyst by the irreversible formation of Pt(IV).

Experimental

General Considerations. All air and moisture sensitive compounds were manipulated using standard high-vacuum line, Schlenk line or cannula techniques, or in a nitrogen atmosphere glove box as previously described.[32] Solvents were dried over sodium/benzophenone ketyl (toluene, THF, Et_2O, petroleum ether), CaH_2 (CH_2Cl_2). Zeise's salt ($K[Cl_3Pt(C_2H_4)]\cdot H_2O$) and Zeise's dimer $[(PtCl_2(C_2H_4)]_2$ were purchased from Strem Chemicals. (tmeda)PtClMe[11] (**2.1**), the neutral ethylene complexes *cis*-$Cl_2PtL(\eta^2$-$C_2H_4)$[33] (L = PPh_3 (**2.23**), $AsPh_3$ (**2.24**), Me_2SO (**2.25**), and *trans*-$Cl_2Pt(\eta^2$-$C_2H_4)(C_5H_5N)$[21] (**2.26**) were all prepared as previously described. The cationic olefin complex $[(tmeda)PtCl(\eta^2$-$C_2H_4)][ClO_4]$ (**2.32**)was prepared as previously described.[22] Na_2PtCl_6 was prepared from $Na_2PtCl_6\cdot 6H_2O$ as previously described.[11] All silver salts were purchased from Aldrich and stored in a glove box. H_2O_2 (30% aqueous solution) was purchased from EM Science and used as received. NMR spectra were recorded on a Bruker AM500 (^{1}H, 500.13 MHz), General Electric QE300 (^{1}H, 300 MHz) or a Varian *Mercury-VX* 300 (^{1}H, 300.1 MHz; ^{19}F, 282.081 MHz; ^{13}C, 125.701 MHz) spectrometer. All ^{1}H NMR shifts are referenced to the residual protons of the NMR solvent.

$[(tmeda)PtMe(\eta^2$-$C_2H_4)][SbF_6]$ (**2.2**). $AgSbF_6$ (522 mg, 1.52 mmol) and **2.1** (500 mg, 1.38 mmol) were added to a medium wall glass bomb. CH_2Cl_2 (~40 mL) was vacuum transferred onto the solids at –78 °C. Ethylene (~3–4 manifolds worth at 1 atm) was then admitted while the reaction was still at –78 °C. The reaction was then sealed and allowed to warm to room temperature overnight behind a blast shield in a fume hood. All volatiles were then removed under vacuum. The residual solid was extracted with

CH_2Cl_2 (30 mL) and filtered through a pad of celite. The celite was washed with more CH_2Cl_2, and then all volatiles were removed under vacuum. This procedure was repeated at least two times in order to remove all of the AgCl byproduct. Recrystallization from CH_2Cl_2 and hexanes afforded a white solid. Yield: 718 mg (88%). ^{1}H NMR (CD_2Cl_2): δ 3.89 (s, 4H, $^3J_{PtH}$ = 65.0 Hz, C_2H_4), 3.06 (t, 2H, CH_2 of tmeda), 2.87–2.77 (overlapping, 8H, $^3J_{PtH}$ = 50.0 Hz, CH_3 and CH_2 of tmeda), 2.59 (s, 6H, $^3J_{PtH}$ = 20.0 Hz, CH_3 of tmeda), 0.36 (s, 3H, $^2J_{PtH}$ = 70.0 Hz, CH_3).

(tmeda)PtMe(OMe)(OH)$_2$ (2.12). **2.2** (32 mg, 0.054 mmol) was dissolved in methanol (2 mL). To this was added added NaOH (1mL 0.1N, 0.1 mmol). A few drops of 30% H_2O_2 was then added and the reaction was stirred for 10 minutes. The reaction was then extracted with CH_2Cl_2 (~10 mL), washed with water (2 x 2 mL) and dried over $MgSO_4$. Evaporation of the solvent yielded an off white residue. ^{1}H NMR of this residue in CD_2Cl_2 revealed that bound ethylene was no longer present. This product is tentatively assigned as the Pt(IV) species and was not purified any further. ^{1}H NMR (CD_2Cl_2): δ 2.81 (s, 3H, $^3J_{PtH}$ = 45 Hz, OCH_3), 2.70 (m, 2H CH_2 of tmeda), 2.56 (s, 3H, CH_3 of tmeda), 2.45 (s, 3H, CH_3 of tmeda), 2.42 (s, 3H, CH_3 of tmeda), 2.38 (s, 3H, CH_3 of tmeda), 2.22 (m, 2H CH_2 of tmeda), 1.29 (s, 3H, $^2J_{PtH}$ = 96 Hz, $PtCH_3$).

(tmeda)PtMe(Cl)(OH)$_2$ (2.13). **2.2** (30 mg, 0.051 mmol) was dissolved in CH_2Cl_2 (2 mL). To this was added $NMe_4OH{\cdot}5H_2O$ (184 mg, 1.02 mmol). To this mixture was added a solution of Na_2PtCl_6 (31.4 mg, 0.051 mmol) in water (2 mL). The reaction was stirred at room temperature for 5 hrs, after which the aqueous layer looked pinkish in

color while the CH_2Cl_2 layer looked pale yellow. An equal volume of water was added to the mixture and then extracted with CH_2Cl_2 (2 x 10 mL). The CH_2Cl_2 layer was washed with water (2 x 10 mL) and dried over Na_2SO_4. Filtration followed by removal of solvent yielded a white residue. ^{1}H NMR of this residue in CD_2Cl_2 revealed that bound ethylene was no longer present. This product is tentatively assigned as the Pt(IV) species and was not purified any further. ^{1}H NMR (CD_2Cl_2): δ 2.78–2.91 (m, 2H, C*H*$_2$ of tmeda), 2.69 (s, 3H, CH_3 of tmeda), 2.62 (s, 3H, CH_3 of tmeda), 2.55 (s, 3H, CH_3 of tmeda), 2.41 (s, 3H, CH_3 of tmeda), 1.3 (s, 3H, $^2J_{PtH}$ = 75 Hz, PtC*H*$_3$).

(tmeda)PtMe(Cl)$_3$ (2.14). In a screw cap NMR tube **2.2** (10 mg, 0.017 mmol) and Na_2PtCl_6 (25 mg, 0.055 mmol) were added. MeOH-*d*$_4$ (0.7 mL) was added and immediately a yellow solution formed accompanied by the formation of a tan precipitate. ^{1}H NMR of this mixture after addition of MeOH-*d*$_4$ showed that the amount of $[Cl_3Pt(\eta^2\text{-}C_2H_4)]^-$ to **2.2** was approximately 2:1. Additionally the Pt(IV) product **2.15** was detected as well as another unidentified Pt(IV)Me peak at δ 1.55 ppm ($^2J_{PtH}$ = 69.3 Hz). Complete consumption of **2.2** was observed after 24 hrs. The major tmeda containing product is assigned as the Pt(IV) species **2.14**. ^{1}H NMR (MeOH-*d*$_4$): δ 2.93 (m, 2H, C*H*$_2$ of tmeda), 2.87 (overlapping m and s, 8H, C*H*$_2$ and C*H*$_3$ of tmeda), 2.72 (s, 6H, $^3J_{PtH}$ = 30 Hz, C*H*$_3$ of tmeda), 2.46 (s, 3H, $^2J_{PtH}$ = 75 Hz, PtC*H*$_3$).

^{1}H NMR for **15** (MeOH-*d*$_4$): δ 3.44 (m, 2H, $^2J_{PtH}$ = 90 Hz, PtC*H*$_2$CH$_2$OCD$_3$), 3.12 (t, 2H, PtCH$_2$C*H*$_2$OCD$_3$).

(H_2O)PtClMe(η^2-C_2H_4) (2.16). To a solution of **2.2** (7.5 mg, 0.013 mmol) in methanol (1 mL) was added excess aqueous HCl. The reaction was stirred for 5 minutes, diluted with H_2O, then extracted with CH_2Cl_2. Evaporation of the solvent afforded a white solid. ^1H NMR in CD_2Cl_2 of this white solid showed an approximate 1:1 mixture of starting **2.2** and a new product, tentatively assigned as **2.16**. Evaporation of the solvent from the aqueous layer and redissolving the remaining residue in D_2O revealed tmeda·2HCl as the only organic product. ^1H (CD_2Cl_2): δ 3.76 (s, 4H, $^3J_{PtH}$ = 79.2 Hz, Pt(η^2-C_2H_4)), 1.55 (s, 2H, $^2J_{PtH}$ = 96 Hz, Pt(H_2O)), 0.56 (s, 3H, $^2J_{PtH}$ = 81.0 Hz, PtCH_3).

Zeise's Salt Catalyzed Oxidation of C_2H_4 with Na_2PtCl_6. In a 6 oz high pressure Fischer-Porter apparatus K[$Cl_3Pt(\eta^2$-$C_2H_4)$] (30.3 mg, 0.0822 mmol) and Na_2PtCl_6 (557 mg, 1.23 mmol) were added. Distilled water was added (10.0 mL) and the apparatus was flushed with ethylene for 5 minutes. The apparatus was then charged with 50 psi of ethylene and heated to 45 °C. The reaction mixture was analyzed by allowing the apparatus to cool to rt and then venting the excess ethylene. 1 mL aliquots were then withdrawn with a gas tight syringe and diluted with 1 mL of distilled water containing a known amount of 1-pentanol. The amounts of 2-chloroethanol to ethylene glycol were then determined by GC analysis of this mixture. The pH of the solution was determined by pH paper. The reaction was also carried out using D_2O instead of water, allowing a ^1H NMR determination of the amount 2-chloroethanol to ethylene glycol. The results obtained by both methods were in good agreement with each other.

Oxidation of Zeise's Salt with H_2O_2. $K[Cl_3Pt(\eta^2\text{-}C_2H_4)]$ (22 mg, 0.0597 mmol) was added to a J. Young NMR tube. This was then dissolved in a 20% DCl/D_2O (0.7 mL) solution. Ethylene was then bubbled through the solution for 5–10 minutes. Next 30% aqueous H_2O_2 (50 μL, 0.597 mmol) was added via microsyringe and capped as quickly as possible. ^1H NMR revealed that a mixture of the complexes **2.18–2.20** had formed, but their separate identities could not be determined. The reaction was then heated to 45 °C for 12 hrs. After the reaction was complete, a known amount of *tert*-butanol was added as an internal standard. ^1H NMR showed only 2-chloroethanol and ethylene. Addition of another 10 equiv. of H_2O_2 and heating for another 12 hours did not affect the amount of 2-chloroethanol formed.

[K][*cis*-$Cl_2Pt(PPh_3)(C_2H_4OH)$] (2.27). In an NMR tube **2.23** (5 mg, $8.99x10^{-3}$ mmol) was dissolved in CD_3OD (0.7 mL). To this was added excess KOH (3–5 mg, 0.0535–0.0891 mmol). A ^1H NMR spectrum taken immediately after addition revealed that all the starting material had been consumed and free ethylene was not present. ^1H NMR (MeOH-d_4): δ 7.80–7.32 (m overlapping, 15H, $(C_6H_5)_3P$), 3.18 (m, 2H, Pt-CH_2CH_2OD), 1.29 (m, 2H, Pt-CH_2CH_2OD). ^{195}Pt satellites were not located.

[K][*cis*-$Cl_2Pt(AsPh_3)(C_2H_4OH)$] (2.28). Prepared analogously to **2.27** from **2.24**. A ^1H NMR spectrum taken immediately after addition revealed that all the starting material had been consumed and free ethylene was not present. ^1H NMR (MeOH-d_4): δ 7.80–7.30 (m overlapping, 15H, $(C_6H_5)_3As$), 3.25 (m, 2H, Pt-CH_2CH_2OD), 1.35 (m, 2H, Pt-CH_2CH_2OD). ^{195}Pt satellites were not located.

[K][*cis*-$Cl_2Pt(DMSO)(C_2H_4OH)$] (2.29). Prepared analogously to **2.27** from **2.25**. A ^1H NMR spectrum taken immediately after addition revealed that all the starting material had been consumed and free ethylene was not present. At least three other unidentified complexes were also present. ^1H NMR (MeOH-d_4): δ 3.57 (m, 2H, Pt-CH_2CH_2OD), 3.4–3.2 (overlapping s, Pt-$(CH_3)_2SO$), 1.80 (t, 2H, $^2J_{PtH}$ = 70 Hz, Pt-CH_2CH_2OD).

OH^- Attack at the Bound Ethylene in 2.26. The procedure is analogous to that of **2.27**. In an NMR tube **2.26** (5 mg, 0.0134 mmol) was dissolved in CD_3OD (0.7mL). To this was added an excess of KOH (5 mg, 0.0891 mmol). A ^1H NMR spectrum taken immediately after addition revealed a mixture of two β-hydroxyethyl compounds in a 5:1 ratio, tentatively assigned as the *trans* and *cis* isomers **2.30** and **2.31**, respectively. ^1H NMR for **2.30** (MeOH-d_4): δ 8.95 (d, 2H, *o*-H on py), 7.81 (t, 1H, *p*-H on py), 7.34 (t, 2H, *m*-H on py), 3.56 (m, 2H, $PtCH_2CH_2OD$), 2.05 (m, 2H, $^2J_{PtH}$ = 95 Hz, Pt-CH_2CH_2OD).

^1H NMR for **2.31** (MeOH-d_4): δ 8.61 (d, 2H, *o*-H on py), 7.40 (t, 1H, *p*-H on py), 7.20 (m overlapping, 2H, *m*-H on py), 3.43 (m, 2H, $PtCH_2CH_2OD$), 1.84 (m, 2H, $^2J_{PtH}$ = 90 Hz, Pt-CH_2CH_2OD).

(tmeda)$PtCl(C_2H_4OH)$ (2.33). Prepared similarly to that reported previously by Maresca and coworkers.[34] KOH (114 mg, 3.16 mmol) was dissolved in H_2O (10 ml). Solid **2.32** (474 mg, 1 mmol) was then added in small portions under vigorous stirring. After addition was complete the reaction mixture was stirred for another 0.5 hrs at room temperature. The precipitated $KClO_4$ was then filtered away yielding a clear aqueous

solution. The aqueous layer was then extracted with CH_2Cl_2 (3 x 75 mL), dried over Na_2SO_4. Removal of solvent under vacuo afforded 310 mg white powder. Yield 80%. ^{1}H NMR (CD_3CN/CD_2Cl_2): δ 3.32 (t, 2H, $^3J_{HH}$ = 10 Hz, $PtCH_2CH_2OH$), 2.84-2.80 (m overlapping, 2H, CH_2 of tmeda), 2.84 (s overlapping, 6H, $^3J_{PtH}$ = 55 Hz, $N(CH_3)_2$ *trans* to Cl), 2.64 (s, 6H, $N(CH_3)_2$ *trans* to CH_2CH_2OH), 2.29 (br, 1H, Pt-CH_2CH_2OH), 1.51 (t, 2H, $^3J_{HH}$ = 10 Hz, $^2J_{PtH}$ = 90 Hz, Pt-CH_2CH_2OH).

(tmeda)PtCl(OD)(OCD$_3$)(C$_2$H$_4$OD) (2.34). In an NMR tube **2.33** (20 mg, 5.16 x 10^{-2} mmol) was dissolved in CD_3OD (0.7 mL). 30% aqueous H_2O_2 (8.89 μL, 1.03 x 10^{-1} mmol) was then added with a microsyringe. A ^{1}H NMR spectrum taken after addition revealed full consumption of starting materials. ^{1}H NMR (CD_3OD): δ 3.70 (m, 1H, Pt-CH_2CH_2OH), 3.39 (dt, 1H, Pt-CH_2CH_2OH), 3.13 (dt, 1H, Pt-CH_2CH_2OH), 3.05 (br t, 1H, Pt-CH_2CH_2OH), 2.8-2.5 (overlapping m, 4H, CH_2 of tmeda), 2.67 (br s, 3H, $N(CH_3)_2$), 2.62 (br s, 3H, $N(CH_3)_2$), 2.60 (br s, 3H, $N(CH_3)_2$), 2.47 (br s, 3H, $N(CH_3)_2$). ^{195}Pt satellites were not located.

Reductive Elimination from 2.34 in CD$_3$OD. Solutions of **2.34** in CD_3OD were prepared as described above in screw cap NMR tubes. To these solutions were added either excess (~ 2–5 equiv) solid KOH or 20% DCl in D_2O and then heated to 80°C in a constant temperature oil bath. After cooling to room temperature the progress of the reactions were monitored by ^{1}H NMR. Under basic conditions reductive elimination should lead to the formation of ethylene glycol or 2-methoxyethanol while under acidic conditions 2-chloroethanol or 2-methoxyethanol is expected. Under basic conditions no

products of reductive elimination were observed. Slow formation of 2-chloroethanol was observed when DCl was added. Furthermore, upon cooling to room temperature (tmeda)$PtCl_2$ was seen to precipitate from solutions containing DCl.

References and Notes

1. Shilov, A. E.; Shul'pin, G. B. *Activation and Catalytic Reactions of Saturated Hydrocarbons in the Presence of Metal Complexes*; Kluwer: Dordrecht, 2000.
2. Parshall, G. W.; Ittel, S. D. *Homogeneous Catalysis*; 2nd ed.; John Wiley & Sons, Inc.: New York, 1992.
3. Crabtree, R. H. *Chem. Rev.* **1995**, *95*, 987.
4. Shilov, A. E. *Activation of Saturated Hydrocarbons by Transition Metal Complexes*; Riedel: Dordrecht, 1984.
5. Shilov, A. E.; Shul'pin, G. B. *Chem. Rev.* **1997**, *97*, 2879.
6. A precise and detailed discussion of the various contributions by different groups towards the elucidation of the mechanism is presented in Stahl, S. S.; Labinger, J. A.; Bercaw, J. E. *Angew. Chem. Int. Ed.* **1998**, *37*, 2180.
7. Hutson, A. C.; Lin, M.; Basickes, N.; Sen, A. *J. Organomet. Chem.* **1995**, *504*, 69.
8. Labinger, J. A.; Herring, A. M.; Lyon, D. K.; Luinstra, G. A.; Bercaw, J. E.; Horvath, I. T.; Eller, K. *Organometallics* **1993**, *12*, 895.
9. Labinger, J.; Herring, A. M.; Bercaw, J. E. *J. Am. Chem. Soc.* **1990**, *112*, 5628.
10. Sen, A.; Benvenuto, M.; Lin, M.; Hutson, A. C.; Basickes, N. **1994**, *116*, 998.
11. Luinstra, G. A.; Wang, L.; Stahl, S. S.; Labinger, J. A.; Bercaw, J. E. *J. Organomet. Chem.* **1995**, *504*, 75.

12. Luinstra, G. A.; Wang, L.; Stahl, S. S.; Labinger, J. A.; Bercaw, J. E. *Organometallics* **1994**, *13*, 755.

13. Rostovtsev, V. V.; Labinger, J. A.; Bercaw, J. E.; Lasseter, T. L.; Goldberg, K. I. *Organometallics* **1998**, *17*, 4530.

14. Although the electrode kinetics were irreversible, redox potential measurements of (tmeda)PtMeCl and (tmeda)$PtCl_2$ revealed that both complexes are harder to oxidize compared to (tmeda)$PtMe_2$; approximately 500 mvolts for the methyl chloride and nearly a volt harder for the dichloride. Scollard, J.D.; Bercaw, J.E. unpublished results.

15. Appleton, T. G.; Clark, H. C.; Manzer, L. E. **1973**, *10*, 335.

16. A similar cationic PtMe(η^2-ethylene) complex has been synthesized containing the unsymmetrical N–N ligand 2-(N,N-dimethylaminomethyl)pyridine. Two isomers are observed in which the ethylene is *trans* to the pyridine group in one isomer and *trans* to the NMe_2 group in the other. The ethylene resonances begin to broaden at -65 °C but could not be frozen out down to -80 °C. Wong-Foy, A.G.; Bercaw, J.E. unpublished results.

17. Scollard, J.D.; Bercaw, J.E. unpublished results.

18. Zamashchikov, V. V.; Rudakov, E. S.; Mitchenko, S. A.; Litvinenko, S. L. *Teor. Eksp. Khim.* **1982**, *18*, 510.

19. Maresca, L.; Natile, G. *Comments Inorg. Chem.* **1994**, *16*, 95.

20. Basickes, N.; Hutson, A. C.; Sen, A.; Yap, G. P. A.; Rheingold, A. L. *Organometallics* **1996**, *15*, 4116.

21. Orchin, M.; Schmidt, P. J. *Inorg. Chim. Acta Reviews* **1968**, 123.

22. Maresca, L.; Natile, G. *J. Chem. Soc. -Dalton Trans.* **1982**, 1903.

23. Tsuji, J. *Palladium Reagents and Catalysts*; Wiley: New York, 1995.

24. Ittel, S. D.; Johnson, L. K.; Brookhart, M. *Chem. Rev.* **2000**, *100*, 1169.

25. Holtcamp, M. W.; Labinger, J. A.; Bercaw, J. E. *J. Am. Chem. Soc.* **1997**, *119*, 848.

26. Holtcamp, M. W.; Henling, L. M.; Day, M. W.; Labinger, J. A.; Bercaw, J. E. *Inorg. Chim. Acta* **1998**, *270*, 467.

27. Crabtree, R. H. *The Organometallic Chemistry of the Transition Metals*; 2nd ed.; Wiley: New York, 1994.

28. Collman, J. P.; Hegedus, L. S.; Norton, J. R.; Finke, R. G. *Principles and Applications of Organotransition Metal Chemistry*; University Science Books: Mill Valley, CA, 1987.

29. Cameron, A. D.; Smith, V. H.; Baird, M. C. *J. Chem. Soc. -Dalton Trans.* **1988**, 1037.

30. Halpern, J.; Jewsbury, R. A. *J. Organomet. Chem.* **1979**, *181*, 223.

31. Strukul, G. *Angew. Chem., Int. Ed. Engl.* **1998**, *37*, 1198.

32. Burger, B. J.; Bercaw, J. E. In *Experimental Organometallic Chemistry*; ACS Symposium Series 357; Wayda, A. L., Darensbourg, M. Y., Eds.; American Chemical Society: Washington, DC, 1987; pp 79.

33. De Renzi, A.; Paiaro, G.; Panunzi, A. *Gazzetta Chim. Ital.* **1972**, *102*, 413.

34. Fanizzi, F. P.; Intini, F. P.; Maresca, L.; Natile, G.; Gasparrini, F. *J. Chem. Soc. - Dalton Trans.* **1990**, 1019.

Chapter 3

Intramolecular C–H Activation by Dicationic α-Diimine Supported Pt(II) Complexes

Abstract

The dicationic complexes ([(ArN=C(Me)–C(Me)=NAr)Pt(solv)$_2$]X$_2$, (Ar = 2,6-(CH$_3$)$_2$C$_6$H$_3$; **3.5a**: solv = CH$_3$CN, X = CF$_3$SO$_3^-$, BF$_4^-$, SbF$_6^-$; **3.5b**: solv = (CH$_3$)$_2$CO, X = BF$_4^-$, SbF$_6^-$) and **3.6** [(CyN=C(H)–C(H)=NCy)Pt(CH$_3$CN)$_2$]X$_2$, (Cy = C$_6$H$_{11}$, X = OTf$^-$, BF$_4^-$, PF$_6^-$, SbF$_6^-$) were synthesized from the corresponding Pt dichlorides with 2 equiv. of AgX. The reaction of **3.5a** with 1-phenylpyrazole, 2-phenylpyridine, 2-vinylpyridine, and 2-(2-thienyl)pyridine in acetone affords the cyclometalated products **3.11–3.14** via intramolecular C–H activation of an sp^2 C–H bond of the unsaturated sidegroup. Pyridines with saturated groups at the 2-position do not undergo a similar cyclometalation reaction. **3.6** undergoes cyclometalation of one of the cyclohexyl groups, an example of sp^3 C–H bond activation. The later reaction proceeds only part way to completion, implying that an equilibrium has been reached; in the case where X = OTf$^-$, the equilibrium favors the starting dication. Furthermore, the intramolecular C–H activation occurs in trifluoroethanol but not in acetone under comparable conditions in contrast to the reactions of **3.5a** with the substituted pyridines.

Introduction

The "Shilov system" represents the first example of homogeneous alkane functionalization[1] in which simple (or unactivated) alkanes, including methane, are oxidized to mixtures of alcohols and alkyl chlorides in aqueous solution. The process is catalytic in $[PtCl_4]^{2-}$ and requires stoichiometric $[PtCl_6]^{2-}$ (eq 1).[2-4]

$$R\text{–}H + PtCl_6^{2-} + H_2O\ (HCl) \xrightarrow[H_2O,\ 120°C]{PtCl_4^{2-}} R\text{–}OH\ (R\text{–}Cl) + PtCl_4^{2-} + 2\ HCl \quad (1)$$

It is generally accepted that the C–H activation or actual cleavage of the C–H bond governs the overall rate and selectivity for this alkane functionalization reaction (eq 2).

(2)

Unfortunately, the instability of the resulting Pt(II) alkyl complex towards protonolyis in protic media and its tendency to disproportionate in aprotic media has precluded the direct mechanistic study of this key reaction in the actual Shilov system.[5-7] We have reported mechanistic studies on the microscopic reverse of the C–H activation reaction —the protonolysis of the Pt alkyl bond— for a series of ligand-stabilized alkyl Pt(II) complexes.[8,9] Insights gained from these studies ultimately led to the development of cationic diamine,[10,11] tris(pyrazolyl)borate,[12,13] and α-diimine[14] supported Pt(II) complexes capable of activating alkanes under mild conditions. Key features of these systems include an electrophilic metal center, a non-coordinating counter-anion, a substitutionally labile fourth ligand, and the use of a non-oxidizable and extremely weakly coordinating solvent.

Cationic group 10 transition metal complexes of the general type $[(N–N)M(CH_3)(solv)]^+[WCA]^-$ (M = Ni, Pd; N–N = α-diimine; solv = Et_2O, CH_3CN; WCA = weakly coordinating anion) have been applied to a variety of important catalytic transformations.[15] Pt(II) complexes $[(N–N)Pt(CH_3)L]^+[BF_4]^-$ (where N–N = *bis*(aryl)diimine; L = CH_3CN, H_2O, CF_3CH_2OH) are thermally more robust than the corresponding Pt(II) diamine (*N,N,N',N'*-tetramethylethylenediamine) complexes, probably because of the α-diimines' ability to bind to the metal both as a moderately strong σ-donor and weak π-acceptor.[16,17] Perhaps more importantly, the versatility of the α-diimine synthesis permits both the steric and electronic parameters of the ligand to be varied relatively easily,[18] making these complexes well-suited for mechanistic studies aimed at elucidating the steric and electronic requirements, as well as the inherent selectivity of the Pt center in the C–H activation of alkanes under mild conditions.[19,20] Two representative α-diimine ligands are shown in Figure 1.

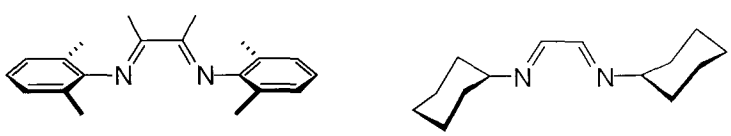

3.1 **3.2**

Figure 1. Representative aryl and alkyl α-diimine ligands.

However, nearly all previous model studies involve a metathesis-like stoichiometry, in which one hydrocarbyl group replaces a methyl group which departs with the hydrogen atom as methane (eq 3). We have not yet demonstrated the exact analog of eq 2, Pt-alkyl formation with proton loss, which is required in a functioning catalyst based on Shilov chemistry. In trying to design such a model, we noted that the methyl groups of Pt(II) cations $[L_2Pt(CH_3)(solv)]^+$ are relatively stable towards protonolysis, compared to the neutral dimethyl or chloromethyl Pt(II) complexes which

are readily protonated to generate methane.[21] For example, the methyl acetonitrile cations $[(N–N)Pt(CH_3)(NCCH_3)]^+[BF_4]^-$ (N–N = **3.1**, **3.2**) can be prepared quantitatively by treating the neutral dimethyl Pt(II) complexes even using a slight excess of HBF_4 in CH_3CN.[14] More remarkably, the methyl group in the cationic Pt(II) complex $[((C_2F_5)_2PCH_2CH_2P(C_2F_5))Pt(Me)CO]^+$ resists protonolysis even in the superacid mixture SbF_5/FSO_3H.[22]

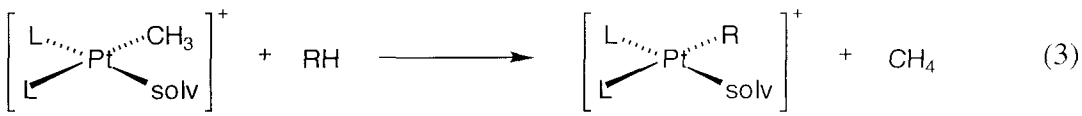

(3)

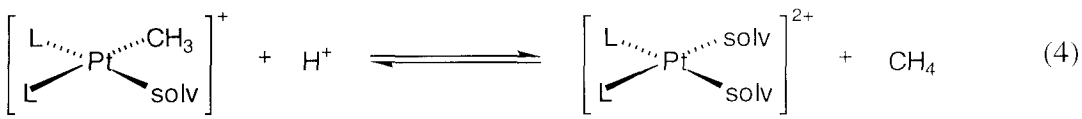

(4)

It is unclear whether this reduced reactivity is primarily a kinetic or equilibrium effect. While the equilibrium shown in eq 4 probably lies to the right in most or all cases, we reasoned that the increased electrophilicity of a dicationic Pt(II) center, as compared to a monocationic one, would favor deprotonation, whether from a coordinated C–H bond or a subsequent Pt(IV) alkylhydride intermediate. This would lead to facile exchange of H^+ with D^+ from the solvent and overall incorporation of deuterium into the alkane substrate, which might be detected even if the equilibrium of eq 4 does lie well to the right. However, studies on intermolecular C–H activation of arenes such as benzene and xylene in trifluoroethanol solvent were inconclusive, since we were unable to rule out competing H/D exchange catalyzed by traces of acid.

Accordingly, we turned our attention to intramolecular C–H activation to generate cyclometalated complexes, where the favorable entropy change of chelation would be

expected to provide an additional driving force. There is ample precedent for this behavior,[23,24] including related platinum complexes.[25-29] We report here C-H bond activation and deprotonation processes for Pt(II) complexes with the diimine auxiliary ligands **3.1** and **3.2**.

Results and Discussion

Preparation of Dicationic Solvento Complexes 3.3 and 3.4. The complexes examined in this study were prepared from the corresponding (N–N)$PtCl_2$ complexes **3.3** (N–N = **3.1**) and **3.4** (N–N = **3.2**). The dichlorides are prepared by adding the appropriate α-diimine to a solution of Zeise's anion in methanol at 0 °C[30] or to a THF solution of the neutral binuclear dimer[31] (Scheme 1).

Scheme 1

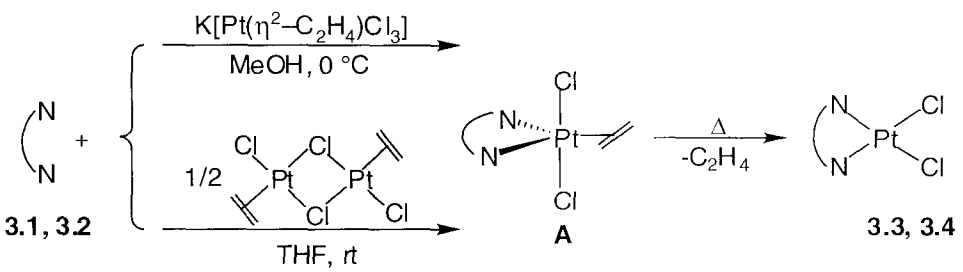

Upon addition of the ligand, the 5-coordinate, 18 e^- intermediate **A** precipitated from methanol solution. This intermediate is generally more soluble in non-polar halogenated solvents and ethers. The propensity of intermediate **A** to liberate ethylene to afford the corresponding dichloride complexes depends on the steric bulk imparted by the substituents on the imine nitrogens in the axial regions above and below the trigonal plane.[32,33] For example, with the bulkier ligand ArN=C(Me)–C(Me)=NAr, Ar = 2,6-$(CH(CH_3)_2)_2C_6H_3$, the 5-coordinate olefin complex was too unstable at room temperature

to be isolated, whereas with ligand **3.2** (RN=C(H)–C(H)=NR, R = cyclohexyl), the olefin complex was isolated exclusively. With ligand **3.1** (ArN=C(Me)–C(Me)=NAr, Ar = 2,6-$(CH_3)_2C_6H_3$), a mixture of the olefin complex and the product **3.3** was isolated. Quantitative conversion to the dichlorides, **3.3** and **3.4**, can be achieved by refluxing the respective 5-coordinate olefin complexes in THF or methylene chloride. The α-diimine ligands are generally unable to displace COD (1,5-cyclooctadiene) from $(COD)PtCl_2$, NBD (norbornadiene) from $(NBD)PtCl_2$, or SMe_2 from $(SMe_2)_2PtCl_2$.[31,33] Surprisingly, treatment of the substitutionally labile Pt(II) complex $[Pt(CH_3CN)_4][OTf]_2$[34] in nitromethane with 1 equiv of an α-diimine did not yield the expected *bis*-acetonitrile complex.

The *bis*-solvento complexes **3.5a**, **3.5b**, and **3.6** were synthesized by abstracting the chlorides with 2 equiv. of a silver salt in a mixture of CH_2Cl_2/CH_3CN or $(CH_3)_2CO$ (eq 5).

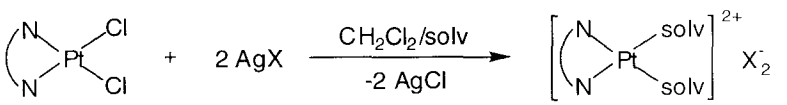

3.3, 3.4 X = OTf^-, BF_4^-, PF_6^-, SbF_6^- (5)

3.5a: N–N = **3.1**; solv = CH_3CN; X = OTf^-, BF_4^-, SbF_6^-
3.5b: N–N = **3.1**; solv = $(CH_3)_2CO$; X = BF_4^-, SbF_6^-
3.6: N–N = **3.2**; solv = CH_3CN; X = OTf^-, BF_4^-, PF_6^-, SbF_6^-

The acetonitrile and acetone adducts were isolated as yellow solids by addition of ether to the reaction mixtures after filtration to remove AgCl. In general, it was necessary to repeat the above procedure several times to remove all the AgCl. Attempts at synthesizing the *bis*-pentafluoropyridine or *bis*-tetrafluoro-4-picoline analogues in

either mixtures of CH_2Cl_2 and the fluorinated pyridines or in neat fluorinated pyridines proved unfruitful due to the insolubility of the $PtCl_2$/AgX mixtures.

The ^1H NMR spectra of the *bis*-acetonitrile and *bis*-acetone complexes in weakly coordinating solvents such as CD_2Cl_2 or CF_3CD_2OD (TFE-d_3) are consistent with a single C_{2v}-symmetric species in solution in each case. In CD_2Cl_2, there is a single resonance for bound acetonitrile in **3.5a** (X = OTf^-, BF_4^-, SbF_6^-) at 2.13 ppm; the ^{19}F NMR spectrum of the OTf^- salt consists of a sharp singlet at -75 ppm, characteristic of non-coordinated OTf^-.[35] When **3.5a** was dissolved in more coordinating solvents such as MeOH-d_4 or D_2O, however, a mixture of products was observed, the major one being $[(N\text{-}N)Pt(CH_3CN)(solv)]^{2+}X_2$, in which one acetonitrile molecule had been replaced by a solvent molecule. In contrast, a D_2O solution of **3.5b** exhibits signals corresponding to two symmetric species, in an approximate 5:1 ratio, as well as free acetone. The major species is assigned as the *bis*-aqua complex $[(N\text{–}N)Pt(D_2O)_2]^{2+}$ which was verified by independent synthesis.[36] The minor species is the C_{2v}-symmetric *bis*-acetone complex **3.5b**; its signal grows in intensity upon addition of acetone. The equilibrium between **3.5b** and the *bis*-aqua complex suggests that acetone has a higher affinity for the electrophilic platinum center than water. Interestingly, there was no indication of the unsymmetrical $[(N\text{-}N)Pt((CH_3)_2CO)(D_2O)]^{2+}X_2$ complex being formed under these conditions.

The acetone ligands in **3.5b** are more labile than the corresponding acetonitrile ligands in **3.5a**. In fact, clean isolation of the complex **3.5b** was possible only in cases where the anions were BF_4^- or SbF_6^-. Attempted isolation of **3.5b** with OTf^- anion invariably yielded oils that were difficult to purify. ^1H NMR spectra of the crude reaction

mixtures in CD_2Cl_2 showed multiple products. Presumably, OTf^- anion can displace one or even both acetone molecules, affording a mixture of dicationic, monocationic, and neutral Pt species. The fact that OTf^- anion can easily replace bound acetone in **3.5b** but not the acetonitrile in **3.5a** implies that acetonitrile is a better ligand for Pt as one might expect. On the other hand, the equilibrium between **3.5b** and the *bis*-aqua complex and previous measurement of equilibrium constants between $[(N\text{-}N)Pt(Me)(D_2O)][BF_4]$ and $[(N\text{-}N)Pt(Me)(TFE)][BF_4]$[19] indictates that acetone has a higher affinity for the electrophilic Pt(II) center than water molecules, which in turn are better ligands than trifluoroethanol. Thus, a qualitative ordering of acetonitrile > acetone > water > trifluoroethanol can be obtained for the affinity of various solvents for the Pt center with ligand **3.1**.

With α-diimine **3.2**, the only solvento complex that could be isolated relatively cleanly was the *bis*-acetonitrile adduct **3.6**. Attempts to isolate the corresponding *bis*-acetone adducts resulted only in the formation of sticky pale yellow oils consisting of various products. Varying the counteranion from OTf^- to BF_4^- to SbF_6^- did not to help to produce any isolable products.

Substitution Reactions Between 3.5a and 1-Phenylpyrazole and 2-Substituted Pyridines. Addition of 1-phenylpyrazole or a 2-substituted pyridine to a clear yellow solution of **3.5a** resulted in an immediate color change to dark yellow-brown and (by ^1H NMR) liberation of free CH_3CN. At least 95% of the resulting Pt species can be assigned as $[(N\text{-}N)Pt(CH_3CN)(L)]^+$ (N-N = **3.1**, L = 1-phenylpyrazole or 2-R-pyridine), **3.7–3.10** (eq 6).

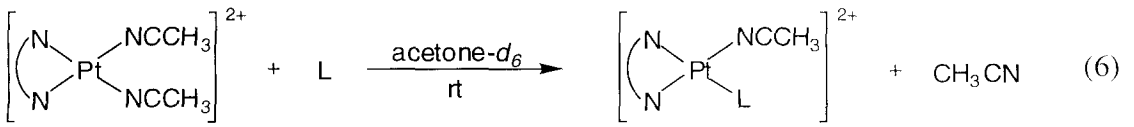

(6)

3.5a

3.7, L = 1-phenylpyrazole
3.8, L = 2-phenylpyridine
3.9, L = 2-vinylpyridine
3.10, L = 2-(2-thienyl)pyridine

Further addition of substrate (up to 2 equiv) does not displace the remaining bound acetonitrile. The increased crowding at the metal center due to the 2-substituted heterocycles may be responsible for the observed substitution pattern in these cases. For example, treatment of **3.5a** with 2 equiv of pyridine or 4-methylpicoline results in formation of the *bis*-pyridine or *bis*-picoline adducts, while treatment of **3.5a** with two equiv of 2-ethylpyridine results in only 1 pyridyl group adding to the metal center.

Displacement of acetonitrile by 2-(2-thienyl)pyridine in **3.5a** can potentially lead to either κ^1- or κ^2-bound 2-(2-thienyl)pyridine. In the κ^1-bound case, coordination can occur either through the S or the N atoms. An examination of the methyl region of the ^{1}H NMR spectrum of the reaction mixture reveals that there are 7 singlets; 6 for the methyl group of the diimine ligand and 1 for the remaining bound acetonitrile, thus establishing the κ^1-mode of binding. Restricted rotation around the Pt–(2-(2-thienyl)pyridine) bond, at least on the NMR time-scale, destroys any mirror planes in the molecule giving rise to the 6 inequivalent methyl groups. Furthermore, the downfield shift of the proton α to the pyridine nitrogen at δ 9.25 ppm compared to the value for free 2-thienylpyridine at δ 8.52 ppm implies that the substrate binds through the nitrogen. Similarly in **3.8**, the proton α to the pyridine nitrogen resonates at δ 9.23 ppm.

Intramolecular C–H Activation of 1-Phenylpyrazole and 2-Substituted Pyridines by 3.5a. Heating reaction mixtures containing a 1:1 or a 2:1 mixture of 1-phenylpyrazole or a 2-substituted pyridine and **3.5a** (or **3.5b**) at 85 °C in acetone for 4–6 hours results in deep burgundy solutions of the cyclometalated products **3.11–3.14** (Scheme 2). The ^{1}H NMR spectrum exhibits a doublet in the region δ 5–6 ppm with Pt satellites ($^3J_{Pt\text{-}H}$ = 26–33 Hz) that grows in intensity over time, assigned to the proton α to the Pt-bonded carbon.

Scheme 2

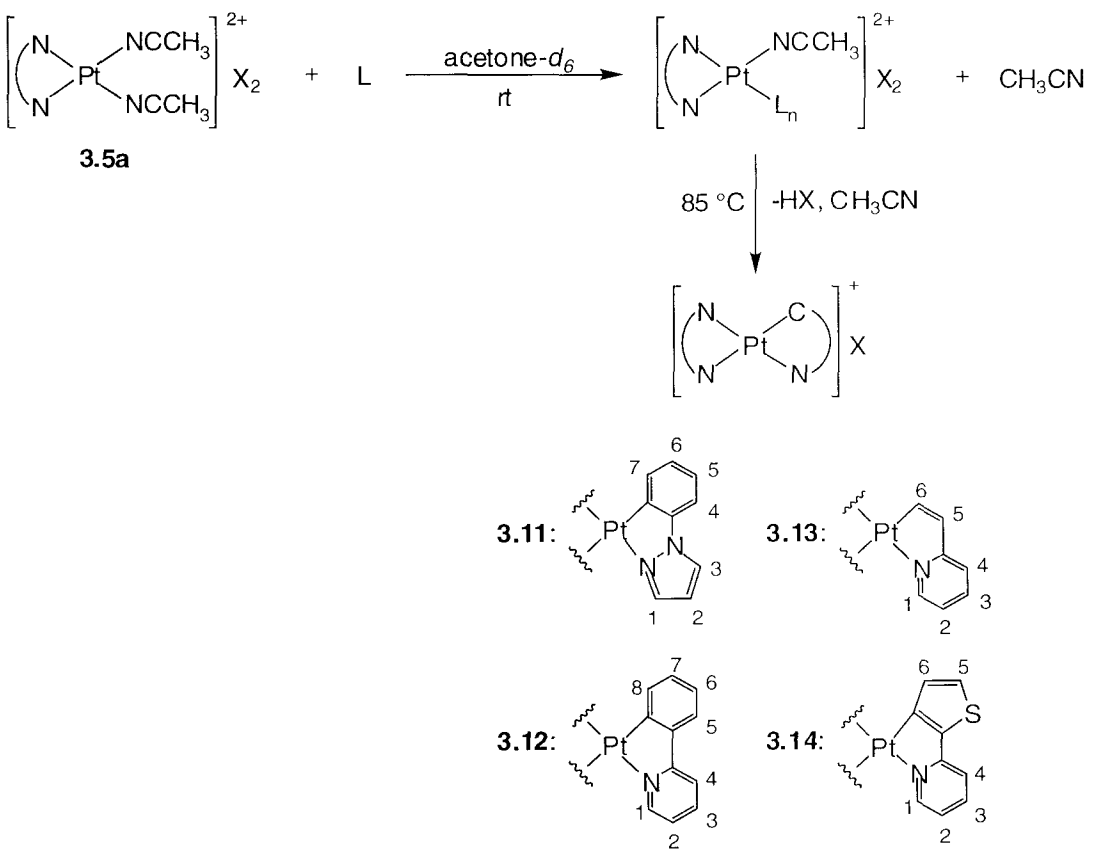

The unusually high upfield shift of this proton is attributed to the ring current shielding of the 2,6-xylyl groups of the diimine ligand. The *ortho*-proton of the pyridyl group is likewise shifted to higher field (~ 6.5–7.0 ppm) in complexes **3.12–3.14**. The

crystal structure of **3.12** (X = BF_4^-) shown in Figure 2 clearly indicates that the protons on C22 and C31 lie in the shielding regions of the arenes on the diimine ligand. Selected metrical parameters for **3.12** are listed in Table 1.

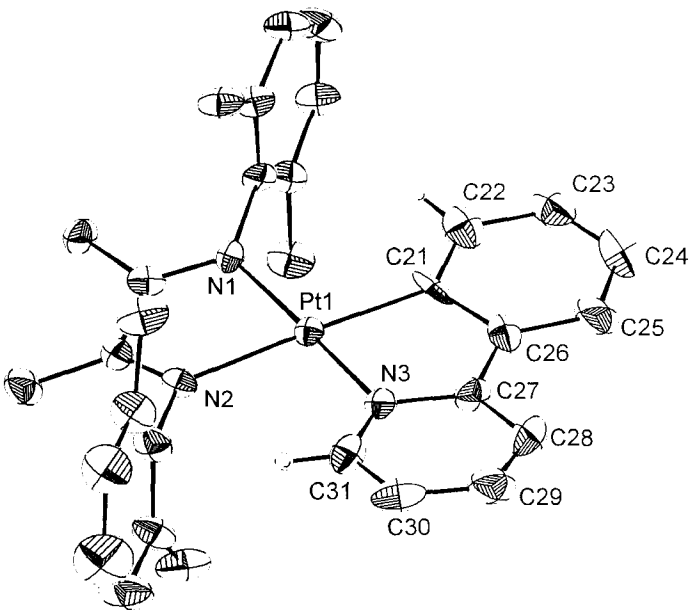

Figure 2. Labeled Diamond drawing of the cationic portion of **3.12** (X = BF_4^-) with ellipsoids at 50% probability.

Table 1. Selected bond lengths and bond angles for the cationic portion of **3.12** (X = BF_4^-).

	Bond Lengths (Å)		
Pt1–N1	2.056(5)	Pt1–N3	2.016(6)
Pt1–N2	2.092(6)	Pt1–C21	2.009(8)
	Bond Angles (°)		
N1–Pt1–N2	76.6(2)	N2–Pt1–N3	101.0(3)
N1–Pt1–N3	176.5(2)	N2–Pt1–C21	174.8(3)
N1–Pt1–C21	101.7(3)	N3–Pt1–C21	80.9(3)
Pt1–N3–C31	127.2(5)	Pt1–C21–C22	112.0(5)

The x-ray structure reveals that C–H bond activation yields a five-membered ring, the common preference. The α-diimine is bound unsymmetrically to the Pt with a moderate lengthening of the Pt-N bond *trans* to the phenyl group relative to that *trans* to

the pyridyl group (2.092 Å versus 2.056 Å), presumably due to higher *trans* influence.[37] Furthermore, the Pt–N (α-diimine) bond distances in **3.12** are significantly longer than those of other α-diimine ligated Pt complexes.

In general, cyclometalation reactions are carried out in the presence of a weak base to trap the equivalent of acid (HX) that is generated.[23,38] Here, a 2:1 molar ratio of substrate to Pt complex yields substantially cleaner reactions than without the extra equivalent of base. In principle one should be able to replace the second equivalent of substrate with another weak base. This is indeed the case for the extremely hindered base, 2,6-di-*t*-butylpyridine; triethylamine, on the other hand, gives significantly lower yields. Inorganic bases such as Na_2CO_3 lead to dramatic color changes affording deep purple or green solutions, exhibiting complex ^{1}H NMR spectra.

The reaction between **3.5a** and 2-(2-thienyl)pyridine could lead to a κ^2 (N,S) chelate, but only the cyclometalated product **3.14** is observed, as unequivocally demonstrated by a crystal structure determination. The structure of **3.14** is shown in Figure 3, with selected bond lengths and bond angles reported in Table 2.

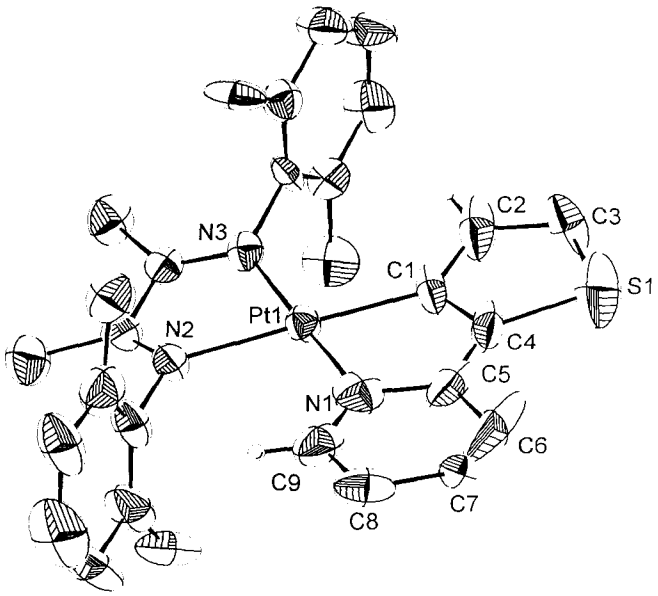

Figure 3. Labeled Diamond drawing of the cationic portion of **3.14** ($X = BF_4^-$) with ellipsoids at 50% probability.

Table 2. Selected bond lengths and bond angles for the cationic portion of **3.14** ($X = BF_4^-$).

	Bond Lengths (Å)		
Pt1–N1	2.013(7)	Pt1–N3	2.009(6)
Pt1–N2	2.095(5)	Pt1–C1	2.006(7)
	Bond Angles (°)		
N1–Pt1–N2	103.3(3)	N2–Pt1–N3	76.1(2)
N1–Pt1–N3	177.9(3)	N2–Pt1–C1	176.2(3)
N1–Pt1–C1	78.1(3)	N3–Pt1–C21	102.6(3)
Pt1–N1–C9	128.9(6)	Pt1–C1–C2	132.5(7)

Surprisingly, reactions of **3.5a** or **3.5b** with 2-substituted pyridines containing sp^3 C–H bonds (2-ethylpyridine, 2-*n*-propylpyridine, 2-*i*-propylpyridine, 2-*t*-butylpyridine, and 8-methylquinoline) did not yield the expected cyclometalated products. In all cases only decomposition was observed. The ^1H NMR spectra of the reaction mixtures indicated the formation of multiple products, of which only the protonated pyridines could be identified unambiguously. Similarly, the anilines 2-*t*-butylaniline and *N*,*N*-

dimethyl-*o*-toluidine yielded only deep green/black unidentifiable mixtures. Changing solvents from acetone to 2-methoxyethanol or trifluoroethanol did not affect the outcome of these reactions.

In order to compare the reactivity of the dicationic platinum complexes to that of the well-studied monocationic systems, complex **3.15** ([(N–N)Pt(Me)(2-$C_6H_5NC_5H_4$)][BF_4]; N–N = **3.1**), was synthesized by treatment of the methyl aqua cation, [(N–N)Pt(Me)(H_2O)]$^+$ (N—N = **3.1**)[20] with 2-phenylpyridine in acetone (eq 7). Thermolysis of this complex in acetone-d_6 does not result in cyclometalation even after prolonged (2 days) heating above 85 °C.

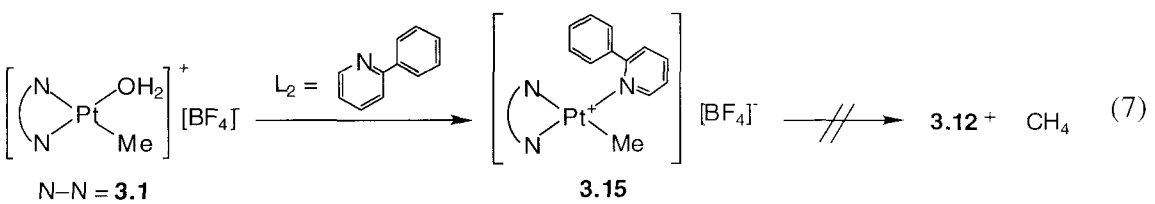

(7)

Intramolecular Cyclometalation of 3.6. To probe the viability of alkyl C–H bond activation by these dicationic complexes, we examined the reaction pattern of **3.6**, which contains a cyclohexyl moiety in its α-diimine ligand framework. Heating a solution of **3.6** in trifluoroethanol-d_3 at 85 °C does result in cyclometalation, albeit slowly, of one of the cyclohexyl groups on the imine nitrogens to yield **3.16** (Scheme 3). **3.16** has been previously synthesized by intramolecular C-H activation of the cationic methyl-acetonitrile complex **3.17b** or the methyl-aqua adduct **3.17a** (right side of Scheme 3) and crystallographically characterized as its BF_4^- salt.[39]

Scheme 3

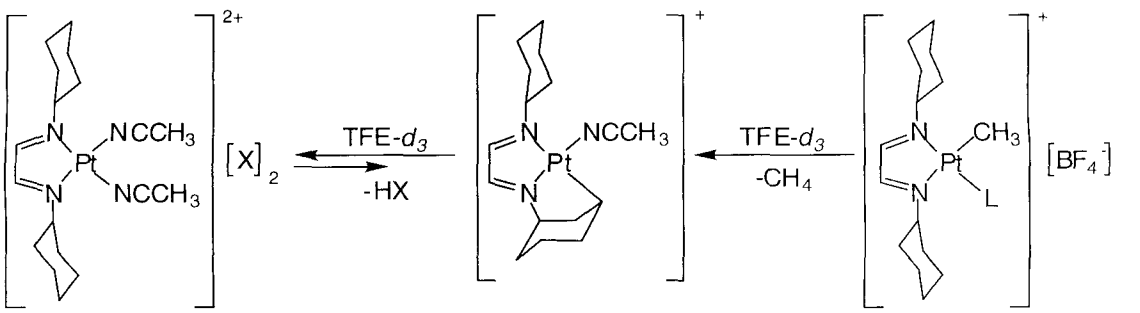

3.6 (X = OTf^-, BF_4^-, SbF_6^-) **3.16** **3.17a**: (L = H_2O) **3.17b**: (L = CH_3CN)

Whereas **3.17a** undergoes cyclometalation at ambient temperature over the course of 24 hrs, the acetonitrile complex **3.17b** and the *bis*-acetonitrile complex **3.6** must be refluxed in trifluoroethanol for the reaction to occur. Furthermore, whereas **3.17a** is converted quantitatively to **3.16** after refluxing in trifluoroethanol for 48 hrs, complete conversion of the dication **3.6** (X = OTf^-) to **3.16** is not observed. Instead, a 2.7:1 mixture of **3.6**:**3.16** was obtained after 12 hrs. Heating for another 24 hrs does not change this ratio.

The reaction is highly solvent-dependent. Switching from TFE-d_3 to acetone-d_6 resulted in a mixture of unidentifiable products. Different anions also affect the outcome of the reaction. Both SbF_6^- and OTf^- anions afforded considerably cleaner reaction mixtures than BF_4^-. With PF_6^- no cyclometalation product was observed, which may be attributed to the extensive decomposition of the PF_6^- anion as indicated by ^{19}F NMR spectroscopy.

Comments on Intramolecular C–H Activation by Dicationic Pt(II). The *bis*-acetonitrile complex **3.5a** reacts readily with 2-aryl- or 2-vinylpyridines to give first

substitution of one acetonitrile by pyridine and then, under relatively mild heating (85 °C), the cyclometalated products **3.11–3.14**. These C–H activation reactions are slower than those of monocationic $[L_2Pt(CH_3)S]^+$ complexes with benzene (eq 3) where S = TFE or H_2O.[14,19,20] This trend almost surely reflects the fact that displacement of the second acetonitrile by the reacting arene C–H (or C=C) bond is more difficult than the corresponding displacement in the monocationic systems, because ligands such as TFE and water are much more weakly bonded to Pt(II) than acetonitrile, and perhaps also because the solvent-Pt(II) bond is probably stronger in a dication. Displacement of a ligand is required, as demonstrated by the fact that conversion of complex **3.15** to **3.12** with liberation of methane (eq 7), a reaction that should be strongly thermodynamically favored, is not observed under comparable conditions. Formation of **3.11–3.14** from **3.5** is driven to completion by the presence of a second equivalent of base, although some conversion is observed even without extra base present.

Based on the earlier studies of the corresponding mono-cationic systems,[8,19,20] we would propose Scheme 4 to account for these observations. Replacement of the second acetonitrile ligand by a C-H bond (perhaps preceded by formation of an η^2-π-arene species[20]) may take place either by direct displacement or by a solvent-assisted pathway to give intermediate **B**. In the cyclometalation of 2-phenylpyridine, the η^1-arenenium, **B´**, species is another possible structure for **B**; such intermediates have been implicated in a number of studies involving Pt and Pd arene cyclometalation.[27,40]

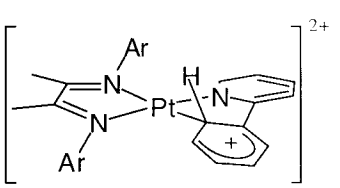

B´

From **B**, the actual cleavage of the C–H bond can proceed via an oxidative addition mechanism (Scheme 4, Path I) to generate a Pt(IV) hydride which is then deprotonated by a base in solution, or alternatively via direct deprotonation of the agostic complex (Scheme 4, Path II). Most of the evidence supports the formation of Pt(IV) hydrides as important intermediates in C–H activation, and we tend to favor the oxidative addition route, although it is conceivable that the involvement of additional external base in the present case could result in a different preferred route.

Scheme 4

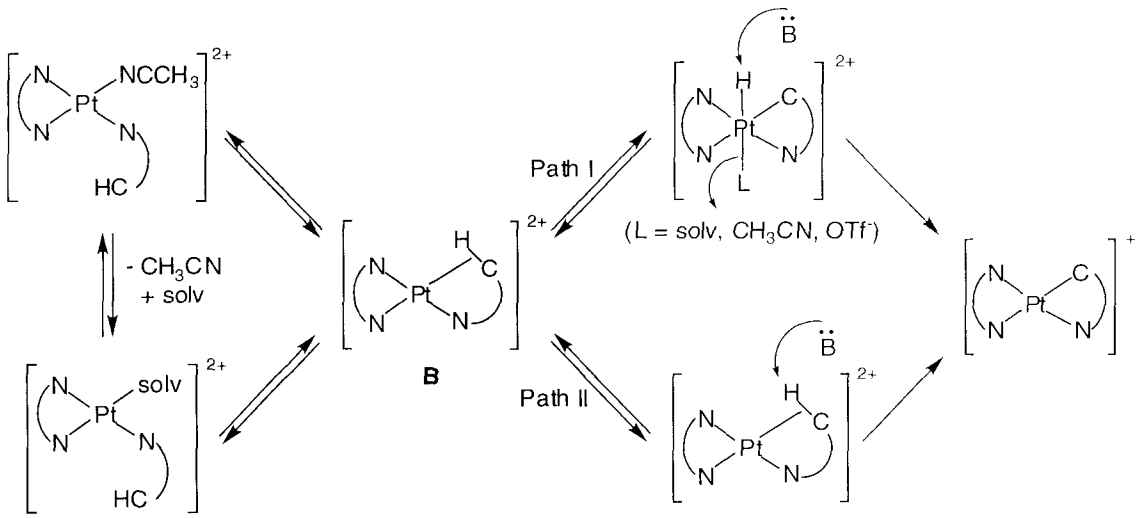

No cyclometalated products were observed when the *bis*-solvento complexes **3.5a** or **3.5b** were treated with pyridines containing adjacent aliphatic or benzylic C–H bonds, although intermolecular alkane activations by $[L_2Pt(CH_3)(H_2O)]^+$ have been observed.[14,19] This presumably reflects the fact that displacement of acetonitrile by an sp^3 C–H bond is less favorable than by vinyl or aryl C–H bonds (vide supra). However, an example of clean intramolecular C–H activation of an sp^3 C–H bond is observed in the formation of **3.16** from **3.6**. This reaction is slower than the formation of **3.16** from the monocationic

platinum methyl-aquo complex **3.17a**, but proceeds at about the same rate as monocationic platinum methyl-acetonitrile complex **3.7b**, again implying that (solvent) ligand displacement is a central factor in determining reactivity. Note that whereas acetone is the solvent of choice for the cyclometalations involving **3.5a**, no cyclometalation of **3.6** was observed in acetone; clean reaction to yield the cyclometalated product was observed only in trifluoroethanol-d_3.

Also, whereas formation of **3.16** from **3.17** proceeds to completion, cyclometallation of **3.6** only proceeds partway, to an equilibrium mixture in which the dicationic complex is favored. In principle addition of a base stronger than solvent to take up the liberated proton should drive the reaction further; addition of the hindered base 2,6-di-*t*-butylpyridine does seem to shift the equilibrium towards the cyclometallated product **3.16**, but there is competing decomposition. Stronger bases such as Na_2CO_3 resulted in highly colored solutions of which the ^{1}H NMR spectra showed only decomposition products. Nonetheless, the observation of the cyclometalated product **3.16** implies that electrophilic C–H activation at a dicationic Pt(II) center with proton liberation is possible. The fact that the equilibrium lies in favor of the starting material and not the highly entropically favored cyclometalated species suggests that direct observation of a Pt alkyl via intermolecular C–H activation may be difficult, requiring indirect methods such as H/D exchange to access whether C–H activation has occurred, but a catalytic cycle involving such a step, driving the unfavorable equilibrium forward by coupling to a subsequent rapid reaction, is a potentially viable strategy.

Experimental

General Considerations. All air and moisture sensitive compounds were manipulated using standard high-vacuum line, Schlenk line or cannula techniques, or in a nitrogen atmosphere glove box as previously described.[41] Solvents were dried over sodium/benzophenone ketyl (toluene, THF, Et_2O, petroleum ether), CaH_2 (CH_2Cl_2), Drierite (acetone), and 3Å molecular sieves/$NaHCO_3$ (trifluroethanol-d_3). Zeise's salt ($K[Cl_3Pt(C_2H_4)]\cdot H_2O$) and Zeise's dimer $[(PtCl_2(C_2H_4)]_2$ were purchased from Strem Chemicals. All silver salts were purchased from Aldrich and stored in a glove box. 1-Phenylpyrazole, 2-phenylpyridine, 2-vinylpyridine, and 2-ethylpyridine were purchased from Aldrich. 2-(2-Thienyl)pyridine was purchased from Lancaster. α-Diimines **1** and **2** were prepared as previously described.[42,43] NMR spectra were recorded on a General Electric QE300 (^{1}H, 300.1 MHz), a Varian ^{UNITY}*INOVA* 500 (^{1}H, 499.853 MHz; ^{13}C, 125.701 MHz) or a Varian *Mercury-VX* 300 (^{1}H, 300.1 MHz; ^{19}F, 282.081 MHz; ^{13}C, 125.701 MHz) spectrometer. All ^{1}H NMR shifts are relative to the residual NMR solvent and assignments are numbered as shown below. X-ray structure determinations were performed on a Bruker SMART 1000 CCD detector under a cold stream of N_2 gas. Data reduction was done with Bruker SAINT v6.2. All structures were solved by direct methods using SHELXS-97 and refined with SHELXL-97. Elemental Analyses were performed at the Caltech Elemental Analysis Facility or by Midwest Microlab, Indianapolis, IN.

(ArN=C(Me)–C(Me)=NAr)PtCl$_2$, (Ar = 2,6-(CH$_3$)$_2$C$_6$H$_3$), 3.3. $K[Cl_3Pt(\eta^2\text{-}C_2H_4)]\cdot H_2O$ (1.0 g, 2.71 mmol) was dissolved in methanol and cooled to 0 °C in an ice bath. To this

was added ligand **3.1** (0.873 g, 2.98 mmol) in small portions under vigorous stirring. A dark brown-red precipitate formed immediately upon addition. As this brown-red precipitate is the 5-coordinate ethylene complex and is unstable with respect to loss of ethylene at room temperature, filtering this intermediate is unnecessary. Instead the reaction was allowed to warm to room temperature and stirred until a color change to light brown was observed (3 hrs). The solid was then filtered, washed with methanol (10 mL) and Et_2O (10 mL). Drying over a water aspirator yielded a light brown powder. Yield: 1.5 g (100%). The dichloride is only sparingly soluble in most organic solvents giving rise to poorly resolved ^{1}H NMR spectra. ^{1}H NMR (DMSO-d_6, δ): 7.17 (s, 6H, 2,6-$(CH_3)_2C_6H_3$), 2.21 (s, 12H, 2,6-$(CH_3)_2C_6H_3$), 1.74 (s, 6H, N=CCH_3). Anal. Calcd. for $C_{20}H_{24}Cl_2N_2Pt$ (Found): C, 43.02 (42.97); H, 4.33 (4.40); N, 5.02 (4.97).

(CyN=C(H)–C(H)=NCy)PtCl$_2$, (Cy = C$_6$H$_{11}$), 3.4. $K[Cl_3Pt(\eta^2\text{-}C_2H_4)]\cdot H_2O$ (0.405 g, 1.10 mmol) was dissolved in methanol and cooled to 0 °C in an ice bath. To this was added ligand **3.2** (0.266 g, 1.21 mmol) in small portions under vigorous stirring. A bright yellow precipitate formed upon addition. The reaction was stirred for 0.5 hr, then the resulting precipitate was filtered and washed with cold methanol (5–10 mL) and dried. This solid was then dissolved in THF (30 mL) and refluxed for 1 hr after which time a orange-brown solid formed. This was cooled in an ice bath, then filtered to yield a flocculent orange-brown solid. Yield: 324 mg (60%). The dichloride is only sparingly soluble in most organic solvents. ^{1}H NMR (CD_2Cl_2, δ): 8.40 (s, 2H, $^3J_{PtH}$ = 100 Hz, N=CH), 4.69 (m, 2H, NC$H$$(CH_2)_5$), 2.36 (m, 4H, Cy C$H_2$), 1.16–1.91 (m, 16H,

overlapping Cy CH_2). Anal. Calcd. for $C_{20}H_{24}Cl_2N_2Pt$ (Found): C, 34.57 (33.93); H, 4.97 (4.73); N, 5.76 (5.39).

[(ArN=C(Me)–C(Me)=NAr)Pt(CH_3CN)$_2$]X_2, (Ar = 2,6-$(CH_3)_2C_6H_3$; X = $CF_3SO_3^-$, BF_4^-, SbF_6^-), 3.5a. To a stirred suspension of **3.3** (1.04 g, 1.86 mmol) in CH_2Cl_2 (75 mL) containing CH_3CN (2 mL) was added AgOTf (0.978 g, 3.81 mmol). As the reaction proceeded, the color of the suspended solids slowly turned light yellow. The mixture was stirred while protected from light at room temperature for 12 hrs, after which time a dull yellow precipitate formed. The entire mixture was then evaporated to dryness. Acetone (10 mL) and acetonitrile (1 mL) were then added to this residue and filtered through a pad of Celite to yield a yellow-orange solution. The solvent was removed in vacuo. Redissolving in acetone and acetonitrile followed by filtering through Celite was repeated until all the AgCl was removed. Precipitation with Et_2O of a 10:1 acetone:acetonitrile solution afforded the product as a bright yellow powder. Yield: 1.01 g (63%). ^{1}H NMR (CD_2Cl_2, δ): 7.35 (t, 2H, $^3J_{HH}$ = 6.00 Hz, *p*-H 2,6-$(CH_3)_2C_6H_3$), 7.31 (d, 4H, $^3J_{HH}$ = 6.00 Hz, *m*-H 2,6-$(CH_3)_2C_6H_3$), 2.45 (s, 6H, N=CCH_3), 2.44 (s, 12H, 2,6-$(CH_3)_2C_6H_3$). ^{13}C {^{1}H} NMR (CD_2Cl_2, δ): 188.4, 141.4, 130.9, 130.7, 129.6, 120.7, 20.6, 18.2, 3.5, ($CF_3SO_3^-$ not found). ^{19}F {^{1}H} NMR (CD_2Cl_2, δ) -79.1. Anal. Calcd. for $C_{26}H_{30}F_6N_4O_6PtS_2$ (Found): C, 35.99 (36.58); H, 3.48 (3.63); N, 6.46 (6.35). Analogous procedures were used for X = BF_4^- and SbF_6^-. For X = BF_4^-, **3.3** (0.300 g, 0.357 mmol) was combined with $AgBF_4$ (0.214 g, 1.10 mmol). Workup afforded a yellow powder. Yield: 0.334 g (83.7%). ^{1}H NMR in CD_2Cl_2 is the same as for the X = OTf^-. ^{19}F {^{1}H} NMR (CD_2Cl_2, δ) –152.3. Anal. Calcd. for $C_{24}H_{30}B_2F_8N_4Pt$ (Found): C, 38.79 (39.01); H,

4.07 (3.9); N, 7.54 (7.08). For X = SbF_6^-, **3.3** (0.100 g, 0.179 mmol) was combined with $AgSbF_6$ (0.123 g, 0.367 mmol). Workup afforded a bright yellow powder. Yield: 143 mg (66%). ^{1}H NMR ($(CD_3)_2CO$, δ): 7.43 (br m, 6H, 2,6-$(CH_3)_2C_6H_3$), 2.60 (s, 6H, N=CCH_3), 2.50 (s, 12H, 2,6-$(CH_3)_2C_6H_3$), 2.34 (s, 6H, CH_3CN). Anal. Calcd. for $C_{24}H_{30}F_{12}N_4PtSb_2$ (Found): C, 27.69 (27.66); H, 2.90 (3.01); N, 5.38 (5.25).

[(ArN=C(Me)–C(Me)=NAr)Pt(Me$_2$CO)$_2$]X$_2$, (Ar = 2,6-(CH$_3$)$_2$C$_6$H$_3$; X = BF$_4^-$, SbF$_6^-$), 3.5b. A solution of **3** (100 mg, 0.179 mmol) $AgSbF_6$ (123 mg, 0.367 mmol) and in dry acetone (7 mL) was stirred at room temperature while protected from light for 3 hrs. The resulting mixture was filtered through a pad of Celite and the solvent removed in vacuo to afford a red-orange oil. This was redissolved in dry acetone (5 mL) and filtered through a pad of Celite followed by removal of solvent in vacuo. The above procedure was repeated at least one more time until all the AgCl was removed. The crude product was purified by repeated precipitation of acetone (2mL) solutions with Et_2O under vigorous stirring. Drying in vacuo afforded a bright yellow solid. Product is very hygroscopic. Yield 68 mg (35.2%). ^{1}H NMR ($(CD_3)_2CO$, δ): 7.46 (t, 2H, $^3J_{HH}$ = 6.28 Hz, *p*-H 2,6-$(CH_3)_2C_6H_3$), 7.40 (d, 3H, $^3J_{HH}$ = 6.28 Hz, *m*-H 2,6-$(CH_3)_2C_6H_3$) 2.61 (s, 6H, N=CCH_3), 2.57 (s, 12H, 2,6-$(CH_3)_2C_6H_3$). Anal. Calcd. for $C_{26}H_{36}F_{12}N_2O_2PtSb_2$ (Found): C, 29.04 (27.78); H, 3.37 (3.38); N, 2.61 (2.45). For X = BF_4^-, **3** (200 mg, 0.358 mmol) was combined with $AgBF_4$ (143 mg, 0.734 mmol) in dry acetone (15 mL). Workup as above afforded a bright yellow powder. Yield 132 mg (47.4%). ^{1}H NMR appears to be consistent with the formation of the *bis*-acetone complex; however, the product is again extremely hygroscopic and yielded poor analysis.

[(CyN=C(H)–C(H)=NCy)Pt(CH_3CN)$_2$]X_2, (Cy = C_6H_{11}, X = OTf^-, BF_4^-, PF_6^-, SbF_6^-), 3.6. The solids **3.4** (135 mg, 0.278 mmol) and AgOTf (149.6 mg, 0.583 mmol) were suspended in a mixture of CH_2Cl_2 (10 mL) and CH_3CN (0.5 mL) and stirred for 3 hrs at room temperature while protected from light. The resulting mixture was filtered through a pad of Celite and the solvent removed in vacuo. The yellow-orange oil was taken up in acetone and a small amount of CH_3CN, filtered, and all the volatiles were removed in vacuo. Addition of Et_2O to a concentrated acetone solution of this mixture yields a viscous, yellow-orange oil. All attempts to recystallize or precipitate a solid resulted in the formation of this oil. Redissolving the oil in acetone, followed by removal of the solvent in vacuo a number of times affords a foam that could be triturated with Et_2O to yield a very sticky slightly yellow solid. Prolonged exposure to air results in the solid turning to an orange oil. Yield: 66 mg (30%) ^{1}H NMR (TFE-d_3 δ): 8.25 (s, 2H, $^3J_{PtH}$ = 106.4 Hz, N=C*H*), 3.77 (m, 2H, *ipso* H on CyN), 2.73 (s, 6H, Pt(NC*Me*)$_2$), 2.31–1.23 (m, 20H, CH_2 on CyN). ^{13}C {^{1}H} NMR (CD_3CN, δ): 172.85, 71.02, 32.95, 25.78, 25.71. Anal. Calcd. for $C_{20}H_{30}F_6N_40_6PtS_2$ (Found): C, 30.19 (29.27); H, 3.80 (3.78); N, 7.04 (6.38). Isolation of the BF_4^- salt was similarly complicated by the product precipitating as a viscous oil. This occurred to a lesser extent with SbF_6^- as the counteranion while with PF_6^- the final product precipitated as a nice off-white solid.

[(ArN=C(Me)–C(Me)=NAr)Pt(κ^2-(C,N)-1-$C_6H_4N_2C_3H_3$)]X, (Ar = 2,6-$(CH_3)_2C_6H_3$; X = OTf^-), 3.11. A solution of **3.5a** (X = OTf^-) (153 mg, 177 mmol) and 1-phenylpyrazole (46.7 μL, 353 mmol) in acetone (70 mL) was refluxed for 6 hrs, at which point the solution was deep red. The solvent was removed in vacuo to yield a red-orange residue.

This was dissolved in CH_2Cl_2 (40 mL) and washed with aqueous HOTf (0.1 M, 2 x 20 mL), water (20 mL), and then dried over Na_2SO_4. Solvent was removed in vacuo and the crude product was purified by repeated precipitation of concentrated acetone (2 mL) solutions with Et_2O to afford a red-brown powder. Yield 66 mg (48%). ^{1}H NMR ($(CD_3)_2CO$, δ): 8.54 (d, 1H, $^3J_{HH}$ = 2.90 Hz, H^3 on $N_2C_3H_3$), 7.49-7.47 (br m, 5H, 2,6-$(CH_3)_2C_6H_3$ and H^4 on C_6H_4), 7.03 (t, 1H, $^3J_{HH}$ = 8.8 Hz, H^5 on C_6H_4), 6.61 (t, 1H, $^3J_{HH}$ = 8.7 Hz, H^6 on C_6H_4), 6.51 (t, 1H, $^3J_{HH}$ = 2.90 Hz, H^2 on $N_2C_3H_3$), 5.40 (d, 1H, $^3J_{HH}$ = 2.90 Hz, H^1 on $N_2C_3H_3$), 5.18 (dd, 1H, $^3J_{HH}$ = 2.90 Hz, $^3J_{PtH}$ = 30 Hz, H^7 on C_6H_4). ^{13}C {^{1}H} NMR ($(CD_3)_2CO$, δ): 184.5, 180.6, 145.5, 145.2, 145.1, 139.3, 132.5, 132.3, 131.6, 130.0, 129.7, 127.3, 125.7, 123.8, 122.4 (q, $^1J_{CF}$ = 323 Hz), 112.2, 108.7, 21.2, 20.0, 17.83, 17.82, (was not able to detect ^{195}Pt coupling to C bonded to Pt). Anal. Calcd. for $C_{30}H_{31}F_3N_4O_3PtS$ (Found): C, 46.21 (46.01); H, 4.01 (4.09); N, 7.19 (6.96).

[(ArN=C(Me)–C(Me)=NAr)Pt(κ^2-(C,N)-1-$C_6H_4NC_5H_4$)]X, (Ar = 2,6-$(CH_3)_2C_6H_3$; X = OTf), 3.12. A solution of **3.5a** (X = OTf) (63 mg, 0.073 mmol) and 2-phenylpyridine (20.5 μL, 0.146 mmol) in acetone (10 mL) was heated at 85 °C overnight in a re-sealable Schlenk tube. The resulting dark red solution was diluted with water (30 mL), extracted with CH_2Cl_2 (2x 10 mL), then dried over Na_2SO_4. The solvent was removed in vacuo and the crude product was purified by repeated precipitation of concentrated acetone (2 mL) solutions with Et_2O at –20 °C to afford an orange-brown powder. Yield: 24 mg (41%). ^{1}H NMR ($(CD_3)_2CO$, δ): 7.96-8.05 (overlapping m, 2H, H^3 and H^4 on NC_5H_4), 7.61 (d, 1H, $^3J_{HH}$ = 7.61 Hz, H^5 on C_6H_4), 7.40-7.47 (br m, 6H, 2,6-$(CH_3)_2C_6H_3$), 7.00 (t, 1H, $^3J_{HH}$ = 7.61 Hz, H^6 on C_6H_4), 6.87 (dd, 1H, $^3J_{HH}$ = 6.3 Hz, $^3J_{PtH}$ = 34 Hz, H^1 on NC_5H_4), 6.81 (t,

1H, $^3J_{HH}$ = 6.3 Hz, H^2 on NC_5H_4), 6.65 (t, 1H, $^3J_{HH}$ = 7.54 Hz, H^7 on C_6H_4), 5.27 (dd, 1H, J_{HH} = 8.1 Hz, $^3J_{PtH}$ = 39 Hz, H^8 on C_6H_4), 2.44 (s, 3H, N=CCH_3), 2.36 (s, 6H, 2,6-(CH_3)$_2$C$_6$H$_3$), 2.34 (s, 3H, N=CCH_3), 2.28 (s, 6H, 2,6-(CH_3)$_2$C$_6$H$_3$). ^{13}C {^{1}H} NMR ((CD$_3$)$_2$CO, δ): 184.14, 180.47, 168.17, 148.68, 147.10, 145.58, 144.61, 142.13, 138.66, 132.16, 132.02, 131.31, 130.33, 129.97, 129.78, 129.72, 129.21, 126.81, 124.55, 122.77, 120.41, 21.44, 20.67, 17.96, 17.92. Anal. Calcd. for $C_{32}H_{32}F_3N_3O_3PtS$ (Found): C, 48.6 (47.13); H, 4.08 (4.10); N, 5.31 (5.08).

[(ArN=C(Me)–C(Me)=NAr)Pt(κ^2-(C,N)-(2-C$_2$H$_2$NC$_5$H$_4$)]X, (Ar = 2,6-(CH$_3$)$_2$C$_6$H$_3$; X = OTf), 3.13. A solution of **3.5a** (X = OTf) (100 mg, 0.115 mmol) and 2-vinylpyridine (27.4 μL, 0.230 mmol) in acetone (40 mL) was heated to reflux for four hours. The solvent was then removed in vacuo to 1/4 the volume. This was diluted with CH_2Cl_2 (30 mL), washed with aqueous HOTf (0.1 M, 2 x 20 mL), water (20 mL), and then dried over Na_2SO_4. Solvent was removed in vacuo and the crude product was purified by repeated precipitation of concentrated acetone (2 mL) solutions with Et_2O/hexanes to afford a rust-colored powder. Yield: 44 mg (52%) ^{1}H NMR ((CD$_3$)$_2$CO, δ): 7.84 (t, 1H, $^3J_{HH}$ = 7.7 Hz, H^3 on NC_5H_4), 7.45–7.34 (br m, 6H, 2,6-(CH$_3$)$_2$C$_6$$H_3$), 7.30 (d, 1H, $^3J_{HH}$ = 7.5 Hz, H^4 on NC_5H_4), 6.78 (t, 1H, $^3J_{HH}$ = 7.8 Hz, H^2 on NC_5H_4), 6.32 (dd, 1H, $^3J_{HH}$ = 5.9 Hz, $^3J_{PtH}$ = 30 Hz, H^1 on NC_5H_4), 6.30 (dd, 1H, $^3J_{HH}$ = 7.9 Hz, $^3J_{PtH}$ = 89 Hz, H^6 on C_2H_2), 5.84 (dd, 1H, $^3J_{HH}$ = 7.9 Hz, $^3J_{PtH}$ = 82 Hz, H^5 on C_2H_2), 2.48 (s, 3H, N=CCH_3), 2.35 (s, 6H, 2,6-(CH_3)$_2$C$_6$H$_3$), 2.33 (s, 6H, 2,6-(CH_3)$_2$C$_6$H$_3$), 2.31 (s, 3H, N=CCH_3). ^{13}C {^{1}H} NMR ((CD$_3$)$_2$CO, δ): 182.59, 180.57, 171.88, 156.84 (d, $^1J_{PtC}$ = 1041 Hz), 148.47, 145.07, 144.73, 143.02, 142.85, 139.50, 130.89, 130.66, 130.13, 129.73, 129.41, 122.4 (q, $^1J_{CF}$ =

323 Hz), 121.67, 121.39, 20.50, 2014, 17.94, 17.85. Anal. Calcd. for $C_{28}H_{30}F_3O_3PtS$ (Found): C, 45.40 (45.17); H, 4.08 (4.15); N, 5.67 (5.45).

[(ArN=C(Me)–C(Me)=NAr)Pt(κ^2-(C,N)-(2-C_4H_2S)NC_5H_4)]X, (Ar = 2,6-$(CH_3)_2C_6H_3$; X = OTf), 3.14. A solution of **3.5a** (X = OTf) (100 mg, 0.115 mmol) and 2-(2-thienyl)pyridine (37.2 mg, 0.230 mmol) in acetone (25 mL) was heated to reflux for 4 hrs. The solvent was then removed. The resulting dark red residue was dissolved in CH_2Cl_2 (50 mL), washed with aqueous HOTf (0.1 M, 2 mL), water (10 mL), and then dried over Na_2SO_4. Solvent was removed in vacuo and the crude product was purified by repeated precipitation of concentrated CH_2Cl_2 (2 mL) solutions with Et_2O/hexanes to afford a maroon solid. Yield: 48.3 mg (52%) ^{1}H NMR ($(CD_3)_2CO$, δ): 7.88 (t, 1H, $^3J_{HH}$ = 7.6 Hz, H^3 on NC_5H_4), 7.53–7.40 (overlapping, 7H, 2,6-$(CH_3)_2C_6H_3$ and H^3 on NC_5H_4), 7.24 (d, 1H, $^3J_{HH}$ = 5.0 Hz, H^5 on C_4H_2S), 6.68 (t, 1H, $^3J_{HH}$ = 6.9 Hz, H^2 on NC_5H_4), 6.52 (dd, 1H, $^3J_{HH}$ = 6.0 Hz, $^3J_{PtH}$ = 37 Hz, H^1 on NC_5H_4), 5.57 (dd, 1H, $^3J_{HH}$ = 5.0 Hz, $^3J_{PtH}$ = 13.3 Hz, H^6 on C_4H_2S) 2.44 (s, 3H, N=CCH_3), 2.39 (s, 6H, 2,6-(CH_3)$_2C_6H_3$), 2.33 (s, 6H, 2,6-(CH_3)$_2C_6H_3$), 2.31 (s, 3H, N=CCH_3). ^{13}C {^{1}H} NMR ($(CD_3)_2CO$, δ): 184.06, 181.07, 163.57, 148.09, 146.46, 144.75, 143.94, 143.08, 142.74, 132.08, 131.58, 131.20, 130.36, 130.04, 129.95, 127.83, 127.69, 122.4 (q, $^1J_{CF}$ = 323 Hz), 120.71, 119.01, 20.86, 20.62, 17.95, 17.85. Anal. Calcd. for $C_{30}H_{30}F_3N_3O_3PtS_2$ (Found): C, 45.22 (44.99); H, 3.80 (3.89); N, 5.27 (5.09).

[(ArN=C(Me)–C(Me)=NAr)Pt(CH_3)(2-$C_6H_5NC_5H_4$)][BF_4], (Ar = 2,6-$(CH_3)_2C_6H_3$) 3.15. To a solution of (ArN=C(Me)–C(Me)=NAr)$PtMe_2$ (Ar = 2,6-$(CH_3)_2C_6H_3$) (100 mg,

0.193 mmol) in acetone (15 mL), cooled to –20 °C, was added HBF_4(aq) (48%, 25.2μL, 0.193 mmol). Upon addition of the acid the color of the solution turned yellow-orange from dark red. The reaction was stirred for 15 min, after which 2-phenylpyridine (55.2 mL, 0.386 mmol) was added. The reaction was allowed to stir for 2 hrs. while warming to room temperature. Solvent was then removed under vacuo and resulting red-orange residue was precipitated from acetone with Et2O. Recrystallisation from CH_2Cl_2 and Et_2O afforded an orange solid. Yield: 45 mg (31%) ^{1}H NMR (CD_2Cl_2, δ): 8.64 (dd, 1H, $^3J_{HH}$ = 5.1 Hz, $^3J_{PtH}$ = 49 Hz, α-H on NC_5H_4), 7.8–7.7 (m overlapping, 3H, $C_6H_4NC_5H_4$), 7.54–7.42 (m overlapping, 3H, $C_6H_4NC_5H_4$), 7.30–7.17 (m overlapping, 5H, 2,6-$(CH_3)_2C_6H_3$), 7.0–6.95 (m overlapping, 2H, 1H from $C_6H_4NC_5H_4$ and 1H from 2,6-$(CH_3)_2C_6H_3$), 2.30 (s, 3H, N=CCH_3), 2.20 (s, 3H, N=CCH_3), 2.18 (s, 3H, 2,6-(CH_3)$_2$C$_6$H$_3$), 1.84 (s, 3H, 2,6-(CH_3)$_2$C$_6$H$_3$), 1.83 (s, 3H, 2,6-(CH_3)$_2$C$_6$H$_3$) 1.17 (s, 3H, 2,6-(CH_3)$_2$C$_6$H$_3$), 0.67 (3H, $^2J_{PtH}$ = 77.1 Hz, Pt(CH_3)). Anal. Calcd. for $C_{32}H_{36}BF_4N_3Pt$ (Found): C, 51.62 (50.05); H, 4.87 (4.80); N, 5.64 (5.31).

X-ray Structure Determinations of 3.12 and 3.14. Dark red crystals of **3.12** and **3.14** suitable for x-ray structure determinations were grown by layering concentrated solutions of **3.12** (CH_2Cl_2) and **3.14** (acetone) each with Et_2O at –40 °C. The position of the Pt atom in **3.12** was located with a Patterson map. The presence of the Pt atom creates a pseudo-mirror plane perpendicular to the b-axis and passing through the Pt position. The positions of the remaining atoms in the difference Fourier maps were complicated by this pseudo-mirror, but it was possible to distinguish actual peaks from ghost peaks. Numerous absorption correction schemes were tried, but all resulted in unsatisfactory

refinement results; therefore, the uncorrected data was used in the final refinement. All large peaks in the final difference Fourier map are near the Pt atom.

Refinement of F^2 against ALL reflections. The weighted R-factor (*w*R) and the goodness of fit (S) are based on F^2, conventional R-factors (R) are based on F, with F set to zero for negative F^2. The threshold expression of $F^2 > 2s(F^2)$ is used only for calculating R-factors(gt), etc., and is not relevant to the choice of reflections for refinement. R-factors based on F^2 are statistically about twice as large as those based on F, and R-factors based on ALL data will be even larger.

All esds (except the esd in the dihedral angle between two l.s. planes) are estimated using the full covariance matrix. The cell esds are taken into account individually in the estimation of esds in distances, angles and torsion angles; correlations between esds in cell parameters are only used when they are defined by crystal symmetry. An approximate (isotropic) treatment of cell esds is used for estimating esds involving l.s. planes.

References and Notes

1. Gol'dshleger, N. F.; Es'kova, V. V.; Shilov, A. E.; Shteinman, A. A. *Zh. Fiz. Khim.* **1972**, *46*, 1353.

2. Shilov, A. E.; Shul'pin, G. B. *Activation and Catalytic Reactions of Saturated Hydrocarbons in the Presence of Metal Complexes*; Kluwer Academic Publishers: Boston, MA, 2000.

3. Stahl, S.; Labinger, J. A.; Bercaw, J. E. *Angew. Chem., Int. Ed.* **1998**, *37*, 2181.

4. Shilov, A. E.; Shul'pin, G. B. *Chem. Rev.* **1997**, *97*, 2879.

5. Wang, L.; Stahl, S. S.; Labinger, J.; Bercaw, J. E. *J. Mol. Catal. A-Chem.* **1997**, *116*, 269.

6. Luinstra, G. A.; Wang, L.; Stahl, S. S.; Labinger, J. A.; Bercaw, J. E. *J. Organomet. Chem.* **1995**, *504*, 75.

7. Zamashchikov, V. V.; Rudakov, E. S.; Mitchenko, S. A.; Litvinenko, S. L. *Teor. Eksp. Khim.* **1982**, *18*, 510.

8. Stahl, S. S.; Labinger, J. A.; Bercaw, J. E. *J. Am. Chem. Soc.* **1996**, *118*, 5961.

9. Stahl, S. S.; Labinger, J. A.; Bercaw, J. E. *J. Am. Chem. Soc.* **1995**, *117*, 9371.

10. Holtcamp, M. W.; Henling, L. M.; Day, M. W.; Labinger, J. A.; Bercaw, J. E. *Inorg. Chim. Acta* **1998**, *270*, 467.

11. Holtcamp, M. W.; Labinger, J. A.; Bercaw, J. E. *J. Am. Chem. Soc.* **1997**, *119*, 848.

12. Wick, D. D.; Goldberg, K. I. *J. Am. Chem. Soc.* **1997**, *119*, 10235.

13. Reinartz, S.; White, P. S.; Brookhart, M.; Templeton, J. L. *Organometallics* **2001**, *20*, 1709.

14. Johansson, L.; Ryan, O. B.; Tilset, M. *J. Am. Chem. Soc.* **1999**, *121*, 1974.

15. For a review of α-diimine ligated late transition metal olefin polymerization complexes see: S. D. Ittel, L. K. Johnson, M. Brookhart, *Chem. Rev.* **2000**, 100, 1169.

16. Rendina, L. M.; Puddephatt, R. J. *Chem. Rev.* **1997**, *97*, 1735.

17. Van Koten, G.; Vrieze, K. *Adv. Organomet. Chem.* **1982**, *21*, 151.

18. Ittel, S. D.; Johnson, L. K.; Brookhart, M. *Chem. Rev.* **2000**, *100*, 1169.

19. Zhong, H. A.; Labinger, J. A.; Bercaw, J. E. submitted for publication.

20. Johansson, L.; Tilset, M.; Labinger, J. A.; Bercaw, J. E. *J. Am. Chem. Soc.* **2000**, *122*, 10846.

21. Holtcamp, M. W.; Labinger, J. A.; Bercaw, J. E. *Inorg. Chim. Acta* **1997**, *265*, 117.

22. Houlis, J. F.; Roddick, D. M. *J. Am. Chem. Soc.* **1998**, *18*, 2536.

23. Ryabov, A. D. *Chem. Rev.* **1990**, *90*, 403.

24. Dyker, G. *Angew. Chem. Int. Ed. Engl.* **1999**, *38*, 1698.

25. Rybtchinski, B.; Milstein, D. *J. Am. Chem. Soc.* **1999**, *121*, 4528.

26. Thorn, D. L. *Organometallics* **1998**, *17*, 348.

27. Canty, A. J.; Van Koten, G. *Acc. Chem. Res.* **1995**, *28*, 406.

28. Griffiths, D. C.; Young, G. B. *Organometallics* **1989**, *8*, 875.

29. Whitesides, G. M. *Pure & Appl. Chem.* **1981**, *53*, 287.

30. Maresca, L.; Natile, G.; Cattalini, L. *Inorg. Chim. Acta* **1975**, *14*, 79.

31. Clark, H. C.; Manzer, L. E. *J. Am. Chem. Soc.* **1973**, *95*, 3812.

32. Albano, V. G.; Natile, G.; Panunzi, A. *Coord. Chem. Rev.* **1994**, *133*, 67.

33. Cucciolito, M. E.; De Felice, V.; Panunzi, A.; Vitagliano, A. *Organometallics* **1989**, 1180.

34. Wendt, O. F.; Kaiser, N.-F. K.; Elding, L. I. *J. Chem. Soc., Dalton Trans.* **1997**, 4733.

35. By ^{19}F NMR Johansson et al. have observed that OTf^- can displace the bound CH_3CN in the cationic complex $[(N–N)Pt(Me)(CH_3CN)]^+$ (N–N = 3,5-$(CF_3)_2C_6H_3N$=C(Me)–C(Me)3,5-$(CF_3)_2C_6H_3N$) in CD_2Cl_2 to yield the neutral

methyl triflate complex with a ^4J(Pt–F) coupling constant of 14.4 Hz. L. Johansson, Ph D. thesis, University of Oslo (Oslo, Sweden), **2000**, Chapter 3.

36. Treatment of **3** with 2 equiv of AgOTf in CH_2Cl_2 followed by extraction of the resulting precipitate with D_2O afforded the dicationic *bis*-D_2O species.

37. Appleton, T. G.; Clark, H. C.; Manzer, L. E. *Coord. Chem. Rev.* **1973**, *10*, 335.

38. Martín-Matute, B.; Mateo, C.; Cárdenas, D. J.; Echavarren, A. M. *Chem. Eur. J.* **2001**, *7*, 2341.

39. Johansson, L., Ph D. Thesis, University of Oslo, **2000**.

40. Cámpora, J.; López, J. A.; Palma, P.; Valerga, P.; Spillner, E.; Carmona, E. *Angew. Chem. Int. Ed. Engl.* **1999**, *38*, 147.

41. Burger, B. J.; Bercaw, J. E. In *Experimental Organometallic Chemistry*; ACS Symposium Series 357; Wayda, A. L., Darensbourg, M. Y., Eds.; American Chemical Society: Washington, DC, 1987; pp 79.

42. Tom Dieck, H.; Svoboda, M.; Greiser, T. *Z. Naturforsch., B: Anorg. Chem., Org. Chem.* **1981**, *36B*, 823.

43. Svoboda, M.; Tom Dieck, H.; Krueger, C.; Tsay, Y.-H. *Z. Naturforsch., B: Anorg. Chem., Org. Chem.* **1981**, *36B*, 814.

Chapter 4

Synthesis and Characterization of a Dinuclear μ-Hydroxo-Bridged α-Diime Pt(II) Complex

Abstract

The diaqua complex $[(ArN{=}C(Me){-}C(Me){=}NAr)Pt(H_2O)_2]X_2$, **4.3**, (Ar = 2,6-$(CH_3)_2C_6H_3$; X = OTf^-, BF_4^-) decompose in aqueous solution to yield a red-orange precipitate. Spectroscopic characterization of the precipitate by ^1H, IR, and conductivity measurements is consistent with a C_{2v} symmetric structure containing hydroxo groups. Confirmation of the dicationic, dinuclear Pt(II) complex, **4.4**, where the two Pt centers are bridged by two OH groups was revealed by x-ray crystallography. Details of the synthesis and the resulting cleavage of the dimer under acidic and basic conditions is discussed. Lastly an equilibrium mixture of the diaqua complex and μ-OH bridged dimer generated in trifluoroethanol-d_3 was tested to determine if this mixture could activate the C–H bonds of cyclohexane which could be detected by deuterium incorporation from the solvent. Prior to decomposition of the complexes, no deuterium incorporation was observed.

Introduction

Considerable effort has been directed toward identifying new catalysts for alkane and arene functionalization. From mechanistic studies on model systems,[1,2] well-defined Pt(II) complexes were developed that could react with alkanes and arenes.[3,4] The latest generation of well-defined Pt(II) complexes are based on σ-aryldiimine ligated cationic Pt(II) complexes such as **4.1**. Alongside this was the key innovation of using the extremely weakly coordinating solvent trifluoroethanol for the C–H activation reactions.

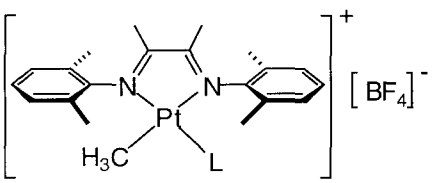

(L = H_2O, CF_3CH_2OH, CH_3CN)

4.1

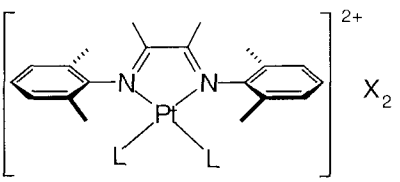

(L = CH_3CN, $(CH_3)_2CO$;
X = OTf^-, BF_4^-)

4.2

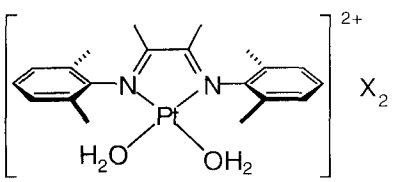

($X = OTf^-$, BF_4^-)

4.3

In chapter 3, it was discussed how attempts were made to employ dicationic complexes such as **4.2** for inter- and intra-molecular alkane and arene C–H activation. In addition to the acetonitrile and acetone solvated complexes, we were also interested in the possibility of the diaquo complex **4.3** as a potential catalyst since in the original Shilov system the active form of the catalyst has been concluded to be the neutral diaquo complex $PtCl_2(H_2O)_2$ from hydrolysis of the $[PtCl_4]^{2-}$ starting material (eq 1).[5,6]

$$PtCl_4^{2-} \xrightleftharpoons{H_2O} PtCl_3(H_2O)^- + Cl^- \xrightleftharpoons{H_2O} PtCl_2(H_2O)_2 + 2Cl^- \text{ etc.} \quad (1)$$

In trying to isolate the diaquo complex **4.3**, another minor product was always observed in substantial quantities. **4.3** eventually converted to this unknown product even in the solid state. A crystal structure determination finally established the identity of this unknown species as a dinuclear complex in which two cationic Pt(II) centers were bridged by OH groups. This chapter describes the synthesis and characterization of **4.3** and its pH dependent decomposition to a $(\mu\text{-OH})_2$ dimer. In addition, protonolysis studies of the monocation **4.1** with DOTf were carried out in triflouroethanol-d_3 in the absence of and in the presence of added water to compare the nature of the resulting Pt species.

Results and Discussion

Synthesis and Characterization of the Hydroxo Bridged Dimer [(N–N)Pt(μ-OH)]$_2$[X]$_2$ (N–N = 2,6-(CH$_3$)$_2$C$_6$H$_3$N=C(Me)–C(Me)N=2,6-(CH$_3$)$_2$C$_6$H$_3$); X = OTf$^-$, BF$_4^-$), 4.4. Treatment of a suspension of the light brown dichloride (ArN=C(Me)–C(Me)=NAr)PtCl$_2$ (Ar = 2,6-(CH$_3$)$_2$C$_6$H$_3$) with 2 equiv of AgX (X = OTf$^-$, BF$_4^-$) in CH_2Cl_2 yields a bright yellow precipitate. Extraction of this yellow precipitate with water affords a clear yellow solution and AgCl. When D_2O was used to extract this mixture two C_{2v}-symmetric species formed in an approximate 2:1 ratio as determined by ^{1}H NMR spectroscopy. The major product was the diaqua species **4.3**. Over time **4.3** disappeared with the concomitant formation of the minor product. Heating drives this conversion to completion. The final red-orange product is substantially more soluble in organic solvents compared to water and can be isolated and purified by recrystallization

from acetone–ether mixtures. The IR spectrum of this complex in nujol shows a broad band at 3425 cm^{-1}, indicative of a bound OH group.[7-9] Conductivity experiments in acetone gave a molar conductivity of Λ_M = 335 Ω^{-1} cm^{-1} mol^{-1}, which is on the high end but still consistent with a 2:1 electrolyte.[10] In dry CD_2Cl_2, the complex displays a singlet at –0.85 ppm which integrates to 2 protons, again indicating the presence of a hydroxy group.[11-13] In wet CD_2Cl_2, this peak is often too broad to be observed.

Based on literature precedents and these analytical data, the compound was tentatively as a μ-hydroxo-bridged platinum(II) dimer **4.4** (Figure 1).

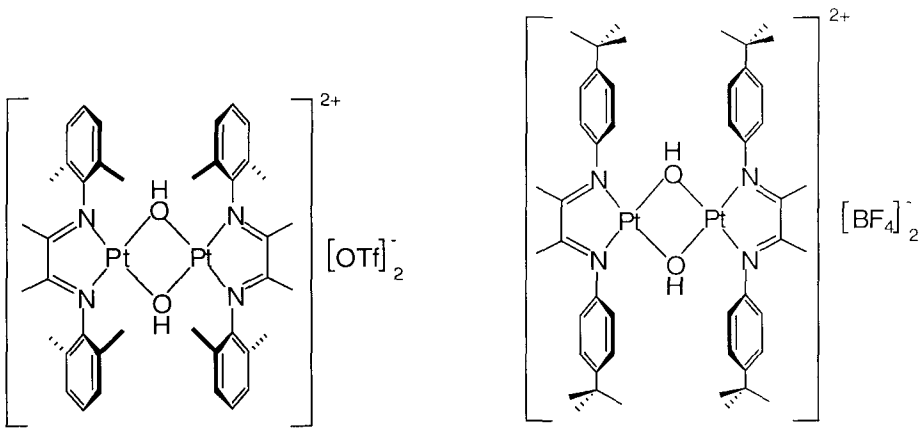

Figure 1. α-aryldiimine ligated μ-hydroxo-bridged dimers of Pt(II).

This assignment has been unequivocally confirmed by x-ray diffraction studies. Red crystals suitable for x-ray diffraction studies were grown by vapor diffusion of ether into an acetone solution of **4.4** (X = OTf) at –40 °C. Figure 2 shows a front view of the complex, confirming its dinuclear structure. Selected bond lengths and bond angles are listed in Table 1.

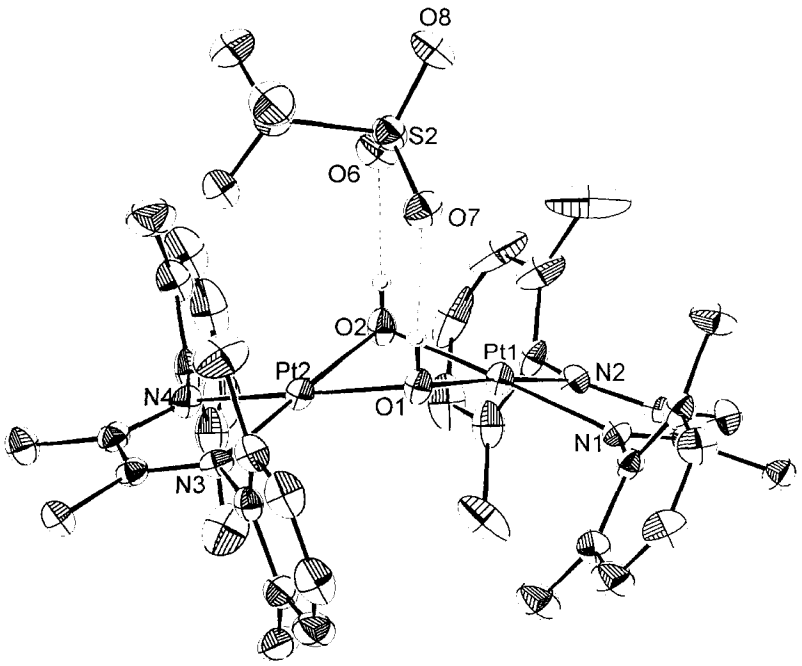

Figure 2. Labeled Diamond drawing of the cationic portion of **4.4** (X = OTf) with ellipsoids at 50% probability. The two OTf anions and a disordered acetone molecule have been omitted for clarity.

Table 1. Selected bond lengths and bond angles for the cationic portion of **4.4** (X = OTf).

	Bond Lengths (Å)		
Pt1–N1	1.987(3)	Pt2–N3	1.982(3)
Pt1–N2	1.983(3)	Pt2–N4	1.975(3)
Pt1–O1	2.034(2)	Pt2–O1	2.049(2)
Pt1–O2	2.019(3)	Pt2–O2	2.028(3)
O1···O7	2.793(4)	Pt1–Pt2	2.9743(3)
O2···O6	2.847(4)		
	Bond Angles (°)		
O1–Pt1–O2	79.52(10)	O1–Pt2–O2	78.97(10)
O1–Pt1–N1	101.70(11)	O1–Pt2–N3	102.74(11)
O1–Pt1–N2	175.55(11)	O1–Pt2–N4	178.29(11)
O2–Pt1–N2	99.68(12)	O2–Pt2–N4	99.58(11)
O2–Pt1–N1	178.64(12)	O2–Pt2–N3	177.87(12)
N1–Pt1–N2	79.05(12)	N3–Pt2–N4	78.69(12)
Pt1–O1–Pt2	93.50(10)	Pt1–O2–Pt2	94.60(11)

Sharp and coworkers have recently reported the synthesis and x-ray crystal structures of a number of μ-hydroxo, μ-amido, μ-methoxy, and μ-chloro bridged dimers of α-diimine-ligated Pt and Pd complexes.[11] Both the Pt–O and Pt–N bond lengths of **4.4** are within the range of those reported by Sharp for the analogous μ-hydroxo-bridged dimer $[(ArN{=}C(Me){-}C(Me){=}NAr)Pt(\mu\text{-}OH)]_2[BF_4]_2$ (Ar = 4-^{t}Bu-C_6H_4), **4.5** (Figure 1) which has average Pt–O bond length of 2.028 Å and average Pt–N bond length of 1.987 Å.[11] The bond angles about the Pt centers in **4.4** are likewise similar to those of **4.5**: the O–Pt–O and N–Pt–N angles are both approximately 80° and the O–Pt–N angles are approximately 100°.

The bridging hydroxo hydrogens in **4.4** were located in the difference Fourier map and each are hydrogen-bonded to two oxygen atoms of a single triflate anion. In **4.5** the hydroxo hydrogens are *trans* to each other while, in **4.4** they adopt a *cis*-configuration. Another major structural difference between **4.4** and **4.5** lies with the dihedral angle between the two planes defined by O1–Pt1–O2 and O1–Pt2–O2. In **4.4**, this value is 142°, whereas a value of 170° is observed in **4.5**.

Both planar and non-planar Pt_2O_2 cores have been observed.[14-16] In general bent structures are favored by a weak metal···metal interaction. This preference is further strengthened when the terminal ligands are good σ-donors or good π-acids.[14] Planar structures are favored when the terminal ligands are π-basic or poor σ-donors.[14] However, because the metal···metal interaction is relatively weak (≤ 5 kcal/mol),[15] steric interactions between the ancillary ligands can often override these electronic considerations.[14,17] For example, most of the reported μ-hydroxo-bridged Pt(II) dimers containing nitrogen-based ligands possess a nearly planar Pt_2O_2 core.[11,18-24] This has been

rationalized in terms of nitrogen based ligands as being poor σ-donors (as compared to phosphines). However, the Pt_2O_2 core of [(2,9-dimethyl-1,10-phenanthroline)Pt(μ-OH)]$_2$[OTf$^-$]$_2$ is severely bent with a dihedral angle of 136.9° due to steric repulsion of the dimethyl substituents between the two halves of the dimer (Figure 3).[25] In contrast the parent [(1,10-phenanthroline)Pt(μ-OH)]$_2$[OTf$^-$]$_2$ is nearly planar (Figure 3).[19]

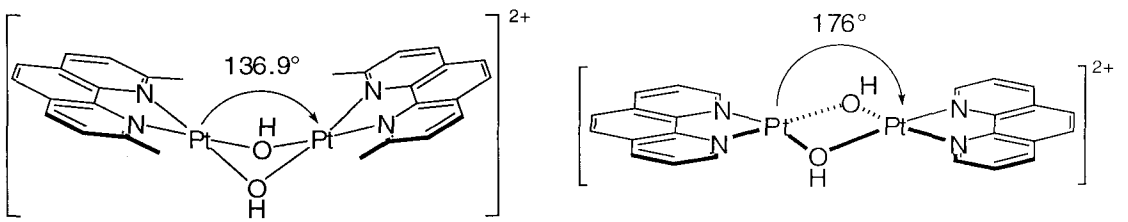

Figure 3. Bent and planar 1,10-phenanthroline based Pt(II) μ-OH bridged dimers.

As can be seen in Figure 2, the 2,6-xylyl rings of the α-diimine ligand are nearly perpendicular (dihedral angles range from 77° – 98°) to the square plane containing the platinum atom and the α-diimine nitrogens, effectively minimizing any steric interactions between the ligands on the two Pt centers. Thus there are no obvious steric repulsions that could account for the bent structure of **4.4**. An electronic preference due to the π-acid character of the α-diimine ligand might be one possible explanation. However, all of the other reported α-diimine containing μ-OH bridged structures reported by Sharp are nearly planar such as **4.5**. The most reasonable explanation to account for the bent structure of **4.4** is that it is a consequence of the hydrogen-bonding between the μ-OH hydrogens and the triflate anion. In order to minimize unfavorable steric interractions between the OTf$^-$ anion coming in from the top (Figure 2) and the aryl groups on the nitrogens, the two Pt centers bend towards each other about the O1–O2 vector. In

solution, this complex is expected to be rapidly interconverting between the bent and planar structures due to the inherently small energy differences between the two configurations.[14]

Cleavage of 4.4 Under Acidic and Basic Conditions in Aqueous Media. The solubility of **4.4** is highly anion-dependent. Whereas the di-triflate salt is slightly soluble in water at neutral pH and ambient temperature, the BF_4^- analog is nearly insoluble. However, refluxing either of the salts in strongly acidic HOTf solution (pH ≤ 1) for an hour resulted in cleavage of the dimer to yield a pale yellow solution of **4.3** (eq 3). Following the reaction by ^1H NMR spectroscopy in a solution of D_2O/ DOTf (~ 0.05 M DOTf) confirms that only **4.3** is left in solution.

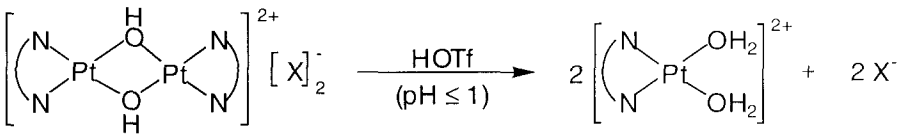

4.4 **4.3** (3)

Figures 4a and 4b show the ^{1}H NMR spectra of **4.4** in neutral D_2O and the resulting diaqua complex **4.3** after refluxing with added DOTf for 1 hour. Figure 5 shows the absorption spectra of the dimer **4.4** and that of the monomer **4.3**. Table 2 lists the absorption maxima and their corresponding molar absorptivities.

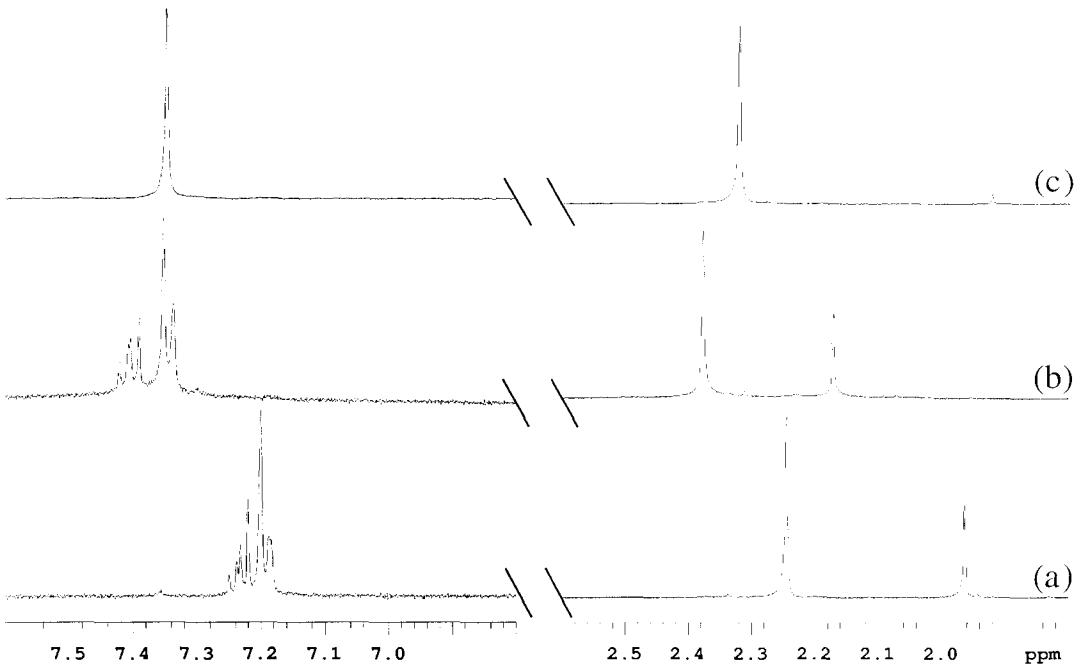

Figure 4. ^{1}H NMR of (a) μ-OH dimer **4.4** (X = OTf^-) in neutral D_2O; (b) diaqua **4.3** in 0.05M DOTf solution; (c) dihydroxy **4.6** in 0.1 M KOH in D_2O solution. (Peak intensities in the aryl and methyl regions are scaled differently.)

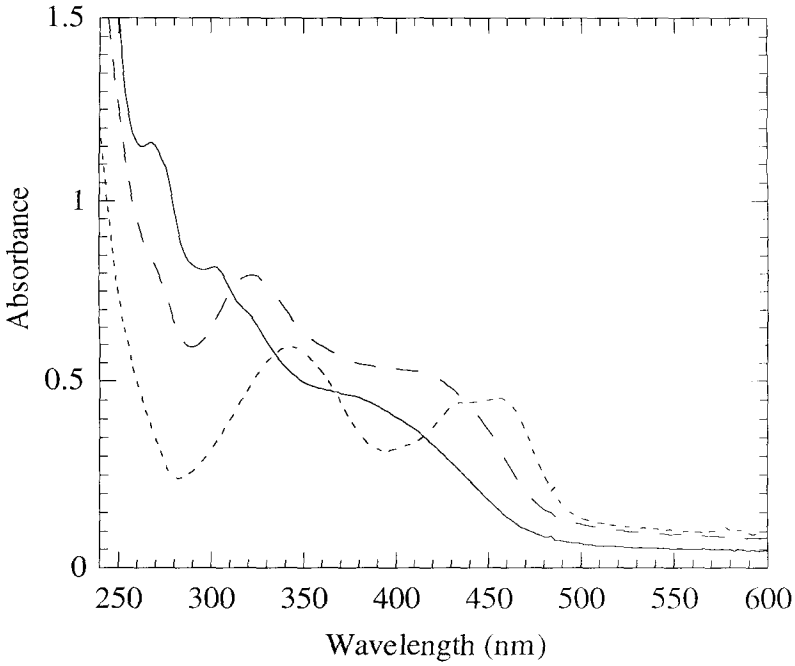

Figure 5. Electronic spectra of **4.3** (——, 1.12 x 10^{-4} M), **4.4** (– – –, 9.27 x 10^{-5} M), and **4.6** (---, 1.52 x 10^{-4} M).

Table 2. Tabulated absorption maxima λ_{max} and molar absorptivities for **4.3**, **4.4**, and **4.6** in aqueous solution.

Complex	λ_{max}, nm (ε, $M^{-1}\cdot cm^{-1}$)			
4.3	268	302	320	374
$[(N\text{-}N)Pt(H_2O)_2][OTf]_2$	(10,368)	(7293)	(6181)	(4138)
4.4	264	322	414	
$[(N\text{-}N)Pt(\mu\text{-}OH)]_2[OTf]_2$	(9562)	(8577)	(5656)	
4.6	342	438	456	
$[(N\text{-}N)Pt(OH)_2$	(3901)	(2915)	(2989)	

Slow addition of an D_2O solution of KOH to **4.4** results in the formation of a new species, which is tentatively assigned as the mononuclear di-hydroxo complex **4.6** by literature precedents (eq 4).[26,27] Its ^1H NMR spectrum is shown in Figure 4c and its

UV/vis trace is shown in Figure 5. In the ^{1}H NMR spectrum of **4.6**, the methyl groups in the backbone of the α-diimine have been almost completely deuterated, as seen by the small peak at δ 1.92 ppm. In addition the singlet in the aryl region integrates to six protons versus the 12 xylyl methyl protons at δ 2.34 ppm. All six protons coincidentally resonate at exactly the same frequency, giving rise to the singlet instead of the expected triplet/doublet pattern. Efforts to prepare and isolate **4.6** by metathesis of the chloride ligands in (ArN=C(Me)–C(Me)=NAr)$PtCl_2$ (Ar = 2,6-$(CH_3)_2C_6H_3$) with NaOH have not yet been successful due to the high solubility of the resulting product in basic solutions.

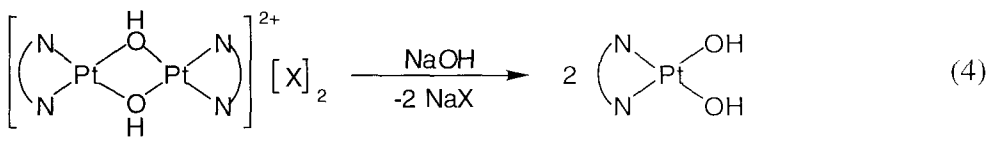

4.4 **4.6** (4)

It is important that the addition of base is slow. If 2 equiv. of aqueous KOH or NaOH were added quickly in one portion to **4.4**, a dark purple precipitate formed. Surprisingly, addition of acid did not re-dissolve this precipitate. In contrast, when base was added slowly in small portions, the purple color precipitate that initially formed quickly dissipated to afford a clear yellow solution.

A similar behavior has been observed for the analogous μ-OH bridged Pt(II) complexes of bipyridine and phenanthroline, where addition of OH^- to aqueous solutions of the dimers $[(N–N)Pt(\mu\text{-}OH)]_2[ClO_4]_2$ (N–N = bipyridine, phenanthroline) deposited red solids formulated to be the trihydroxo-bridged complexes $[(N–N)Pt(\mu\text{-}OH)_3Pt(N–N)]^+$ (eq 5).[7] Conductivity as well as spectrophotometric titrations with NaOH seems to support this formulation where only 1 equiv of OH^- adds to the dimer, although the precise structure is still not known with certainty.[7] Eventual conversion to the known

dihydroxy complex occurred at pH 10. The purple precipitate may be a similar multi-hydroxo bridged species.

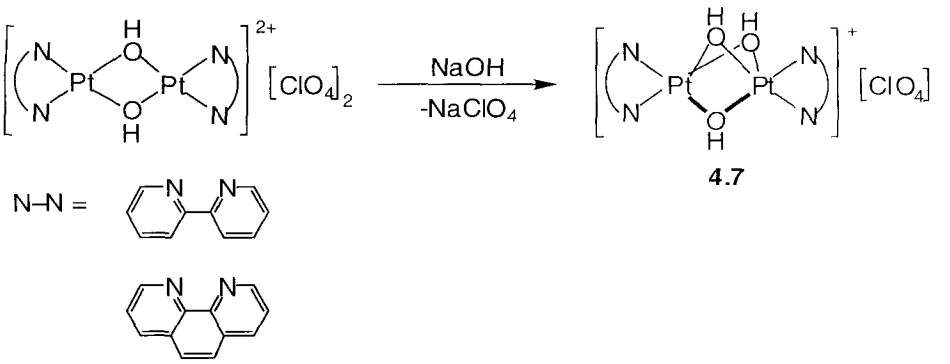

4.7 (5)

Therefore a spectrophotometric titration with 0.100M NaOH was carried out to examine the effect of added base to **4.4**. Figure 6 shows the changes in absorbance of the UV/Vis spectra of **4.4** as 0.22 equivalents of NaOH was added. Isosbestic points are observed at 335 nm, 368 nm, and 425 nm. For every equivalent of dimer in solution 2 equivalents of OH^- was consumed, and is therefore not consistent with a structure such as **4.7**. These spectral changes also indicate that once ~3 equivalents of base per molecule of dimer were introduced, further addition of base led to no additional changes to the spectra.

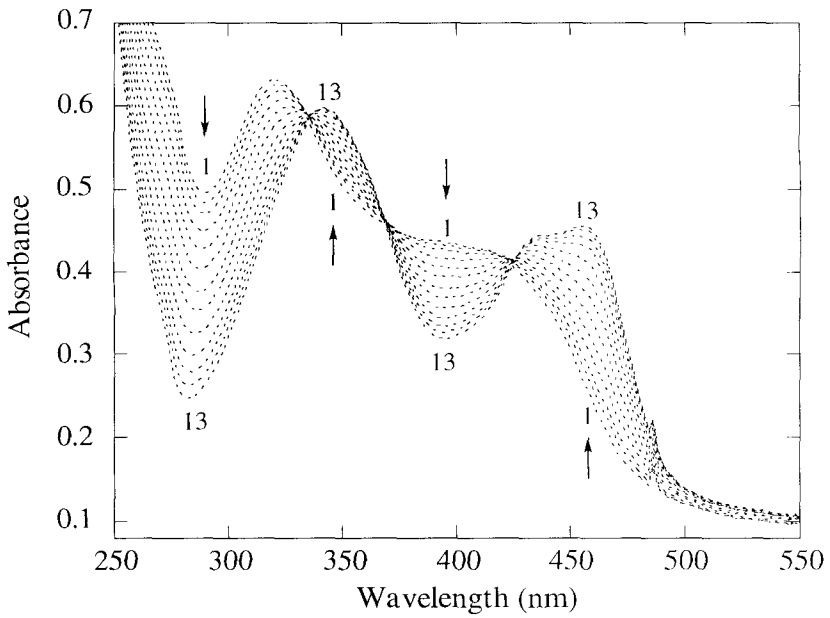

Figure 6. Titration of **4.4** (7.61 x 10^{-5} M) with 0.100M NaOH. Mole ratios of added OH^-:**4.4** are 0:1(trace 1) and 2.8:1(trace 13). Further addition of NaOH does not result in additional changes to trace 13.

Possible Mechanisms for the Formation and Cleavage of the (μ-OH)^2 Dimer

4.4. Bridging hydroxo complexes have been reported for all Group 10 metals.[28] In general these complexes are relatively un-reactive, and have consequently found little application in catalysis. However, there are evidences indicating that the monomeric metal hydroxo- and alkoxo complexes derived from these dimers may be important intermediates in metal catalyzed C–O bond forming reactions.[29-35]

For Pt(II), cationionic μ-hydroxo bridged dimers of the type $[L_2Pt(\mu\text{-}OH)]_2^{2+}$,[14] neutral dimers of the type $[LPt(R)(\mu\text{-}OH)]_2$,[36] and the anionic dimer $[(C_6F_5)_2Pt(\mu\text{-}OH)]_2^{2-}$ are known.[37] Ancilliary ligands in these dimers range from phosphines, arsines, sulfoxides, amines, to aromatic imines. In general the dimers are synthesized in high yield by halide abstraction of a halide containing Pt starting material with Ag salts of

weakly coordinating anions in wet organic solvents. The dimers are formed even in coordinating solvent such as THF, acetone, and ethanol, demonstrating that dimer formation is rather favorable, and is the "thermodynamic sink" for many of the platinum complexes with these ligand systems.

There have been several reports on the studies of the pH dependent equilibria for a number of Pt and Pd complexes containing bidentate and monodentate nitrogen ligands (Scheme 1).[7,26,27,38,39]

Scheme 1

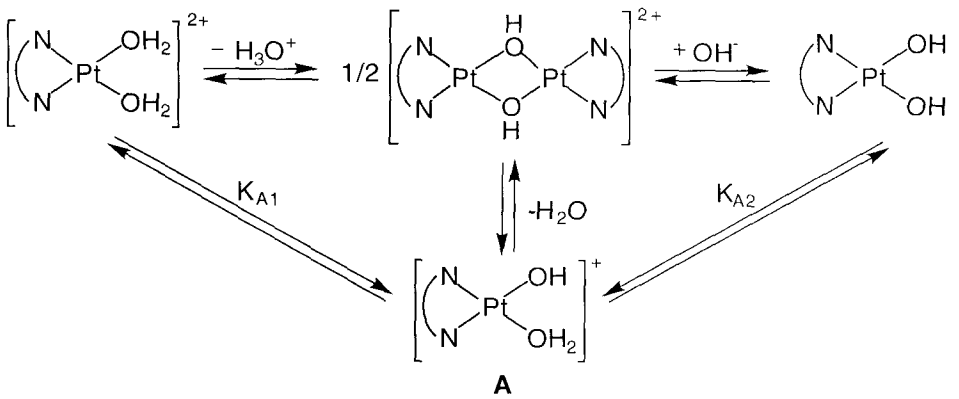

A

In principle, pK_{a1} and pK_{a2}, the first and second acid dissociation constants of the diaquo complexes, can be determined by titration with a strong base. In practice, due to the rapid formation of hydroxo bridged dimers, accurate numbers are often difficult to measure. However, a few accurate determinations of pK_a values have been made for a number of *cis*-diaqua complexes containing amine ligands such as NH_3 (pK_{a1} = 5.93, pK_{a2} = 7.87),[27] *trans*-1,2-diaminocyclohexane (pK_{a1} = 6.14, pK_{a2} = 7.56),[40] and ethylenediamine (pK_{a1} = 5.8, pK_{a2} = 7.6).[39] In these cases, the intermediate **A** is slow to dimerize and can thus be titrated. These data indicate that the aqua ligands are only weakly acidic in the amine and diamine ligated platinum complexes. With imine-type

bidentate N–N ligands such as bipyridine or phenanthroline, however, the diaqua complexes are substantially more acidic. For example, at pH = 2, only the bridged hydroxo dimers are observed.[7]

This enhancement of acidity of the bound water molecules in complexes with chelated imine ligands has been attributed to the π-acid character as well as the weaker σ-donation of the ligands which increases the electrophilicity of the Pt center.[7,26,41] In contrast, the amine based Pt complexes are not as electrophilic because the amine ligands are strictly σ–donating. Qualitatively, the behavior of α-diimine based Pt(II) systems are similar to that of the bipyridine and phenanthroline complexes. For example, only under strongly acidic solutions is the diaqua complex **4.3** stable. Such observations can again be explained by the substantial π-acceptor character of the α-diimine ligands in their bonding to transition metals.[42]

A possible mechanism for the formation and cleavage of **4.4** is shown in Scheme 2. It is likely that the process occurs by a series of proton transfer and ligand substitution steps that proceed through the singly bridged intermediate **C′**. The first step is loss of a proton from the diaqua complex **4.3** to generate **A** . **A** can then react with another equivalent of itself to generate **C′**, but more likely it reacts with another equivalent of **4.3** to give **C** and water. Proton loss to arrive at **C′** is followed by formation of the second OH bridge to yield **4.4** with loss of water. Starting from **4.4**, the reverse of this process will result in cleavage of the dimer, giving back **4.3**.

Scheme 2

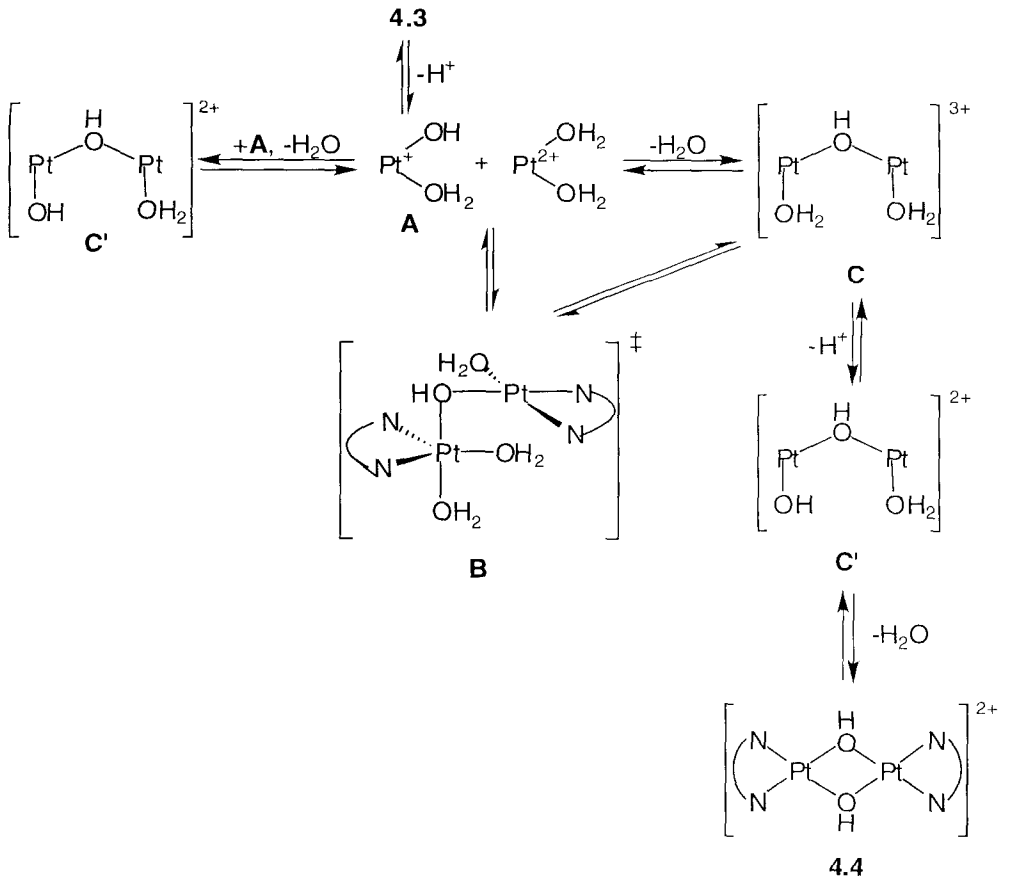

The alternative in which two molecules of **A** form the dimer directly and liberate two equiv of water is unlikely since the microscopic reverse would require that two water molecules simultaneously cleave two hydroxo bridges. Similar singly bridged structures have been invoked as intermediates in the acid or base hydrolysis of μ-$(OH)_2$ bridged dicobalt(III) complexes.[43,44] Additionally, Appleton had reported the synthesis and characterization of such a structure in the hydrolysis of *cis*-$(NH_3)PtCl_2$.

Finally, in addition to the increased acidity imparted by the a-diimine ligand, another reason why dimer formation may be so fast in nitrogen ligands with π-acid character is because these ligands are much better at stabilizing the five coordinate transition structure **B** compared to amine ligands.

Scheme 3

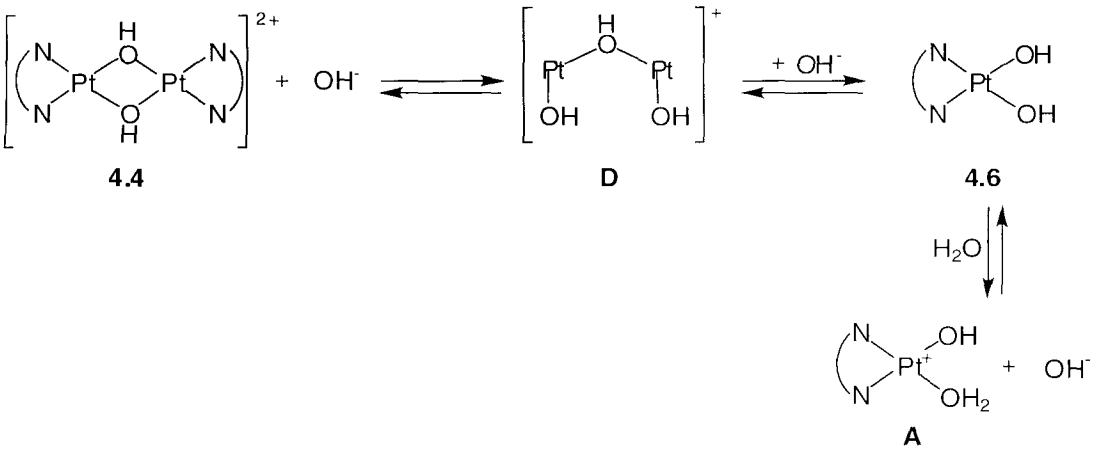

4.4 **D** **4.6** **A**

A possible mechanism that accounts for the 3 equivalents of OH^- used to cleave the dimer **4.4** to the neutral dihydroxo complex **4.6** is shown in Scheme 3. Two equivalents are used to cleave the dimer while the third is necessary in order to shift the equilibrium between **4.6** and **A** towards **4.6**. This is reasonable since one of the Pt–OH groups is expected to be basic. For instance pK_{a2}'s quoted above are all greater than 7. Again the cleavage is expected to be stepwise, proceeding through an intermediate such as **D**. Unfortunately, the formation of the precipitate in the reaction precludes the observation of this intermediate in solution by UV/Vis, and from inspection of the spectra shown in Figure 6, it appears that **4.4** converts to **4.6** in a single step which is misleading.

Protonolysis of the Cation 4.1 in Trifluoroethanol with HOTf. Complex **4.1** is an active complex for the C–H activation of alkanes and arenes at mild temperatures (22 °C for the activation of benzene where L = H_2O, CF_3CH_2OH; 45 °C where L = CH_3CN). As discussed in chapter 3, the methyl group in Pt(II) cations like **4.1** are relatively stable towards protonolysis, in comparison to the dimethyl or methylchloride analogs. However, eventual decomposition of **4.1** to a mixture of products was observed over the

course of several weeks at room temperature in trifluoroethanol solution.[45] One of the major constituents in the decomposition mixture was spectroscopically identified as the μ-OH bridged dimer. It was observed that decomposition was accelerated by high platinum concentrations while retarded by added water. The mechanism by which the dimer forms in this case is still unclear.[45]

Given the propensity of the diaqua complex **4.3** to undergo dimer formation, **4.3** seems like a likely intermediate that is slowly generated by adventitious acid present in solution. Therefore a direct study of the protonolysis of **4.7** (Figure 7) with excess DOTf was undertaken in trifluoroethanol-d_3 (TFE-d_3). DOTf was used in order to keep the amount of water that was introduced into the system to a minimum. Since dimer formation is rapid from the diaqua complex, keeping the amount of water present in the system to a minimum may allow other intermediates to be detected.

Figure 7 shows the result of addition of 5 equiv. of DOTF to a 0.0116 mM solution of **4.7** in 0.7 mL TFE-d_3. After 12 hrs all of the Pt methyl groups have been protonated off the Pt center as CH_4 and CH_3D (spectrum (a)). No other methane isotopomers were identified. From the methyl group region two C_s-symmetric species remain in solution and are tentatively assigned as the OTf^- bound monocations $[(N–N)Pt(OTf)(H_2O)]^+$ (**4.8**) and $[(N–N)Pt(OTf)(TFE\text{-}d_3)]^+$ (**4.9**). The water present is from adventitious water found in the TFE-d_3 solvent.

Addition of 2 μL of D_2O (~ 12 equiv.) immediately results in the formation of the diaqua complex **4.3** as the major species in solution (spectrum (b)). It can be seen here that all of **4.9** has been consumed while there is still a small amount left of the aqua cation. After heating this sample for 24 hrs at 45 °C, resonances for at least two new

species start to appear (spectrum (c)). One of these is the μ-OH bridged dimer **4.4** while the other specie(s), implied by the appearance of a pair of singlets centered around δ 2.0 *ppm* of equal intensity, remains unknown at this time. Due to all the overlapping resonances in the aryl region, more information cannot be obtained. The ratio between **4.3** and the monoaqua complex **4.8** remains the same as in spectrum (b).

The results of adding 15 μL of D_2O and heating for 6 hrs at 60 °C is shown in spectrum (d). Complex **4.8** is no longer present and an approximate 2:1 mixture of diaqua complex **4.3** to μ-OH dimer **4.4** is observed. The pair of mystery singlets are still present and do not seem to be affected by the addition of the D_2O. Spectrum (e) shows the results after heating the sample for a week at 60 °C. Only a small decrease in the

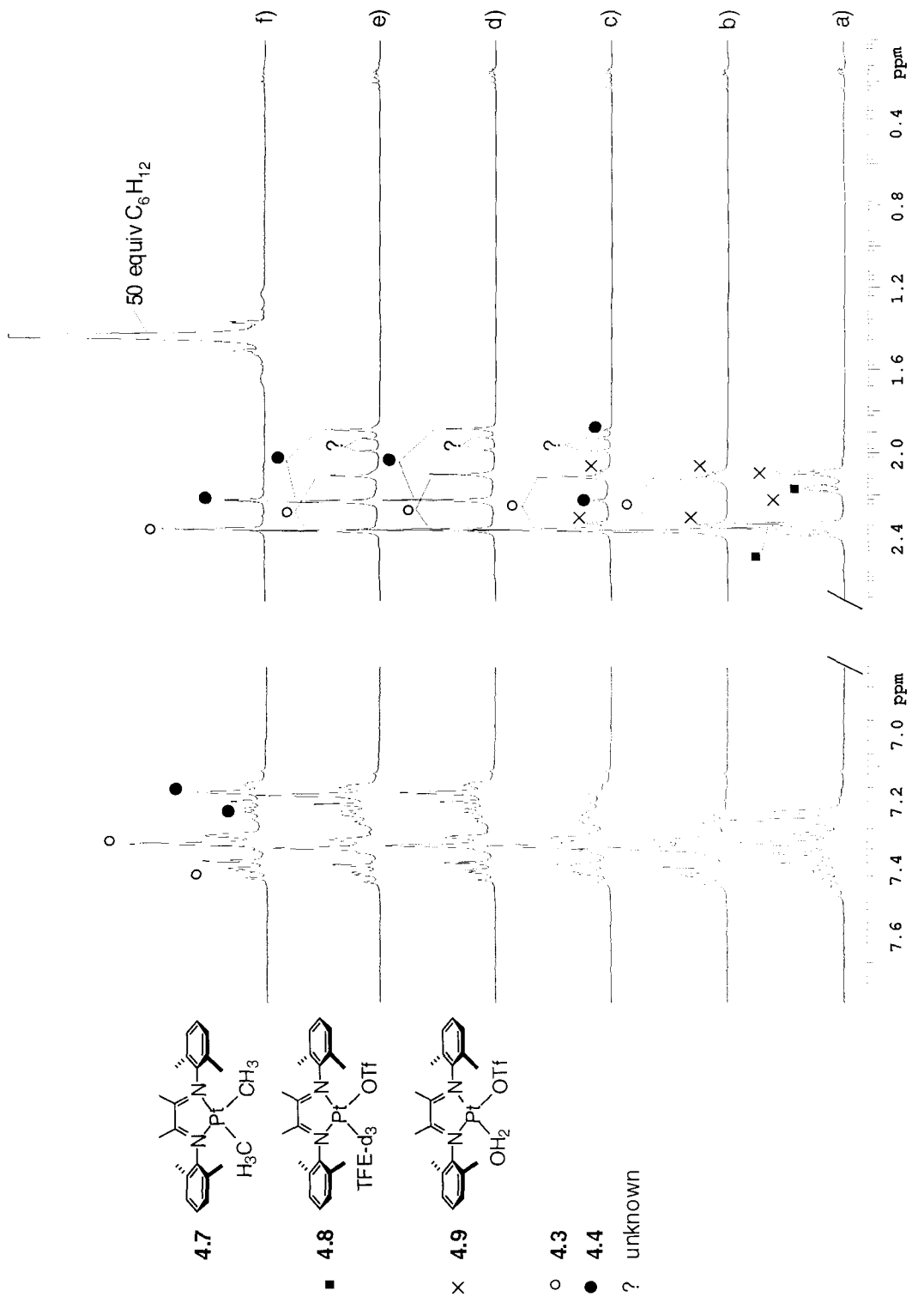

Figure 7. Alkyl and aryl region of the ^{1}H NMR in TFE-d_3 for the protonolysis of **4.7**, with DOTf.

ratio of monomer to dimer is observed compared to spectrum (d), implying that the reaction has reached equilibrium. Additionally, the intensities and position of the unknown pair of singlets at δ 2.0 ppm has not changed.

Since it appeared that an equilibrium mixture of the diaqua and μ-$(OH)_2$ dimer was reached, 50 equivalents of cyclohexane was added and heated to determine if it would undergo C–H activation. Spectrum (f) shows the result of adding 50 equiv of cyclohexane to the reaction mixture and heating for 24 hrs at 130 °C. First it can be seen that the amount of monomer to dimer has slightly increased. Second, the protons of the methyl group on the back bone of the α-diimine ligand of complexes **4.3** and **4.4** have been completely deuterated. Unfortunately, deuterium has not been incorporated into the cyclohexane, which would be an indication that activation of the cyclohexane C–H bonds had occurred. Heating the mixture for another 2 days at 130 °C results in a darkening of the solution to a red-brown color and the formation of a small amount of a black precipitate, which is presumably Pt^0.

From these experiments, it may be concluded that the "decomposition products" observed earlier are variously solvated Pt(II) species where the α-diimine ligand remains intact. Ligand decomposition does not appear to be significant under these conditions. Furthermore, these various species will eventually convert to a mixture of the diaquo and hydroxo-bridged dimers at high enough water concentrations.

Conclusions

The μ-$(OH)_2$ bridged dimer **4.4** has been isolated and characterized by x-ray crystallography. It can be cleaved in strongly acid solutions to the monomeric diaqua

complex **4.3**, or under basic conditions to yield the neutral dihydroxo complex **4.6**. Protonolysis of the dimethyl complex **4.7** in TFE–d_3 with excess DOTf and a minimal amount of water shows that first the monocations **4.8** and **4.9** are generated. Addition of water generates a mixture of the diaqua and μ-$(OH)_2$ bridged dimer complexes. Unfortunately, these complexes do not appear to activate alkane C–H bonds under typical shilov conditions. It is possible that due to the 2+ charge at the metal center, oxidative addition of the C–H bond is no longer favorable compared to the monocationic systems.

Experimental

General Considerations. All air and moisture sensitive compounds were manipulated using standard high-vacuum line, Schlenk line or cannula techniques, or in a nitrogen atmosphere glove box as previously described.[46] Solvents were dried over sodium/benzophenone ketyl (toluene, THF, Et_2O, petroleum ether), CaH_2 (CH_2Cl_2), Drierite (acetone), and 3Å molecular sieves/$NaHCO_3$ (trifluroethanol-d_3). Zeise's salt ($K[Cl_3Pt(C_2H_4)]\cdot H_2O$) and Zeise's dimer $[(PtCl_2(C_2H_4)]_2$ were purchased from Strem Chemicals. All silver salts were purchased from Aldrich and stored a glove box. (N–N)$PtCl_2$ (N–N = 2,6-$(CH_3)_2C_6H_3N$=C(Me)–C(Me)N=2,6-$(CH_3)_2C_6H_3$) was prepared as in chapter 3. **4.1** was prepared as previously described.[47] NMR spectra were recorded on Varian ^{UNITY}*INOVA* 500 (^{1}H, 499.853 MHz; ^{13}C, 125.701 MHz) or a Varian *Mercury-VX* 300 (^{1}H, 300.1 MHz; ^{19}F, 282.081 MHz; ^{13}C, 125.701 MHz) spectrometer. All ^{1}H NMR shifts are relative to the residual NMR solvent. X-ray structure determinations were performed on a Bruker SMART 1000 CCD detector under a cold stream of N_2 gas. Data reduction was done with Bruker SAINT v6.2. All structures were solved by direct

methods using SHELXS-97 and refined with SHELXL-97. Elemental Analyses were performed at either the Caltech Elemental Analysis Facility or by Midwest Microlab, Indianapolis, IN.

[(ArN=C(Me)–C(Me)=NAr)Pt(μ-OH)]$_2$OTf$_2$ (Ar = 2,6-(CH$_3$)$_2$C$_6$H$_3$) 4.4. (N–N)PtCl$_2$ (300 mg, 0.537 mmol) and AgOTf (283 mg, 1.10 mmol) were added as solids together and suspended in CH_2Cl_2 (50 mL). Acetone (2 mL) to ensure that the AgOTf dissolved. The mixture was stirred vigorously overnight covered in foil. Solvent was then removed in vacuo and extracted with water (50 mL). A small amount of acetone (2 mL) is used to extract the last bit of yellow color out of the precipitate. If the reaction were run on 30 mg or less of Pt, acetone was not used. The solvent was then removed under vacuo. To the resulting red-orange residue was added water (50 mL) which yield a red-orange solid and a yellow solution. The solution was concentrated to ~ 10 mL and the solid was filtered. Drying under vacuo afforded a rust colored solid. Yield: 235 mg (67%) ^{1}H NMR (D_2O, δ): 7.23 (t, 2H, $^3J_{HH}$ = 7.4 Hz, *p*-H on 2,6-(CH$_3$)$_2$C$_6$*H*$_3$), 7.20 (d, 4H, $^3J_{HH}$ = 7.4 Hz, *m*-H on 2,6-(CH$_3$)$_2$C$_6$*H*$_3$), 2.24 (s, 12H, H on 2,6-(C*H*$_3$)$_2$C$_6$H$_3$), 1.96 (s, 6H, N=CC*H*$_3$). ^{1}H NMR (CD_2Cl_2, δ): OH observed at –0.85. IR (nujol): 3424.6 cm^{-1} (OH); 1457.8, 1376.4 (C=N). ^{13}C{^{1}H} NMR ((CD$_3$)$_2$CO, δ): 183.65, 142.33, 130.98, 129.9, 129.73, 122.20 (q, $^1J_{C\text{-}F}$ = 326.6 Hz) 19.17, 17.84. Anal. Calcd. for $C_{42}H_{50}F_6N_4O_8Pt_2S_2$ (Found): C, 38.59 (37.48); H, 3.86 (3.71); N, 4.29 (4.53). Anal. Calcd. for BF_4^- salt, $C_{40}H_{50}B_2F_8N_4O_2Pt_2$ (Found): C, 40.62 (37.69); H, 4.26 (4.28); N, 4.74 (4.71). Molar conductivity was carried out on BF_4^- salt. Λ = 335 Ω^{-1} cm^{-1} mol^{-1}.

[(ArN=C(Me)–C(Me)=NAr)Pt(H_2O)$_2$]OTf_2 (Ar = 2,6-$(CH_3)_2C_6H_3$) 4.3. The yellow filtrate above is lyophilized to yield a yellow solid. This solid slowly turns slightly orange standing at room temperature for a day. ^{1}H NMR (D_2O/(4 μL DOTf), δ): 7.40 (t, 2H, $^3J_{HH}$ = 8.4 Hz, *p*-H on 2,6-$(CH_3)_2C_6H_3$), 7.34 (d, 4H, $^3J_{HH}$ = 8.4 Hz, *m*-H on 2,6-$(CH_3)_2C_6H_3$), 2.38 (s, 12H, H on 2,6-$(CH_3)_2C_6H_3$), 2.17 (s, 6H, N=CCH_3).

Protonation of 4.7 in TFE-d_3. To a screw cap nmr tube equipped with a rubber septum was added **4.7** (4.2 mg, 0.00811 mmol). The solid was suspended in TFE-d_3 (0.7 mL). Next DOTf (3.6 μL, 0.0406 mmol) was added through the septum. Immediately the suspension dissolved to give a clear yellow solution. The first spectrum acquired after addition shows that one methyl group has been immediately protonated off the metal to yield a mixture of the methyl aqua cation and the methyl TFE cation. The sample was then heated in a constant temperature bath for the times described in the text.

X-ray Structure Determination 4.4. Red blocks of **4.4** suitable for x-ray structure determinations were grown by layering concentrated solutions of **4.4** (acetone) with Et_2O at –40 °C. The crystal was mounted on a glass fiber with Paratone–N oil. Data was collected at low temperature. Five runs of data were collected with 15 second long, -0.3° wide ω-scans at five values of φ (0, 120, 240, 180, and 300°) and Θ at –28° The position of the hydrogen atoms of the OH bridge were located in the difference Fourier map. Absorption correction was not necessary.

References and Notes

1. Stahl, S. S.; Labinger, J. A.; Bercaw, J. E. *J. Am. Chem. Soc.* **1996**, *118*, 5961.
2. Stahl, S. S.; Labinger, J. A.; Bercaw, J. E. *J. Am. Chem. Soc.* **1995**, *117*, 9371.
3. Holtcamp, M. W.; Labinger, J. A.; Bercaw, J. E. *Inorg. Chim. Acta* **1997**, *265*, 117.
4. Holtcamp, M. W.; Labinger, J. A.; Bercaw, J. E. *J. Am. Chem. Soc.* **1997**, *119*, 848.
5. Zamashchikov, V. V.; Rudakov, E. S.; Yaroshenko, A. P. *React. Kinet. Catal. Lett.* **1983**, *22*, 39.
6. Labinger, J. A.; Herring, A. M.; Bercaw, J. E. *Adv. Chem. Ser.* **1992**, *230*, 221.
7. Wimmer, S.; Castan, P.; Wimmer, F. L.; Johnson, N. P. *J. Chem. Soc.-Dalton Trans.* **1989**, 403.
8. Casellato, U.; Vitago, P. A.; Vidali, M. *Coord. Chem. Rev.* **1981**, *36*, 183.
9. Addison, C. C.; Sutton, D. *Prog. Inorg. Chem.* **1967**, *8*, 195.
10. Geary, W. J. *Coord. Chem. Rev.* **1971**, *7*, 81.
11. Kannan, S.; James, A. J.; Sharp, P. R. *Polyhedron* **2000**, *19*, 155.
12. Bandini, A. L.; Banditelli, G.; Demartin, F.; Manassero, M.; Minghetti, G. *Gazz. Chim. Ital.* **1993**, *123*, 417.
13. Lopez, G.; Ruiz, J.; Garcia, G.; Vicente, C.; Marti, J. M.; Hermoso, J. A.; Vegas, A.; Martinez-Ripoll, M. J. *J. Chem. Soc.-Dalton Trans.* **1992**, 53.
14. Aullon, G.; Ujaque, G.; Lledos, A.; Alvarez, S. *Chem. Eur. J.* **1999**, *5*, 1391.
15. Aullon, G.; Ujaque, G.; Lledos, A.; Alvarez, S.; Alemany, P. *Inorg. Chem.* **1998**, *37*, 804.

16. Capdevila, M.; Clegg, W.; Gonzalez-Duarte, P.; Lledos, A. *Inorg. Chem.* **1996**, *35*, 490.

17. Connick, W. B.; Marsh, R. E.; Schaefer, W. P.; Gray, H. B. *Inorg. Chem.* **1997**, *36*, 913.

18. Schnebeck, R.-D.; Freisinger, E.; Lippert, B. *Eur. J. Inorg. Chem.* **2000**, 1193.

19. Fekl, U.; van Eldik, R. *Eur. J. Inorg. Chem.* **1998**, 389.

20. Koz'min, P. A.; Fedorova, T. N.; Kuznetsova, G. N.; Surazhskaya, M. D.; Baranovsky, I. B. *Zh. Neorg. Khim.* **1997**, *42*, 1834.

21. Rochon, F. D.; Melanson, R.; Morneau, A. *Magn. Reson. Chem.* **1992**, 697.

22. Min, D.; Larsen, R. D.; Emerson, K.; Abbott, E. H. *Inorg. Chem.* **1990**, *29*, 73.

23. Lippert, B.; Lock, C. J. L.; Rosenberg, B.; Zvagulis, M. *Inorg. Chem.* **1978**, *17*, 2971.

24. Faggiani, R.; Lippert, B.; Lock, C. J. L.; Rosenberg, B. *J. Am. Chem. Soc.* **1977**, *99*, 777.

25. Fekl, U.; van Eldik, R.; Richardson, C.; Robinson, W. T. *Inorg. Chem.* **2001**, *40*, 3247.

26. Wimmer, F. L.; Wimmer, S.; Afcharian, A.; Castan, P.; Fabre, P. L. *J. Chem. Res.* **1999**, *(M)*, 1048.

27. Appleton, T. G.; Hall, J. R.; Ralph, S. F.; Thompson, C. S. M. **1989**, *28*, 1989.

28. Grushin, V. V.; Alper, H. *Organometallics* **1996**, *15*, 5242.

29. Paneghetti, C.; Gavagnin, R.; Pinna, F.; Strukul, G. *Organometallics* **1999**, *18*, 5057.

30. Fujii, A.; Hagiwara, M.; Sodeoka, M. *J. Am. Chem. Soc.* **1999**, *121*, 5450.

31. Strukul, G. *Angew. Chem., Int. Ed. Engl.* **1998**, *37*, 1198.

32. Hamed, O.; Henry, P. M. *Organometallics* **1997**, *16*, 4903.

33. Ganguly, S.; Mague, J. T.; Roundhill, D. M. *Inorg. Chem.* **1992**, *31*, 3831.

34. Backvall, J.-E.; Bjorkman, E. E.; Pettersson, L.; Siegbahn, J. *J. Am. Chem. Soc.* **1985**, *107*, 7265.

35. Backvall, J.-E.; Bjorkman, E. E.; Pettersson, L.; Siegbahn, J. *J. Am. Chem. Soc.* **1984**, *106*, 4369.

36. Slawin, A. M. Z.; Smith, M. B.; Woollins, J. D. *J. Chem. Soc.-Dalton Trans.* **1996**, 4567.

37. Ruiz, J.; Cutillas, N.; Samperdo, J.; Lopez, G.; Hermoso, J. A. *J. Organomet. Chem.* **1996**, *526(1)*, 67.

38. Barton, S. J.; Barnham, K. J.; Habtemariam, A.; Sue, R. E.; Sadler, P. J. *Inorg. Chim. Acta* **1998**, *273*, 8.

39. Lim, M. C.; Martin, R. B. *J. Inorg. Nucl. Chem.* **1976**, *38*, 1911.

40. Gill, D. S.; Rosenberg, B. *J. Am. Chem. Soc.* **1982**, *104*, 4598.

41. Rendina, L. M.; Puddephatt, R. J. *Chem. Rev.* **1997**, *97*, 1735.

42. Van Koten, G.; Vrieze, K. *Adv. Organomet. Chem.* **1982**, *21*, 151.

43. El-Awady, A. A.; Hugus, Z. Z. J. *Inorg. Chem.* **1971**, *10*, 1415.

44. Hoffman, A. B.; Taube, H. *Inorg. Chem.* **1968**, *7*, 903.

45. Zhong, H. A.; Labinger, J. A.; Bercaw, J. E.; submitted for publication.

46. Burger, B. J.; Bercaw, J. E. In *Experimental Organometallic Chemistry*; ACS Symposium Series 357; Wayda, A. L., Darensbourg, M. Y., Eds.; American Chemical Society: Washington, DC, 1987; pp 79.

47. Johansson, L.; Tilset, M.; Labinger, J. A.; Bercaw, J. E. *J. Am. Chem. Soc.* **2000**, *122*, 10846.

Appendix 1

X-ray Crystallographic Data for 1.13a

Table 1. Crystal data and structure refinement for AWF19 (CCDC 163000).

Empirical formula	$C_{20}H_{41}BCl_2NSi_2Zr$ $(C_6H_{14}N_2)_2Li$
Formula weight	759.97
Crystallization Solvent	THF/petroleum ether
Crystal Habit	Plate
Crystal size	0.25 x 0.22 x 0.04 mm^3
Crystal color	Purple

Data Collection

Preliminary Photos	Rotation
Type of diffractometer	CCD area detector
Wavelength	0.71073 Å MoKα
Data Collection Temperature	98(2) K
θ range for 9996 reflections used in lattice determination	2.15 to 28.44°
Unit cell dimensions	a = 11.9650(11) Å b = 15.2494(15) Å β= 95.956(2)° c = 23.179(2) Å
Volume	4206.5(7) $Å^3$
Z	4
Crystal system	Monoclinic
Space group	$P2_1/n$
Density (calculated)	1.200 Mg/m^3
F(000)	1624
Data collection program	Bruker SMART
θ range for data collection	1.60 to 28.53°
Completeness to θ = 28.53°	94.1 %
Index ranges	$-15 \le h \le 16$, $-20 \le k \le 20$, $-31 \le l \le 30$
Data collection scan type	ω scans at 5 ϕ settings
Data reduction program	Bruker SAINT v6.2
Reflections collected	61580
Independent reflections	10057 [R_{int}= 0.2142]
Absorption coefficient	0.472 mm^{-1}
Absorption correction	None
Max. and min. transmission (calculated)	0.9827 and 0.8907

Table 1 (cont.)

Structure solution and Refinement

Structure solution program	SHELXS-97 (Sheldrick, 1990)
Primary solution method	Direct methods
Secondary solution method	Difference Fourier map
Hydrogen placement	Geometric positions
Structure refinement program	SHELXL-97 (Sheldrick, 1997)
Refinement method	Full matrix least-squares on F^2
Data / restraints / parameters	10057 / 0 / 416
Treatment of hydrogen atoms	Riding
Goodness-of-fit on F^2	1.394
Final R indices [I>2σ(I), 5514 reflections]	R1 = 0.0736, *w*R2 = 0.1252
R indices (all data)	R1 = 0.1504, *w*R2 = 0.1389
Type of weighting scheme used	Sigma
Weighting scheme used	$w=1/\sigma^2(Fo^2)$
Max shift/error	0.004
Average shift/error	0.000
Largest diff. peak and hole	1.201 and -1.282 e.Å^{-3}

Special Refinement Details

The largest peaks in the final difference Fourier were associated with the lithium counterion.

Refinement of F^2 against ALL reflections. The weighted R-factor (*w*R) and goodness of fit (S) are based on F^2, conventional R-factors (R) are based on F, with F set to zero for negative F^2. The threshold expression of $F^2 > 2\sigma(F^2)$ is used only for calculating R-factors(gt) etc. and is not relevant to the choice of reflections for refinement. R-factors based on F^2 are statistically about twice as large as those based on F, and R-factors based on ALL data will be even larger.

All esds (except the esd in the dihedral angle between two l.s. planes) are estimated using the full covariance matrix. The cell esds are taken into account individually in the estimation of esds in distances, angles and torsion angles; correlations between esds in cell parameters are only used when they are defined by crystal symmetry. An approximate (isotropic) treatment of cell esds is used for estimating esds involving l.s. planes.

Appendix 2

X-ray Crystallographic Data for 1.14a

Table 1. Crystal data and structure refinement for AWF10.

Empirical formula	$C_{33}H_{69}BCl_2LiN_5SiZr$
Formula weight	743.89
Crystallization Solvent	Heptane/TMEDA/THF
Crystal Habit	Block
Crystal size	0.37 x 0.37 x 0.29 mm^3
Crystal color	Deep Blue

Data Collection

Preliminary Photos	None	
Type of diffractometer	CAD-4	
Wavelength	0.71073 Å MoKα	
Data Collection Temperature	85 K	
Theta range for reflections used in lattice determination	15.5 to 16.2°	
Unit cell dimensions	a = 16.287(3) Å b = 11.569(2) Å c = 21.570(4) Å	α= 90° β= 90° γ = 90°
Volume	4064.3(13) $Å^3$	
Z	4	
Crystal system	Orthorhombic	
Space group	$Pna2_1$	
Density (calculated)	1.216 Mg/m^3	
F(000)	1592	
Theta range for data collection	1.6 to 27.5°	
Completeness to θ = 27.47°	99.9 %	
Index ranges	$0 \le h \le 21, -15 \le k \le 15, -20 \le l \le 27$	
Data collection scan type	ω scans	
Reflections collected	11734	
Independent reflections	5927 [R_{int}= 0.0263; GOF_{merge}= 1.13]	
Absorption coefficient	0.459 mm^{-1}	
Absorption correction	None	
Number of standards	3 reflections measured every 75min.	
Variation of standards	-0.24%.	

Table 1 (cont.)

Structure solution and Refinement

Structure solution program	SHELXS-97 (Sheldrick, 1990)
Primary solution method	Direct methods
Secondary solution method	Difference Fourier map
Hydrogen placement	Calculated sites
Structure refinement program	SHELXL-97 (Sheldrick, 1997)
Refinement method	Full matrix least-squares on F^2
Data / restraints / parameters	5927 / 38 / 430
Treatment of hydrogen atoms	Fixed geometry, B(H)=1.2B(C)
Goodness-of-fit on F^2	2.535
Final R indices [I>2σ(I)]	R1 = 0.0483, wR2 = 0.1002
R indices (all data)	R1 = 0.0555, wR2 = 0.1019
Type of weighting scheme used	Observed
Weighting scheme used	$w=1/\sigma^2(Fo^2)$
Max shift/error	0.000
Average shift/error	0.000
Absolute structure parameter	-0.10(5)
Largest diff. peak and hole	1.732 and -1.543 e.$Å^{-3}$

Special Refinement Details

Disorder is observed in the borylide ligand. The tri-methylsilyl and the tertiarybutyl groups bonded to N1 have alternate positions where they swap places. The disorder ratio is approx. 70:30. The major component was refined with anisotropic displacement parameters and the minor component was refined isotropically. Both components were restrained. The minor component was restrained to the geometry of the major component. The nitrogen-silicon and nitrogen-carbon distances were restrained to chemically reasonable values. The carbon-carbon distances of the tertiarybutyl group were also restrained. The tertiary carbon of the tertiarybutyl group required restraints on the anisotropic displacement parameter in order to keep it positive definite.

Refinement of F^2 against ALL reflections. The weighted R-factor (wR) and goodness of fit (S) are based on F^2, conventional R-factors R are based on F, with F set to zero for negative F^2. The threshold expression of $F^2 > 2\_(F^2)$ is used only for calculating R-factors(gt) etc. and is not relevant to the choice of reflections for refinement. R-factors based on F^2 are statistically about twice as large as those based on F, and R- factors based on ALL data will be even larger.

All esds (except the esd in the dihedral angle between two l.s. planes) are estimated using the full covariance matrix. The cell esds are taken into account individually in the estimation of esds in distances,

angles and torsion angles; correlations between esds in cell parameters are only used when they are defined by crystal symmetry. An approximate (isotropic) treatment of cell esds is used for estimating esds involving l.s. planes.

Appendix 3

X-ray Crystallographic Data for 1.15

Table 1. Crystal data and structure refinement for AWF11.

Empirical formula	$(C_{22}H_{38}BCl_2LiN_2Zr)_2$
Formula weight	1020.82
Crystallization Solvent	Heptane
Crystal Habit	Rhomboid
Crystal size	0.33 x 0.33 x 0.22 mm^3
Crystal color	Red

Data Collection

Preliminary Photos	None	
Type of diffractometer	CAD-4	
Wavelength	0.71073 Å MoKα	
Data Collection Temperature	85 K	
θ range for reflections used in lattice determination	12.8 to 16.8°	
Unit cell dimensions	a = 13.165(11) Å b = 13.31(3) Å c = 16.992(10) Å	α= 91.95(12)° β= 106.19(6)° γ = 118.08(13)°
Volume	2475(6) $Å^3$	
Z	2	
Crystal system	Triclinic	
Space group	P-1	
Density (calculated)	1.370 Mg/m^3	
F(000)	1064	
θ range for data collection	1.77 to 22.47°	
Completeness to θ = 22.47°	100.0 %	
Index ranges	$-14 \le h \le 13, -14 \le k \le 14, -18 \le l \le 18$	
Data collection scan type	ω scans	
Reflections collected	15332	
Independent reflections	6464 [R_{int}= 0.036; GOF_{merge}= 1.90]	
Absorption coefficient	0.671 mm^{-1}	
Absorption correction	Not measured	
Number of standards	Not measured	
Variation of standards	Not measured	

Table 1 (cont.)

Structure solution and Refinement

Structure solution program	SHELXS-97 (Sheldrick, 1990)
Primary solution method	Direct methods
Secondary solution method	Difference Fourier map
Hydrogen placement	Calculated geometric sites
Structure refinement program	SHELXL-97 (Sheldrick, 1997)
Refinement method	Full matrix least-squares on F^2
Data / restraints / parameters	6464 / 348 / 523
Treatment of hydrogen atoms	Restrained
Goodness-of-fit on F^2	6.801
Final R indices [$I>2\sigma(I)$]	R1 = 0.1596, *w*R2 = 0.3301
R indices (all data)	R1 = 0.1779, *w*R2 = 0.3320
Type of weighting scheme used	Sigma
Weighting scheme used	$w=1/\sigma^2(Fo^2)$
Max shift/error	0.003
Average shift/error	0.000
Largest diff. peak and hole	5.466 and -1.850 e.Å^{-3}

Special Refinement Details

The crystals of AWF11 did not diffract x-rays well and this structure determination was undertaken for the sole purpose of determining the molecular connectivity.

The crystal structure of this compound contains two molecules in the unit cell and therefore one molecule in the asymmetric unit. However one molecule sits on a center of symmetry at x=_, y=_, z=_ and the other sits on a center of symmetry at x=_, y=0, z=0. This means that the asymmetric unit contains only one-half of each molecule rather than one connected molecule. The drawings therefore have only half the atoms labeled because the others are related by an inversion center in the center of the molecule.

The variances [$\sigma^2(Fo^2)$] were derived from counting statistics plus an additional term, $(0.014I)^2$, and the variances of the merged data were obtained by propagation of error plus the addition of another term, $(0.014<I>)^2$.

Refinement of F^2 against ALL reflections. The weighted R-factor (*w*R) and goodness of fit (S) are based on F^2, conventional R-factors (R) are based on F, with F set to zero for negative F^2. The threshold expression of $F^2 > 2\sigma(F^2)$ is used only for calculating R-factors(gt) etc. and is not relevant to the choice of reflections for refinement. R-factors based on F^2 are statistically about twice as large as those based on F, and R-factors based on ALL data will be even larger.

All esds (except the esd in the dihedral angle between two l.s. planes) are estimated using the full covariance matrix. The cell esds are taken into account individually in the estimation of esds in distances, angles and torsion angles; correlations between esds in cell parameters are only used when they are defined by crystal symmetry. An approximate (isotropic) treatment of cell esds is used for estimating esds involving l.s. planes.

Appendix 4

X-ray Crystallographic Data for 1.16a

Table 1. Crystal and Intensity Collection Data for

AWF4: Cp* Diphenyl, DiMeAminoborollide $ZrCl_2 \cdot Li(THF)_4 \cdot$ Solvent

Formula: $C_{49.2}H_{65}BCl_2LiNO_4Zr$	Formula weight: 914.34
Crystal color: Dichroic bl-gr, rd-br	Habit: Plates, needles
Crystal size: $0.26 \times 0.30 \times 0.37$ mm	$\rho_{calc} = 1.264$ g cm^{-3}
Crystal System: Monoclinic	Space group: $P2_1/n$ (#14)
$a = 11.753(5)$Å	
$b = 33.270(12)$Å	$\beta = 96.91(3)^\circ$
$c = 12.368(4)$Å	
V = 4801.0(30)Å^3	$Z = 4$
Lattice parameters: 25 reflections,	$11.5\ ^\circ \leq \theta \leq 12.5^\circ$
$\mu = 3.82$ cm^{-1}	
CAD-4 diffractometer	ω scan
MoKα, $\lambda = 0.71073$Å	Graphite monochromator
2θ range: 3°–50°	$-13 \leq h \leq 13, -39 \leq k \leq 39, 0 \leq l \leq 14$
T = 160K	$F_{000} = 1924.8$
Number of reflections measured: 19479	Number of independent reflections: 8409
Number with $F_o^2 > 0$: 7144	Number with $F_o^2 > 3\sigma(F_o^2)$: 4817
Standard reflections: Three, every hour	Variation: 0.78% total decay
GOF_{merge} : 1.34 for 8081 multiples	R_{merge} : 0.069 for 5045 duplicates
Number used in refinement: 8409	Criterion: All reflections used

Final R(F_o): 0.061 for 4817 reflections with $F_o^2 > 3\sigma(F_o^2)$

Final R(F_o): 0.097 for 7144 reflections with $F_o^2 > 0$

Final weighted R(F_o^2) : 0.122 for 8409 reflections

Final goodness of fit: 1.84 for 527 parameters and 8409 reflections

$(\Delta/\sigma)_{max}$ in final least squares cycle: 0.00

$\Delta\rho_{max}$: 0.85 eÅ^{-3}, $\Delta\rho_{min}$: -0.92 eÅ^{-3} in final difference map

Appendix 5

X-ray Crystallographic Data for 3.12

Table 1. Crystal data and structure refinement for AWF16 (CCDC 166553).

Empirical formula	$C_{31}H_{32}N_3Pt\,BF_4$
Formula weight	728.50
Crystal Habit	Plate
Crystal size	0.22 x 0.14 x 0.04 mm^3
Crystal color	Brown/yellow

Data Collection

Preliminary Photos	Rotation
Type of diffractometer	CCD area detector
Wavelength	0.71073 Å MoKα
Data Collection Temperature	98(2) K
θ range for 14812 reflections used in lattice determination	2.77 to 27.78°
Unit cell dimensions	a = 10.5686(14) Å b = 11.8223(15) Å β= 106.199(2)° c = 11.9120(16) Å
Volume	1429.3(3) $Å^3$
Z	2
Crystal system	Monoclinic
Space group	$P2_1$
Density (calculated)	1.693 Mg/m^3
F(000)	716
Data collection program	Bruker SMART
θ range for data collection	1.78 to 28.45°
Completeness to θ = 28.45°	95.2 %
Index ranges	$-13 \le h \le 13, -15 \le k \le 15, -15 \le l \le 15$
Data collection scan type	ω scans at 8 ϕ settings
Data reduction program	Bruker SAINT v6.2
Reflections collected	27944
Independent reflections	6691 [R_{int}= 0.1045]
Absorption coefficient	4.960 mm^{-1}
Absorption correction	Not applied
Max. and min. transmission (Calculated)	0.8455 and 0.4110

Table 1 (cont.)

Structure solution and Refinement

Structure solution program	SHELXS-97 (Sheldrick, 1990)
Primary solution method	Patterson method
Secondary solution method	Difference Fourier map
Hydrogen placement	Geometric calculated sites
Structure refinement program	SHELXL-97 (Sheldrick, 1997)
Refinement method	Full matrix least-squares on F^2
Data / restraints / parameters	6691 / 1 / 367
Treatment of hydrogen atoms	Riding
Goodness-of-fit on F^2	1.448
Final R indices [I>2σ(I), 5799 reflections]	R1 = 0.0393, *w*R2 = 0.0839
R indices (all data)	R1 = 0.0489, *w*R2 = 0.0853
Type of weighting scheme used	Sigma
Weighting scheme used	$w=1/\sigma^2(Fo^2)$
Max shift/error	0.008
Average shift/error	0.000
Absolute structure parameter	-0.003(11)
Largest diff. peak and hole	2.406 and -1.081 e.Å^{-3}

Special Refinement Details

The position of the Pt atom was located with a Patterson map. The presence of the Pt atom creates a pseudo-mirror plane perpendicular to the b-axis and passing through the Pt position. The positions of the remaining atoms in the difference Fourier maps were complicated by this pseudo-mirror but it was possible to distinguish actual peaks from ghost peaks.

Numerous absorption correction schemes were tried but all resulted in unsatisfactory refinement results, therefore the uncorrected data was used in the final refinement. All large peaks in the final difference Fourier map are near the Pt atom.

Refinement of F^2 against ALL reflections. The weighted R-factor (*w*R) and goodness of fit (S) are based on F^2, conventional R-factors (R) are based on F, with F set to zero for negative F^2. The threshold expression of $F^2 > 2\sigma(F^2)$ is used only for calculating R-factors(gt) etc. and is not relevant to the choice of reflections for refinement. R-factors based on F^2 are statistically about twice as large as those based on F, and R-factors based on ALL data will be even larger.

All esds (except the esd in the dihedral angle between two l.s. planes) are estimated using the full covariance matrix. The cell esds are taken into account individually in the estimation of esds in distances, angles and torsion angles; correlations between esds in cell parameters are only used when they are defined

by crystal symmetry. An approximate (isotropic) treatment of cell esds is used for estimating esds involving l.s. planes.

Appendix 6

X-ray Crystallographic Data for 3.14

Table 1. Crystal data and structure refinement for AWF18.

Empirical formula	$C_{29}H_{29}BF_4N_3PtS$
Formula weight	733.51
Crystallization Solvent	Acetone
Crystal Habit	Plate
Crystal size	0.26 x 0.19 x 0.07 mm^3
Crystal color	Red

Data Collection

Preliminary Photos	Rotation
Type of diffractometer	CCD area detector
Wavelength	0.71073 Å MoKα
Data Collection Temperature	98(2) K
θ range for 8688 reflections used in lattice determination	2.29 to 25.62°
Unit cell dimensions	a = 10.6141(19) Å b = 11.884(2) Å β= 105.081(3)° c = 11.927(2) Å
Volume	1452.6(4) $Å^3$
Z	2
Crystal system	Monoclinic
Space group	$P2_1$
Density (calculated)	1.677 Mg/m^3
F(000)	718
Data collection program	Bruker SMART
θ range for data collection	1.77 to 28.48°
Completeness to θ = 28.48°	94.0 %
Index ranges	$-13 \le h \le 14, -15 \le k \le 15, -15 \le l \le 15$
Data collection scan type	ω scans at 6 ϕ settings
Data reduction program	Bruker SAINT v6.1
Reflections collected	21549
Independent reflections	6740 [R_{int}= 0.0597]
Absorption coefficient	4.950 mm^{-1}
Absorption correction	SADABS
Max. and min. transmission	1.000 and 0.734

Table 1 (cont.)

Structure solution and Refinement

Structure solution program	SHELXS-97 (Sheldrick, 1990)
Primary solution method	Patterson method
Secondary solution method	Difference Fourier map
Hydrogen placement	Geometric sites
Structure refinement program	SHELXL-97 (Sheldrick, 1997)
Refinement method	Full matrix least-squares on F^2
Data / restraints / parameters	6740 / 1 / 357
Treatment of hydrogen atoms	Restrained
Goodness-of-fit on F^2	1.308
Final R indices [I>2σ(I), 5339 reflections]	R1 = 0.0396, *w*R2 = 0.0657
R indices (all data)	R1 = 0.0564, *w*R2 = 0.0674
Type of weighting scheme used	Sigma
Weighting scheme used	$w=1/\sigma^2(Fo^2)$
Max shift/error	0.013
Average shift/error	0.000
Absolute structure parameter	0.055(9)
Largest diff. peak and hole	1.593 and -0.978 e.Å^{-3}

Special Refinement Details

Refinement of F^2 against ALL reflections. The weighted R-factor (*w*R) and goodness of fit (S) are based on F^2, conventional R-factors (R) are based on F, with F set to zero for negative F^2. The threshold expression of $F^2 > 2\sigma(F^2)$ is used only for calculating R-factors(gt) etc. and is not relevant to the choice of reflections for refinement. R-factors based on F^2 are statistically about twice as large as those based on F, and R-factors based on ALL data will be even larger.

All esds (except the esd in the dihedral angle between two l.s. planes) are estimated using the full covariance matrix. The cell esds are taken into account individually in the estimation of esds in distances, angles and torsion angles; correlations between esds in cell parameters are only used when they are defined by crystal symmetry. An approximate (isotropic) treatment of cell esds is used for estimating esds involving l.s. planes.

Appendix 7

X-ray Crystallographic Data for 4.4

Table 1. Crystal Data and Structure Analysis Details for awf20.

Empirical formula	$C_{43.50}H_{53}F_6N_4O_{8.50}Pt_2S_2$
	$[C_{40}H_{50}N_4O_2Pt_2]^{2+} \cdot 2[CF_3O_3S]^{1-} \cdot 0.5(C_3H_6O)$
Formula weight	1336.20 [1009.04, 2(149.06), 0.5(58.08)]
Crystallization solvent	acetone
Crystal shape	rough block
Crystal color	dichroic red/orange
Crystal size	0.19 x 0.19 x 0.25 mm

Data Collection

Preliminary photograph(s)	rotation	
Type of diffractometer	Bruker SMART 1000 ccd	
Wavelength	0.71073 Å MoKα	
Data collection temperature	98 K	
Theta range for 8185 reflections used in lattice determination	2.4 to 28.0°	
Unit cell dimensions	a = 20.9159(16) Å	α= 90°
	b = 11.9755(9) Å	β= 111.883(1)°
	c = 21.2787(16) Å	γ = 90°
Volume	4945.8(6) Å^3	
Z	8	
Crystal system	monoclinic	
Space group	$P\,2_1/c$ (# 14)	
Density (calculated)	1.794 g/cm^3	
F(000)	2608	
Theta range for data collection	1.9 to 28.5°	
Completeness to theta = 28.46°	95.4%	
Index ranges	$-27 \le h \le 27, -15 \le k \le 15, -27 \le l \le 28$	
Data collection scan type	ω scans at 7 fixed φ values	
Reflections collected	113310	
Independent reflections	11920 [R_{int}= 0.0553]	
Reflections > 2σ(I)	9752	
Average σ(I)/(net I)	0.0303	
Absorption coefficient	5.81 mm^{-1}	
Absorption correction	semi-empirical from equivalents	
Max. and min. transmission	1.000 and 0.824	
Reflections monitored for decay	first 620 scans recollected at end of runs	

Decay of standards	0%

Table 1 (cont.)

Structure Solution and Refinement

Primary solution method	direct methods
Secondary solution method	difference map
Hydrogen placement	calculated
Refinement method	full-matrix least-squares on F^2
Data / restraints / parameters	11920 / 0 / 793
Treatment of hydrogen atoms	all parameters refined (all calculated on disordered solvent)
Goodness-of-fit on F^2	1.95
Final R indices [I>2σ(I), 9752 reflections]	R1 = 0.0312, wR2 = 0.0533
R indices (all data)	R1 = 0.0462, wR2 = 0.0554
Type of weighting scheme used	sigma
Weighting scheme used	$w=1/\sigma^2(Fo^2)$
Max shift/error	0.083
Average shift/error	0.001
Largest diff. peak and hole	2.58 and -1.31 e·Å^{-3}

Programs Used

Cell refinement	Bruker SMART v5.606, Bruker SAINT v6.26
Data collection	Bruker SMART v5.054
Data reduction	Bruker SAINT v6.26
Structure solution	SHELX-97 (Sheldrick, 1997)
Structure refinement	SHELX-97 (Sheldrick, 1997)
Graphics	Diamond, Bruker SHELXTL v6.12

References

Bruker (1999) SMART (v5.054), SMART (v5.606), SAINT (v6.26) and SHELXTL (v6.12). Bruker AXS Inc., Madison, Wisconsin, USA.

Diamond 2.1. (2000) Crystal Impact GbR, Bonn, Germany.

Spek, A.L. (1990). *Acta Cryst.*, A**46**, C-34.

Sheldrick, G. M. (1997). SHELX-97. Program for Structures Refinement. Univ. of Gottingen, Federal Republic of Germany.

Special Refinement Details

A rough block was cut from a six-sided dichroic red/orange plate (red perpendicular to plate, orange when viewed from an edge) and mounted on a glass fiber with Paratone-N oil. Eight runs of data were collected with 13 second long, –0.3° wide ω–scans at seven different values of φ(0, 51, 103, 154, 206, 257, and 309°) with the detector 5 cm (nominal) distant at a θ of –28°. The initial cell for data reduction was calculated from 999 centered reflections chosen from throughout the data frames. In the triclinic least squares (reciprocal lattice vector tolerance of 0.005), 3 reflections were discarded. For data processing with SAINT v6.26, all defaults were used, except: a fixed box size of 1.8 x 1.8 x 0.6 was used, periodic orientation matrix updating was disabled, the instrument error was set to zero, no Laue class integration restraints were used, and for the post-integration global least squares refinement, no constraints were applied. No decay correction was needed. The crystal boundariess were indexed; but a face-indexed absorption correction was not useful. A SADABS v2.03 correction with g = 0.06 was applied.

No reflections were specifically omitted from the final processed data set; 3,133 of the 116,443 reflections were rejected, with 27 space group-absence violations, 0 inconsistent equivalents, and no reflections suppressed. Refinement of F^2 was against all reflections. The weighted R-factor (*w*R) and goodness of fit (S) are based on F^2, conventional R-factors (R) are based on F, with F set to zero for negative F^2. The threshold expression of $F^2 > 2\sigma(F^2)$ is used only for calculating R-factors(gt) etc. and is not relevant to the choice of reflections for refinement.

The dication is a platinum dimer with two bridging hydroxyl groups. Each square planar platinum is coordinated to the two hydroxyl oxygen atoms and to two nitrogen atoms. The angle between the $PtO_2N_2C_2$ cores (rms deviations from planarity of 0.033 and 0.035 Å) is 37.35(7)°. In the asymmetric unit are also two triflate counterions and one half of an acetone molecule (disordered over a center of symmetry). The hydroxyl groups each form a single hydrogen bond to one of the triflate anions; the two similar bonds are to different oxygen atoms.
This structure appears to be isostructural with that of the water/ethanol solvate (a = 20.5162(10), b = 12.3001(6), c = 21.2920(10), α = 90, β = 111.322(1), γ = 90, and V = 5005.3(4) at T = 158 K), with a disordered water/ethanol mixture replacing the disordered acetone.

The 19 largest positive and negative peaks (two at 2.58 $e \cdot Å^{-3}$, thirteen more > 1.1 $e \cdot Å^{-3}$, only two negative) in the final difference map are all ~ 1 Å from a platinum atom.

The Platon analysis of intermolecular contacts shows no significant interactions other than the hydrogen bonds.